4-2-1999

Microscopic characterization of hydrocarbon-polyelectrolyte interactions during coagulation

Vesna Dimitric Clark
Florida International University

DOI: 10.25148/etd.FI14060847

FLORIDA INTERNATIONAL UNIVERSITY

Miami, Florida

MICROSCOPIC CHARACTERIZATION OF HYDROCARBON-POLYELECTROLYTE INTERACTIONS DURING COAGULATION

A thesis submitted in partial fulfillment of the

requirements for the degree of

MASTER OF SCIENCE

in

ENVIRONMENTAL ENGINEERING

by

Vesna Dimitric Clark

1999

To: Dean Gordon R. Hopkins
College of Engineering

This thesis, written by Vesna Dimitric Clark, and entitled Microscopic characterization of hydorcarbon-polyelectrolyte interactions during coagulation, having been approved in respect to style and intellectual content, is referred to you for judgment.

We have read this thesis and recommend that it be approved.

Shonali Laha

Mehrzad Mehran

Berrin Tansel, Major Professor

Date of Defense: April 2, 1999

The thesis of Vesna Dimitric Clark is approved.

Dean Gordon R. Hopkins
College of Engineering

Dean Richard L. Campbell
Division of Graduate Studies

Florida International University, 1999

DEDICATION

I dedicate this thesis to my parents Slobodanka and Dragan Dimitric, and my grandmother Dara whose love, support and understanding through my life has helped me to accomplish my goals. To my husband Guy Clark, whose love and encouragement is always there when needed. To my sisters, Biljana and Nevenka whose confidence in me was motivating and reassuring.

ACKNOWLEDGMENTS

I wish to thank Dr. Berrin Tansel for her advice, support and encouragement during my graduate studies. Without her guidance I would not have been accomplished as a student or have experienced much of the scientific fulfillment of this work and other events.

I would also like to thank my committee members Dr. Shonali Laha, especially for her inspiration and positive influence, and Dr. Mehrzad Mehran for their advice and review of this manuscript.

I wish to thank to the Drinking Water Research Center for their assistance in the analytical work; especially Ms. Nahid Golkar for her coordination and guidance. Special thanks, to my friend Ricardo Martinez for his help in laboratory assignments. Thanks to my friend Lauralyn B. Carter for her academic support during my graduate studies.

ABSTRACT OF THE THESIS

MICROSCOPIC CHARACTERIZATION OF HYDROCARBON-POLYELECTROLYTE INTERACTIONS DURING COAGULATION

by

Vesna Dimitric Clark

Florida International University, 1999

Miami, Florida

Professor Berrin Tansel, Major Professor

The purpose of this study was to investigate effectiveness of polyelectrolyte in removal of different hydrocarbons and to obtain information on settling velocity, size and density of the floc. Image analysis technique provided multilevel data concerning interactions between hydrocarbons and polyelectrolyte. Captured images were digitized, enhanced by numerous filtering techniques and examined. Additional, video-monitoring system was used to provide information on settling velocity of the flocs. Results indicated that polyelectrolyte Cat-Floc 2953, in comparison to EB-5000, was more efficient in removal of all hydrocarbons, which was supported with turbidity measurements, GS analysis and microscopic analysis.

TABLE OF CONTENTS

LIST OF TABLES

LIST OF FIGURES

1. INTRODUCTION

Coagulation processes are usually used for the removal of turbidity and suspended solids from contaminated water. The coagulation process destabilizes colloids and other suspended solids by the addition of chemicals (coagulants) which agglomerate them into bigger flocs, so that gravitational and inertial forces will predominate and affect the settling characteristics of the particles. Within the last decade, the use of polymers in water and wastewater treatment has been expanded for their ability to break down oil-water emulsions and form more dense flocs.

Image analysis and video monitoring systems provided multilevel data concerning factors that influence effectiveness of cationic polyelectrolytes. The Image analysis system used in this study included a microscope, camera and Image-pro Plus software, while the video monitoring system was comprised of a camera, laser (as light source) and Flow Map 2.0 software. The image analysis system provided information on number, diameter, area of oil droplets attached to floc and size of the floc. Statistical data and histograms were based on these measurements. Measurements including average settling velocity, cross-correlation velocity and direction of flow were obtained by the video monitoring system and Particle image velocimetry (PIV).

The experimental designs included jar tests to identify the optimum conditions for removal of the contaminants by coagulation. This was followed by Gas chromatography analysis both before and after coagulation, to provide data on removal efficiency of selected hydrocarbons. Turbidity and pH were also measured before and after addition of coagulants.

Jar test results indicate that the application of Cat-Floc, a cationic coagulant, in the removal of different hydrocarbons exhibited higher effectiveness than EB-5000. These findings were supported by chemical analysis results. EB-5000 produced denser flocs which will be important for its application in sludge volume reduction, product water quality and effective solid-liquid separation processes, such as sedimentation, filtration and flotation.

Further research in the application of these polymers at higher hydrocarbon concentrations could provide more insight on existing relationships.

2. OBJECTIVES

The purpose of this study was to provide multilevel data concerning interactions between hydrocarbons and polyelectrolytes, using the image analysis system. The primary objectives of the research are:

- to investigate the effectiveness of polyelectrolytes in removal of different hydrocarbons from aqueous solutions;

- to evaluate morphology of floc formation by the image analysis system;

- to characterize the removal of oil droplets from oil-water emulsions by polyelectrolytes;

- to measure effectiveness of different coagulants in terms of number and size of oil droplets attaching to the floc;

- to determine settling velocity, size and density of flocs formed by the utilized polyelectrolytes.

3. LITERATURE REVIEW

The focus of this study was the application of the image analysis system to provide information on the effectiveness of specific polyelectrolytes in the removal of selected hydrocarbons from aqueous solutions. For these reasons literature review was concentrated on the coagulation process and different microscopic techniques for studying floc structure and floc characteristics. The applied techniques, and work completed on selected polymers and hydrocarbons, represent relevant and applicable research on the effectiveness of coagulation process in removal of contaminants from surface water and provides information on floc properties.

3.1. Coagulation theory

Solid particles remain in water suspensions primarily due to their surface charges. Since similar particles carry the same electrical charge, they repel one another, rarely getting close enough to stick together. Particle size is also important: the smaller the particle, the greater is its surface charge to weight ratio (Regula, 1994). A solid, when broken into smaller pieces, has greater surface area per unit volume (specific surface area), more exposed charged particles and increased interparticle repulsion. A heavy concentration of suspended solids causes more collisions and faster settling despite inter-particle repulsions (Regula, 1994). The attraction of solid to water also plays a role in suspension separations. Hydrophilic or water- attracting materials like clays, silicates,

and metal oxides are much harder to settle out than hydrophobic or water-repellent solids (Regula, 1994 and Edzwald, 1993).

The coagulation process involves the addition of a coagulant to fluid followed by rapid mixing, in order to destabilize the colloids and the other organic pollutants of a contaminated mixture. Colloidal stability depends on the relative magnitudes of the forces of attraction and the forces of repulsion. The attraction forces are due to Van der Waals forces, which are effective only in the immediate neighborhood of the colloidal particle. The forces of repulsion are due to the electrostatic forces of the colloidal dispersion. Initial destabilization of particles occurs due to reduction in zeta potential. Zeta potential measures the charge of the colloidal particles and is dependent on the distance through which the charge is effective. The higher the zeta potential, the greater are the repulsion forces between colloids; therefore, the more stable is the colloidal suspension. The destabilized particles aggregate due to provided agitation and Van der Waals attraction forces.

The primary mechanisms by which coagulation can remove organic contaminants involve colloidal destabilization, precipitation and coprecipitation steps (Randtke, 1988). Different chemical coagulants can induce destabilization of particles by different mechanisms or combination of mechanisms (Weber, 1972 and Dennett et al., 1996). Destabilization of colloids can be induced by electrical double layer (EDL) compression, adsorption to produce charge neutralization, adsorption to permit interparticle bridging, and sweep coagulation (Randtke, 1988). Colloidal destabilization allows the removal of the colloids by forming large flocs that can be easily settled or easily filtered. Removal of organic contaminants by coagulation depends on the magnitude to which the dissolved

contaminants adsorb to other particles through chemical complexation, electrostatic attraction, hydrogen bonding or various other means. Adsorption of the organics onto flocs is more effective than precipitation because of the trace quantities of the dissolved organics present in water (Randtke, 1988).

The fundamental purpose of slow mixing is to promote collisions between particles, for floc formation (particle flocculation). The process of flocculation has been theoretically described as the physical collision-agglomeration procedure carried out by various particle transportation mechanisms such as thermal motion (termed as Brownian movement), bulk transportation with fluid motion, and settling of particles (Weber, 1972 and Tambo, 1991). Perikinetic flocculation refers to flocculation in which the interparticle contacts are produced by Brownian movement. In orthokinetic flocculation, the interparticle contacts are caused by fluid motion due to agitation. Flocculation caused by contacts resulting from differential settling, is a process in which rapidly settling particles overtake and collide with particles settling at slower rates. The frequency of particle contacts, and the rate at which particles grow, is controlled by the properties of water (temperature, viscosity, and density), the properties of particles (number concentration, density and size) and characteristics of slow mixing facilities such as detention time, flow pattern and mixing intensity (Regula, 1994). The design and operation of coagulation/flocculation systems are focused on the latter characteristics, because the designer and operator have little control over the properties of water and particles except particle destabilization (and possible production of particles by precipitation) accomplished by rapid mixing.

Some solid-liquid separation processes such as sedimentation, flotation, filtration and membrane separation, always follow coagulation and flocculation. In order to improve the quality of formed flocs, polymers can be utilized as coagulant aids or as primary coagulants (Tambo, 1991). Factors effecting polymer and bridging characteristics include ionic strength, presence of divalent or polyvalent cations and mixing intensity. Increase in ionic strength causes decrease in thickness of the electrical double layer and it is easier for an attached polymer to extend beyond the distance at which any substantial energy barrier against particle approach might exist. In polymer flocculation, the turbulence in the reaction vessel plays an important role in effective mixing, therefore slow mixing is imperative (Regula, 1994).

Coagulation is often very effective in removal of dissolved organic matter (DOM) depending on the charge, solubility and molecular size characteristics of the DOM. The efficiency of removing organic carbon is proportional to molecular size, where larger molecular-weight components are more easily removed. Hydrophobic constituents of DOM (humic and fulvic acids) are preferentially sorbed on suspended colloidal particles (Dennett et al., 1996).

The coagulation process has been used for the removal of turbidity and could to some degree remove natural organic matter (NOM) which can function as a precursor to formation of disinfection by-products (DBP) (Krasner et al., 1995). The concept of enhanced coagulation involves modification of coagulation conditions (type of coagulant, coagulant dosage and coagulation pH) in order to sustain effective turbidity removal and to provide increased removal of NOM (Krasner et al., 1995). Higher dosage provides more metal (using aluminum salts) for either floc or complex formation; lower pH

reduces the charge density of humic and fulvic acids, making them more hydrophobic and adsordable.

3.2. Hydrocarbons

Petroleum or crude oil, is a complex mixture of numerous hydrocarbons, primarily comprised of paraffins (alkanes), olefins (alkenes), naphtanes and aromatics. Principal liquid fuels are produced by fractional distillation of crude oils. Petroleum mixtures consist of more than 200 hydrocarbons, with each compound exhibiting different physical and chemical properties that control its fate and behavior in a specific environment.

The alkene groups, normally found in petroleum products are based on the type and degree of processing involved. The cracking process of crude oils allows for the re-formation of alkane chains. When a mixture of alkanes (12 carbons or more) is converted at high temperatures (500°C), in the presence of a catalyst, the molecules break into smaller branched chains of alkanes by radical substitution. The higher the desired octane content of the fuel, the more branched the alkane chain becomes (Solomons, 1992). The degree of branching of alkanes and alkynes in petroleum fuel oils is limited due to the cracking process.

Aromatic compounds found in petroleum based fuels are normally mono-cyclic or bi-cyclic six-membered rings with methyl susbstituted hydrogens. Compounds in this group include benzene, toluene, ethylbenzene, and xylene (BTEX). Separation techniques are based on the very diverse physical properties of these aromatic compounds.

Solubility is the partitioning of a chemical between the nonaqueous (free product layer) and water phase. Dissolution occurs as soluble petroleum hydrocarbons contact with water. Potential for dissolution is a function of each compound solubility and the presence of co-solvents. At higher original concentrations of mixed fuel, the insoluble layer becomes greater and the soluble portion of mixed fuels reaches a maximum dissolution in water.

Alkanes are mostly insoluble because of a high degree of carbon saturation. The solubility of petroleum hydrocarbons in water generally decreases as the carbon number increases for both chain and ring petroleum hydrocarbons. The addition of a second or third double bond increases solubility proportionally. The presence of a triple bond increases solubility more significantly than the presence of two double bonds. Therefore, the most water soluble petroleum hydrocarbons are those with the lowest molar volume and greatest aromatic characteristics (Solomons, 1992).

Many organic chemicals of environmental concern are hydrophobic. The less soluble a chemical in water, the more likely it is to sorb to the surfaces of sediments or suspended particles. The octanol/water partitioning coefficient, K_{ow}, is related to the solubility of a chemical in water, and the higher the value the more a chemical tends to partition in the organic phase.

High molecular weight organics, those that are naturally hydrophobic, and those that posses functional groups able to result in their adsorption onto floc particles, are most likely to be removed by coagulation (Randtke, 1988). Sorption of hydrophobic compounds is often related to the organic content of the solids (sorbent) indicating a process of an organic-organic partitioning or absorption.

The sorption mechanisms can be defined as: (1) physical adsorption due to van der Waals forces, (2) chemisorption due to chemical bonding or surface coordination reaction, and (3) partitioning of the organic chemical into organic a carbon phase of the particulates. Physical adsorption is a surface electrostatic phenomenon while surface coordination reactions result in a binding between the particulate binding site and the dissolved organic molecule. Dissolution of hydrophobic organic chemicals into the organic phase of the particulate matter is defined as partitioning (Schnoor, 1996).

Some characteristics and sources of selected hydrocarbons are presented in Tables 3.1 and 3.2.

Table 3.1. Some characteristics of selected hydrocarbons.

Compound	Mol. wt.	B. p. (°C)	Sp. gr.	Solubility mg/L at 20 °C	log K_{ow}
Decane	142.29	174.1	0.730	0.009	
Toluene	92.1	110.8	0.867	515	2.73
Styrene	104.14	145.2	0.9045	280	2.95
m-xylene	106.16	139	0.864	0.16*	3.20

*Solubility at 25 °C

Table 3.2. Common sources of selected hydrocarbons.

Compound	Manufacturing source	Users and formulation	Natural and Manmade source
Decane	Petroleum refining	Organic synthesis, solvent, rubber industry, paper processing industry	Constituents in paraffin fraction of petroleum
Toluene	Petroleum refining, coal tar distillation	Benzene derivatives, medicines, dyes, solvent recovery plants	Coal tar and petroleum, gasoline (high octanol number),
Styrene	Organic chemical industry	Synthetic rubber, plastics, resins and insulators	Gasoline (high octane number)
m-xylene	Petroleum refining, coal tar distillation, organic chemical industry	Specialty chemical manufacture, solvent recovery plant	Coal tar, petroleum

As a major pretreatment for filtration, coagulation-sedimentation process was investigated for its potential to remove organic contaminants. Interactions between coagulants and organics (humic and salicylic acid), with different molecular weight ranges, in the absence of suspended solids, have been analyzed. Removal of low molecular weight organic compounds (salycilic acid) by alum coagulation was less effective and indicated adsorption and entrapment destabilization mechanisms. Destabilization of humic acid was due to charge neutralization (Huang et al., 1996).

3.3. Polymers

Within the last decade the use of polymers in water and wastewater treatment has expanded considerably. Polymers are long-chained organic molecules, containing ionizable groups (carboxyl, amino, sulfonic groups) arranged along the chain and can be charged (polyelectrolyte) or neutral. Depending on their charge characteristics in water (positive, negative or neutral), they are grouped as cationic, anionic and nonionic polymers.

Organic polymers are comprised of specific monomers linked linearly or in branched configurations and polymerized into high-molecular-weight substances. They are used in order to influence the stability and coagulation properties of a dispersed system (Schwarz et al., 1997). The important characteristics, which affect the performance of a particular polymer, are charge density, molecular weight, degree of branching, dosage rate and contact time. In comparison with standard coagulants, a polyelectrolyte has higher charge densities, can be applied in smaller doses and can yield formation of large heaver flocs (Lind, 1994). Different chemical coagulants can cause the destabilization of colloids in different ways. Organic polymers destabilize colloids by charge neutralization and interparticle bridging (Weber, 1972; Shwarz et al., 1998 and Gray et al., 1997).

During the contact with colloidal particles, some of the functional groups of polymer adsorb at the particle surface, leaving the remainder of the molecule extending out into solution (Reaction 1 in Figure 3.1). Bridging occurs when another particle, with vacant adsorption sites, connects with the extended segment of polymer and forms a link

between them. If the second particle is not available, in time the extended segment of polymer may eventually adsorb on other sites on the original particle, therefore the polymer is no longer capable of serving as a bridge (Reaction 3 in Figure 3.1). Exceeding optimum dosage of polymer can result into restabilized colloids, since no sites are available for the formation of interparticle bridges (Weber, 1972). Certain conditions can cause a system which has been destabilized and aggregated to restabilize by extended

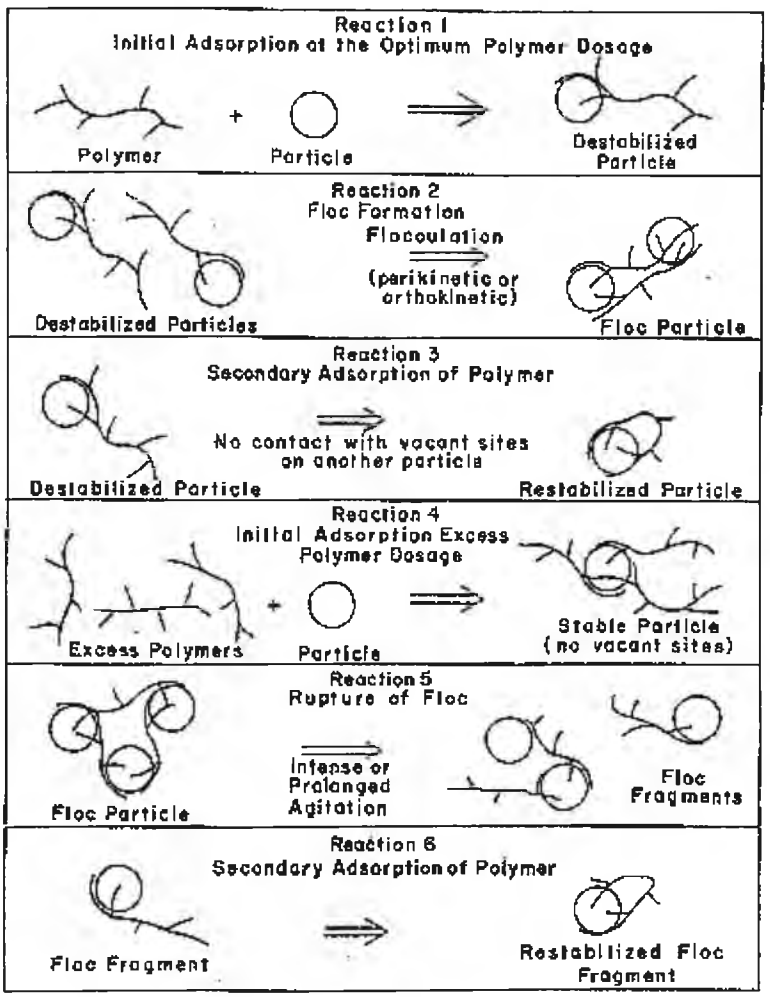

Figure 3.1 Schematic representation of the bridging model for the destabilization of colloids by polymers (Weber, 1972).

agitation. This occurs due to the breaking of polymer-surface bonds and the subsequent folding back of extended segments onto the surface of the particles (Weber, 1972).

Since competing reactions for adsorption and precipitation do not occur for organic polymers, high mixing intensities are not necessary. Interparticle bridging and breaking up of aggregated floc, due to high intensities of turbulence, is important and controlling. Mixing energy is important in increasing the number of collisions between particles and coagulant since faster and more efficient charge neutralization and flocculation would take place at higher mixing intensities. Improved mixing often lowers coagulant dosage, improves clarification, and enhances the action of other treatment chemicals (Lind, 1994).

One investigation reports the reaction mechanism and the effects of aluminum salts, combined with cationic, anionic and nonionic polymers on flocculation processes, while using polyelectrolytes as flocculant aids (Narkins et al., 1991). Results indicated that lower doses of each polyelectrolyte were required, turbidity removal was more efficient and the settling sludge characteristics were improved due to the usage of polyelectrolytes. Flocculation mechanism of cationic polymer could have been either by charge neutralization associated with adsorption and bridging or bridging only. In general, all polymers formed well- settable flocs by the interparticle bridging mechanism. This study provided information on the type of coagulant to be used, process conditions and the concentration ratios of each polymer and the aluminum salt in specific combinations.

The flocculation behavior of oppositely charged polyelectrolytes (two-component system), as flocculants and retention aids, was examined (Petzold et al., 1996) by the

different procedures such as polyelectrolyte titration, dewatering test and measuring the residual turbidity. This study was designed to improve the knowledge of dual systems for flocculation and especially to evaluate influence of polyanion molecular weight. The results of the study indicated that the flocculation mechanism depends upon the molecular weight of a polyanion. Two different mechanisms of flocculation were possible: complexation between oppositely charged polymers, and patchwise adsorption combined with bridging.

The conditioning characteristics of kaolin sludge combined with different cationic polyelectrolytes was examined (Chang et al., 1998) applying the following methods: measuring the capillary suction time (CST), measuring the streaming current (SC), determining the moisture content of dewatering sludge cake and measuring the floc size. According to their results, the moisture content of the kaolin sludge system was found to depend on molecular weight, dosage and charge density of the polyelectrolyte. When the SC value equals zero, the moisture content of dewatered kaolin sludge cake reaches the maximum. The polyelectrolyte dosage necessary to minimize the CST value is independent of the molecular weight of used polyelectrolytes.

The results of the effect of polyelectrolyte density and molecular weight on removal efficiency during an investigation of oil flotation, indicated improved flotation performance with increase in polyelectrolyte charge density, while molecular weight had no effect on flotation (Gray et al., 1997). Turbidity removal advanced as floc size increased, indicating that raising the floc size was the dominant role of the polyelectrolyte in improving flotation performance. Flotation became more robust to variations in

polyelectrolyte concentration as the polyelectrolyte charge density decreased due to lowering adsorption-driving forces between the polyelectrolyte and oil.

3.4. Floc Density

Particle aggregates are formed in coagulation/flocculation processes, and in some cases are already present (in natural waters), where they can greatly influence the transport and fate of contaminants. The two most important properties of aggregates are their size and density, which can both have a significant influence on the effectiveness of solid-liquid separation processes, such as sedimentation, filtration and flotation. Sludge volume reduction, product water quality and overall process performance may depend on these floc properties (Glasgow et al., 1989).

The density of the floc was estimated using Stokes' Law. Since, Stokes' Law is based on the settling of single impermeable spherical particles in a laminar region (Reynolds Number < 0.5). It is not ideal for the determination of floc density due to the heterogeneous structure and irregular shape of the floc (Droppo et al., 1997). The equation used to estimate floc density in this research was:

$$\varpi = 1/18\ D^2(\rho_f - \rho_w)g/\mu \qquad (1)$$

where:

ϖ = settling velocity, m/s

D = diameter of floc, μm

ρ_f = wet density of floc, kg/m^3

ρ_w = density of water, kg/m^3

μ = dynamic viscosity (kinemetic viscosity x ρ_w), Ns/m^2

ϖ and D obtained by the image analysis and ρ_w, μ are constants for a given water temperature, the wet density ρ_f of the floc was calculated.

Factors such as floc composition (organic and inorganic properties), shape, porosity and water content can affect settling rate of a floc. Settling velocity and porosity increase with the floc size while density decreases with increase in floc size (Gregory, 1997, Droppo et al., 1997, Bache et al., 1997). During the growth of a floc, the number of linkages to additional particles or flocs increases creating additional pores. This increased porosity induces an increase in water content that forces the density of the floc towards the density of water and tends to reduce the settling velocity of the floc. Flocs often have a density slightly greater than water and rather a low settling rate (Gregory, 1997).

Figure 3.2 presents a compilation of several existing floc density data in a single graph. Variations in chemical conditions, agitation, flocculant, dispersed-phase and methods of measurement were responsible for differing results. Polymer flocculated systems show larger densities than systems coagulated with inorganic acid salts. All of the results indicated steep increases in density as aggregate size decreased to within 600 - 700 μm. This effect was very pronounced in polymer systems and reflected a change in dominant structural type (Glasgow et al., 1989). Knowledge of settling velocity, density and porosity also is useful for the characterization of sediment environments and for the study and modeling of sediment and contaminant transport (Droppo et al, 1997).

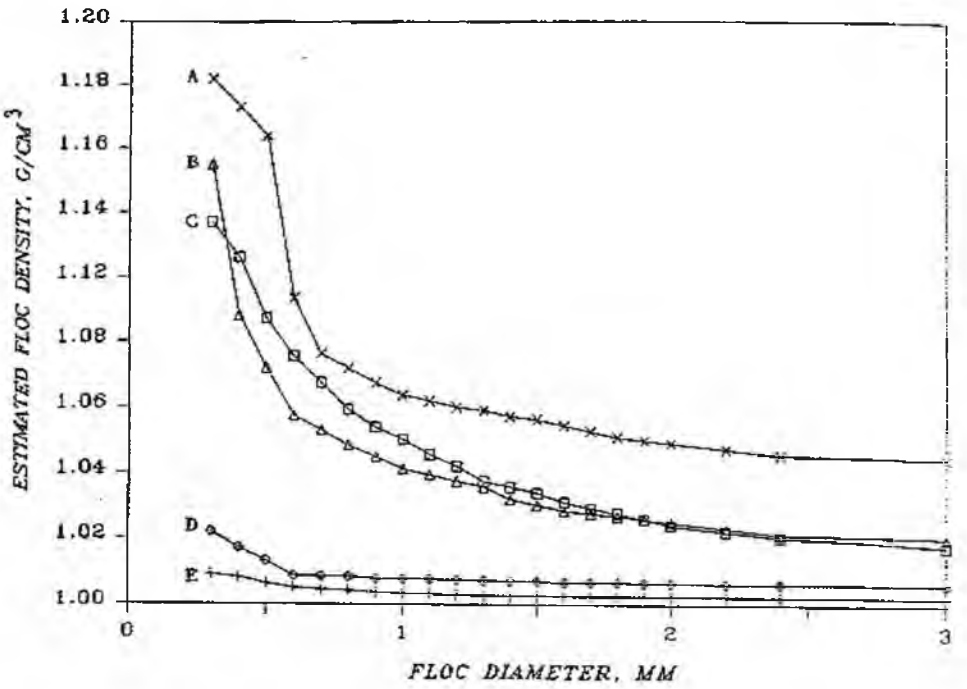

Figure 3.2 Compilation of floc density data from the literature (Glasgow et al., 1989).

Droppo et al. (1996 and 1997) investigated the structural matrix of flocs in freshwater over a large range of magnification using correlative microscopic techniques. The importance of floc characteristics (size, shape, density, porosity, organic composition, inorganic composition) on the physical (eg. transport and settling), chemical (eg. adsorbing/transforming contaminants and nutrients) and biological behavior (eg. biotransfromation and habitat development) of the flocs were examined. The results indicated that internal structure of floc has significant impact on controlling floc behavior. The internal structure of freshwater floc is very complex and is often dominated by fibrillar material containing active microbial community within the floc.

Figure 3.3 presents the interactive physical, chemical and biological factors influencing floc development.

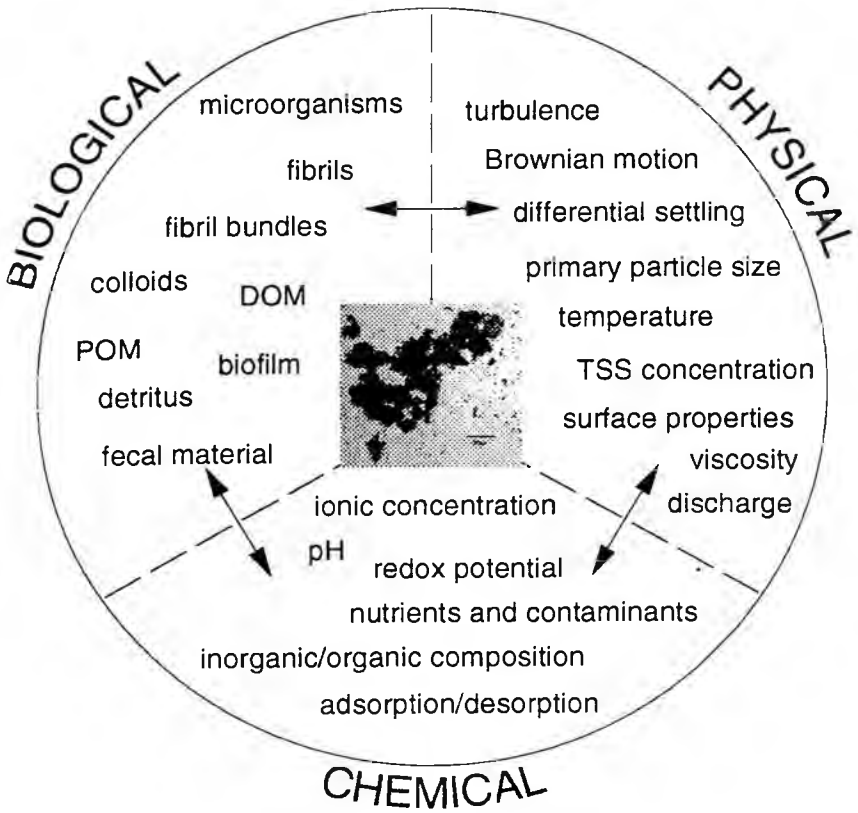

Figure 3.3 Interactive physical, chemical and biological factors influencing floc development (from Droppo et al., 1997).

The addition of polymer can have a profound effect on development of both floc size and settling rate, due to the reaggregation of fragments (Glasgow et al.,1989; Gregory, 1997).

Investigation of the many interesting features of flocculation of both polystyrene latex and kaolin with cationic polyelectrolytes provided important estimates of adsorbed polymer layer thickness (to be ~0.06 μm) and the extent of surface coverage (Glasgow et al., 1989). Such data are essential for modeling floc density changes during aggregate growth.

Bache et al. (1995) investigated the general correspondence between the optimal coagulation conditions identified in jar tests and optimal characteristics of the floc. Floc properties display optimal behavior in response to the operating conditions for both colored waters and turbid suspensions, in terms of floc properties: notably size, effective density and strength. In these experiments for determination of floc strength, single-grid and multi-grid oscillatory mixers are used. Coagulation overdosing leads to reductions in the effective density and diminishing strength due to increasing water content and increasing fraction of positively charged precipitate within the floc.

4. IMAGE ANALYSIS SYSTEM

4.1. Image-pro Plus software

Image-pro Plus version 3.0 software (Media Cybernetics, Silver Spring, MD) perform imaging and analysis capability for acquiring, enhancing and analyzing captured images. The source images obtained in this study by microscope were digitized into pixels (picture elements). Enhancement techniques ranging from simple operations such as brightness and contrast adjustment, to the sophisticated and complex spatial and morphological filtering operations designed to improve and refine visual information, can be applied. The software provides the ability to:

- acquire data images from a camera or microscope;
- read and write data images into all the standard image file formats;
- work with gray scale and color data;
- perform image enhancement using color or contrast filters including fast Fourier transforms (FFT), morphology, field flattening, background subtraction and other spatial and geometric operations;
- trace and count objects manually or automatically. Measure object attributes such as area, angle, perimeter, diameter, roundness, length, as well as characteristics of the defined view area;
- view collected data numerically, statistically or in graphic form (histogram and scattegram);
- sort and classify data according to predefined criteria. Color code of objects by class.

Prior to photographing the particles, a photograph was made of a 1-mm divison scale at the 10X magnification. The photograph of the scale was used to calibrate the image analysis system. Spatial calibration was completed prior to measuring actions.

Measured data were transferred to Microsoft's Excel spreadsheet and displayed. The statistics data sheet provides the following statistics for each measurement:

- Min.: the smallest value for each measurement. Number, placed below the stated minimum identifies the object possessing the minimum measurements.
- Max.: number stated beneath maximum identifies maximum measurement.
- Range: represents the difference between the maximum and minimum values for each specified measurement.
- Mean: define the average (mean) for each measurement
- Std. Dev.: represent standard deviation for each measurement.

Two plotting devices, scattergram and histogram, are provided to allow visualization of data in chart form. A scattergram can be used to illustrate a correlation between two measurements. Measurement histograms provide another way to present the measurement data and to illustrate the distribution of the object population over a measurement range. The histogram's X-scale identifies the measurement's range (from its minimum value to its maximum value), and the Y-scale measures the number of objects within each measured interval.

5. EXPERIMENTAL DESIGN AND INSTRUMENTATION:

5.1. Experimental Design

Standard jar tests were performed and the results were evaluated and compared based on data provided by the image analysis system. The definite removal of hydrocarbons was confirmed by GC (Hewlett Packard Model 5890, Series II) analysis. Subsequently, turbidity measurements provided data on the effectiveness of applied coagulants. Settling velocity provided information on floc density. The design incorporated four variables and twenty settings; more details about design parameters are provided in the following sections. Table 5.1 provides the experimental variables and settings involved in the experimental work.

Table 5.1 Experimental variables and settings.

Variables	Settings
Source Water	Pond water
Coagulant	Cat-Floc 2953 EB-5000
Contaminant concentration	300 ppm 500 ppm
Contaminant type	Decane Toluene m-xylene Styrene Unleaded gasoline

5.1.1. Source water

The sample site was chosen to provide information on surface water characteristics and floc structure. The pond water chosen contains dissolved organic matter, natural organic matter, humics, turbidity and other components, for which removal the coagulation process is effective. The coagulation treatment efficiency of the contaminated water, by specific hydrocarbons, prior and posterior to contamination, was investigated. The important criteria in selecting these types of source waters were to model a situation under which the coagulation process would treat these contaminated waters effectively. Surface water samples were collected from the pond located near the

Engineering Applied Science building, Florida International University, Miami, Florida. Turbidity (Hatch Company laboratory turbidimeter) and pH measurements (Fisher Scientific pH meter) characterized pond water. The samples were contaminated with different petroleum hydrocarbons at concentrations ranging from 300 ppm to 500 ppm, and mixed for one-hour prior to coagulation experiments.

5.1.2. Coagulants

Polyelectrolytes are synthetic organic polymers used in order to bring removal of particles through adsorption and bridging. The selection of Cat-Floc 2953 and EB-5000, used in this research, was based on the coagulant screening tests (refer to Appendix). The liquid cationic polyelectrolytes were obtained from Calgon Corporation (Pittsburgh, Pennsylvania). Cat Floc 2953 and EB-5000 (these are the trade names used by Calgon Corporation) were prepared by adding 1 milliliter of polymer to 100 milliliters of distilled water for ease of handling as recommended by the manufacturer. Table 5.2 provides properties of the coagulant used in the experiments.

Table 5.2 Physical and chemical properties of Cat-Floc2953 and EB-5000.

Parameter	Cat-Floc 2953	EB-5000
Chemical description	Acidic aqueous solution	Acidic aqueous solution
Product class	Cationic coagulant	Cationic coagulant
Ingredients	Poly(dimethyldiallyl-ammonium chloride) ~ 26% by weight Hydrochloric acid 1-5% by weight Sulfuric acid 1-5% by weight	Poly(dimethyldiallyl-ammonium chloride) ~ 26% by weight
Flash point	>200°F	>200°F
Boiling point	>212°F	Not available
Solubility in water	Complete	Complete
Specific gravity	1.18-1.20 at 25°C	1.15-1.20 at 25°C
pH	2.5-3.0 at 25°C	3.5-3.8 at 25°C
% volatile by weight	Not determined	65
Appearance	Clear, pale yellow, slightly viscous liquid	Clear to slightly hazy, pale yellow liquid

5.1.3. Contaminant concentration

The contaminants used in these experiments included decane, toluene, m-xylene, styrene and unleaded gasoline. The types of contaminants were selected based on the conditions required to emulate with the real world situation of a water body contaminated with formerly selected hydrocarbons. The pond water was contaminated with each of these hydrocarbons, in concentrations of 300 ppm and 500 ppm. Hydrocarbons including decane, toluene, m-xylene and styrene were provided by Fisher Scientific Chemical and unleaded gasoline was obtained from a local gas station. Gas Chromatography analysis (Hewlett Packard 5890) using flame ionization detector (FID) were accomplished before and after coagulation process to detect the range and the amount of hydrocarbons removed from the sample. Floc density data were derived from settling velocity measurements.

5.2. Instrumentation

Coagulation unit

The coagulation unit used for the standard jar-tests was a six-paddle mechanical stirrer Model PB-700 manufactured by Phipps & Bird Inc., Richmond, VA. The unit had high and low adjustable speed controls with a maximum speed of 300 rpm.

Gas Chromatograph

The samples, including decane, toluene, m-xylene and styrene, collected for GC analysis were prepared by the liquid–liquid extraction procedure using pentane as solvent. The GC unit was Hewlett Packard Model 5890, Series II equipped with DB-5 column (30m-x 0.45 mm I.D.). The GC was programmed at 35°C for 6 minutes, increasing the temperature by 4°C/min reaching 55°C. Afterward, the oven temperature was increased at the rate of 17°C/min up to 105°C. The temperature of 105°C was retained for the analysis for 1 minute. Helium at flow rate of 6.5 ml/min was used as carrier gas. Make up gas consisting of nitrogen at a flow rate of 30 ml/min, hydrogen at 28 ml/min, and compressed air at 280 ml/min were also used in the GC analysis. Gasoline analyses were accomplished with little changes in GC program. New set up started at temperature of 30°C, retained for 6 minutes. The rate of temperature increase was 6°C/min until reaching 130°C. Subsequently, the oven temperature was increased at the rate of 15°C/min up to 180°C. The temperature of 180°C was retained for the analysis for 8 minutes and increased to 200°C at the rate 25°C/min. Helium with flow rate of 6.8 ml/min was used as a carrier gas.

Stock and working standards of gasoline, styrene, toluene, decane and m-xylene were prepared and refrigerated, prior to the preparation of daily standards. Standard calibration samples were used and the machine was calibrated. Before each set of samples, solvent blanks were run to avoid any carry over of the samples in the GC column. Finally the data printouts were standardized into a format for complete research data organization using computer software programs.

Microscope:

The Olympus System Microscope, model BX40, is the universal optical system, provided by Olympus America Inc., Melville, N.Y.. The objective magnification ranged from 10X to 60X. In this research, the 10X objective magnification provided adequate enlargement of the flocs and oil droplets. The microscope has built-in transmitted Koehler illumination 6V 30W Halogen bulb as light source.

Camera and camera adapter for Image Pro-plus software:

Camera adapter model CMA-D2 was mounted on a Sony Color video camera model DXC-107A/107AP. The DXC-107A/107AP is a color video camera, which uses a CCD (Charge Coupled Device), a solid state image sensor and three automatic shutter speed control (IRIS). The camera automatically adjusts the shutter speed for optimum exposure, even when using a lens with manual IRIS.

Turbidimeter and pH meter:

Hatch Company laboratory turbidimeter, model 2100N was used to provide measured data in NTU units. A machine was calibrated using formazin standard.

A Fisher Scientific pH meter, model AR50 was utilized and standardized prior to its application.

Particle Image Velocimetry system:

The Particle Image Velocimetry (PIV) system provided by DANTEC Inc., was used to obtain the velocity-vector plots containing both amplitude and flow direction for the

whole visualized flow field with high accuracy and high resolution. The system includes four basic sub systems: visualization, camera, video recording and software for analysis. The stabilite 2017 ion laser was used as a continuous wave laser. The beam form CW laser was chopped into pulses by Dantec's 80X41 electro optical shutter. Dantec's camera 80C42 DOUBLE Image 700 may work in three modes. The most powerful operating mode is double-frame cross correlation mode. Captured images are transferred to PIV processor via the digital connector and host computer for data processing and analysis, and the images recorded by the camera where transffered to a video recorder to simultaneously show flow pattern.

6. DATA COLLECTION AND ANALYTICAL METHODS

Initial screening tests were conducted to determine optimum dosages and effectiveness of coagulants in terms of floc formation, floc size and turbidity removal. The screening tests were accomplished using the standard jar-test procedure. The most effective coagulants, Cat-Floc 2953 and EB-5000, as determined from screening tests, were subsequently used for coagulation studies.

After addition of contaminant at concentration 300 ppm or 500 ppm in pond water, the solution was mixed for 24 hours prior to jar tests. Solution samples of 500 ml volume, were placed into 1000 ml (1liter) beakers. The standard jar test procedure includes addition of coagulant in sample and mixing, with agitation rates of 300 rpm for 2 minutes (rapid mixing), followed by 35 rpm for 15 minutes and a settling period of 20 minutes. Turbidity and pH measurements were recorded before the addition of coagulant and after the coagulation process was accomplished.

Settling experiments were conducted after coagulation process was accomplished and flocs formed. 400 mL of each solution was placed in a rectangular glass cell. Using the video monitoring system settling of flocs was observed. A laser was used as the ideal light source for the camera due to its high intensity, directionality and easier optical control. Pixel images were acquired and then transferred to Particle Image Velocimetry 2000 Processor via digital connector and host computer, for data processing and analysis. The host computer was equipped with Software Flow Map 2.0 (Flow Manager). Data were presented as average settling velocity vectors, cross-correlation velocity vectors and streamlines (direction of flow).

Afterward, the samples were refrigerated for a few hours to allow complete settling of flocs. Thirty ml of coagulated water was measured and placed into a turbiditemeter. The data were reported in nephelometric turbidity units (NTU). After the first group of hydrocarbons with concentration of 500-ppm was analyzed, the same preparation and analyzing procedures were followed for 300 ppm water-contaminant mixtures.

The samples for organic analysis were prepared prior to and after the coagulation procedure. Subsequently, the samples were analyzed by a Gas Chromatograph (GC) unit equipped with Flame Ionization detector (FID) and direct flash injection liner, before and after coagulation processes to detect the range and amount of hydrocarbons removed from the samples. The samples collected for GC analysis were prepared by liquid–liquid extraction procedure using pentane as solvent. The extracted samples were placed in to 2 ml auto sampler vials for GC analysis. Preparation of samples and complete chemical analysis were accomplished at the Drinking Water Research Center at Florida International University.

Samples were subsequently prepared for microscopic examination and image analysis. Water drops of coagulated and noncoagulated water were placed on microscopic slides using Pasteur pipettes (Fisher Scientific). Slides are placed on microscopic stage of Olympus System Microscope and observed. Images of flocs were captured using Sony Color video camera CCD-IRIS. The camera was mounted on the microscope and connected to a computer, equipped with Image-pro Plus software. Photograph 1 displays the microscope, camera and computer setting. Data were collected and summarized at the section 7.

6.1. Image-pro Plus analysis system

Image-pro Plus software, used simultaneously with microscope and camera derived multiple levels of information from an analyzed sample. The images captured by microscope were investigated using measured objects attributes such as area, angle, perimeter, diameter, roundness, length, and characteristics of the defined view area.

The spatial calibration was completed prior to measuring actions and the measurements are submitted in micrometers.

Predefined criteria such as diameter range of oil droplets were selected in order to compare data obtained from different images. Collected data were viewed numerically, statistically or in graphic form of histogram and scattergram.

6.2. Microscopic Analysis

The microscope, Sony Color video camera and computer equipped with Image-pro Plus software were used as size and effectiveness analyzing tools for this study. Drops of coagulated water containing flocs were collected with pipettes from beakers and placed on microscopic slides. Flocs were observed with the 10X objective with a light source build in the microscope. Photographs taken by camera were digitized and analyzed using Image-pro Plus. Samples of noncoagulated contaminated water were subsequently prepared for microscopic examination and image analysis.

6.3. Data Collection

Captured images of each hydrocarbon-pond water mixture, with Cat-Floc 2953 and EB-5000, were saved and used for further analysis. Enhancement filtering techniques were applied to provide sharper images. The image analysis system was used to digitize the image and measure average diameter, area of the oil droplet attached on a floc and the area of the floc. The measurements of the flocs and oil droplets were provided in selected range. Statistical data of each image were automatically calculated and displayed in tables. The statistical data were exported to Excel worksheets. Histograms based on computed data provided by Image-pro plus software were created.

Calculations concerning the density of floc were based on floc settling velocity measurements and utilization of Stock's equation (1). Using the video monitoring system settling of flocs was observed. A laser was used as the light source for the camera and Flow Map 2.0 software for analyzes. Obtained data were divided into average settling velocity vectors, cross-correlation velocity vectors and streamlines (direction of flow).

7. RESULTS AND DISCUSSION

The results and discussion of the experimental work are divided into three sections. The first section emphasizes microscopic images and results based on microscopic observations. The second section presents chemical analysis of data and graphical representation. The third part contains measurements of settling velocity and calculations of floc density.

7.1. Microscopic observations

Microscopic images of decane, toluene, xylene, styrene and gasoline were captured and analyzed in this order.

Figures 7.1 to 7.4 and Figures from 7.17 to 7.20 present the microscopic images of decane flocs formed by coagulant Cat-Floc 2953. These flocs exhibit larger number and diameter of oil droplets entrapped (both on the surface and within the floc), compared to one formed by EB-5000. Graphical representation of oil droplet distribution versus diameter (average) and area are provided on figures 7.4 to 7.8 for decane concentration 500 ppm coagulated with Cat-Floc 2953 and 7.21 to 7.24 for decane coagulated with EB-5000.

The observed flocs generally were irregular in shape but tended toward circular shape. Cat-Floc 2953 formed large white flocs (2-4 mm), visible with the naked eye. Size of the floc can have significant implications for the modeling of contaminant movement

as the larger flocs will likely settle out much faster than the finer flocs which travel with their associated contaminant, much further in the system.

In general, flocs formed by EB-5000, had a low resolution due to their yellow color, resulting from the polyelectrolyte liquid. At lower concentration of 300 ppm, decane flocs had appearance of less dense inner structure then EB-5000 flocs at same concentration, which was supported with settling velocity data (Table 7.2)

Toluene images at concentration of 500 ppm are displayed as Figures 7.33 to 7.36 excluding Figures 7.37 to 7.38, representing oil droplet sizes and diameters distribution. The floc structure appears heterogeneous in terms of spatial density across the flocs with the presence of micro-pores. Some of the oil droplets were captured inside the oil-water emulsion bubbles, therefore limiting the feasibility to produce sharper images. The images of the floc sizes, produced by Cat-Floc 2953 occurs on the images larger than EB-5000 but this was not supported with settling velocity data, pointing out possibility of error. During preparation of flocs for microscopic examination the floc structure was partially damaged due to pipette size used in sample preparation.

Area and diameter of m-xylene droplets are displayed on Figures 7.61 , 7.62 and 7.67 and 7.68 for 500 ppm concentration and for 300 ppm concentration on Figures 7.73 to 7.74 and 7.79 to 7.80. Pictures of flocs are displayed on Figure 7.57 to 7.60 and 7.69 to 7.72 for Cat-Floc coagulant and figures 7.63 to 7.66, and 7.75 to 7.78 for EB-5000. Flocs obtained from EB-5000 have irregular shapes with large cavities inside the floc structure while the structure of Cat-Floc 2953 flocs is more chain looking.

Figures through 7.81 to 7.86 are images and image analysis, concerning styrene with coagulant Cat-Floc at 500 ppm concentration while Figures 7.93 to 7.98 are images

at 300 ppm concentration. Coagulant EB-5000 formed flocs exposed on Figures 7.87 to 7.90 for 500 ppm and Figures 7.99 to 7.102 for 300 ppm. Styrene flocs formed with Cat-Floc 2953 have more dense looking structures than EB-5000, which contained some openings in internal structure.

Gasoline flocs formed at concentration of 500 ppm and 300 ppm with Cat-Floc 2953 are shown on Figures 7.105 to 7.108 and 7.117 to 7.120. Flocs of EB-5000 are presented on Figures 7.111 to 7.114 for 500 ppm and 7.123 to 7.126 for 300 ppm concentration. Gasoline floc shapes exhibit irregularities however without cavities inside the flocs. Oil droplets are clearly visible inside the structure and on the surface of floc.

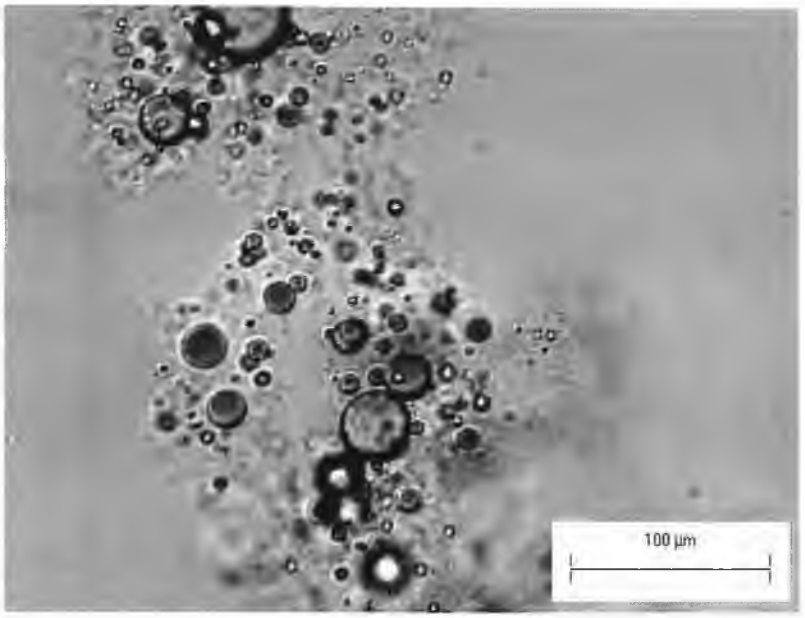

Figure 7.1 Microscopic image of Decane floc at concentration of 500 ppm with Cat-Floc 2953 at optimum dosage.

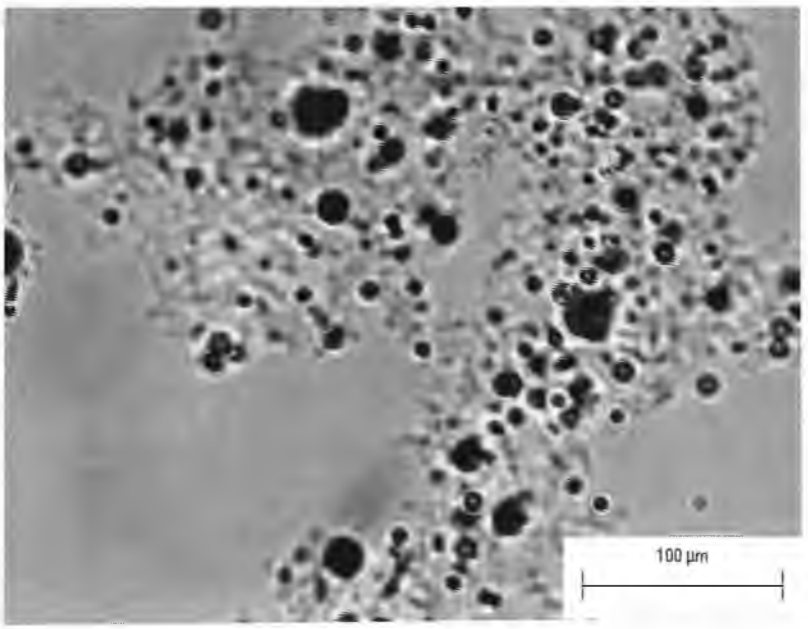

Figure 7.2 Microscopic image of Decane floc at concentration of 500 ppm with Cat-Floc 2953 at optimum dosage.

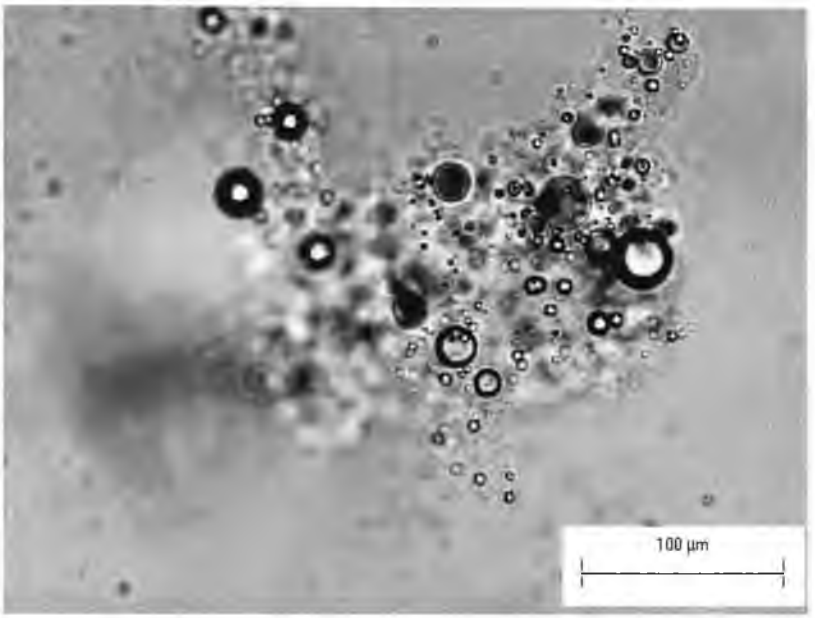

Figure 7.3 Microscopic image of Decane floc at concentration of 500 ppm with Cat-Floc 2953 at optimum dosage.

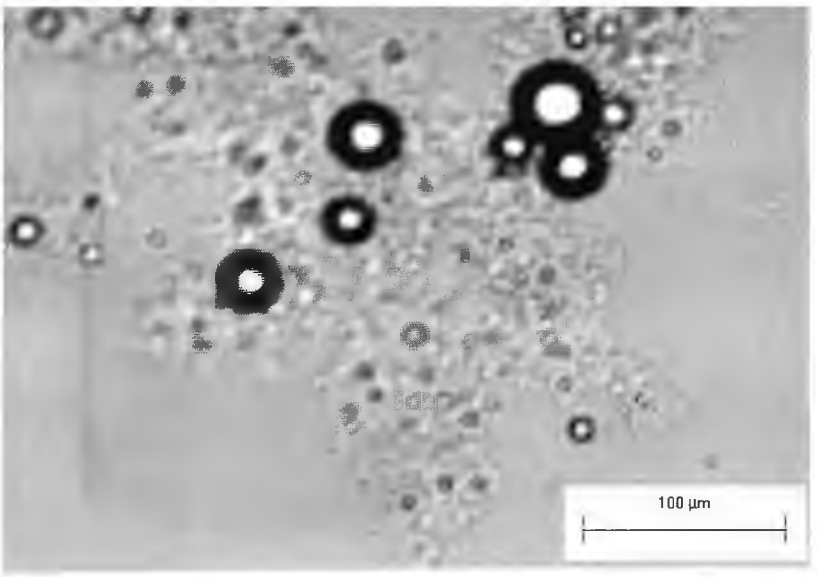

Figure 7.4 Microscopic image of Decane floc at concentration of 500 ppm with Cat-Floc 2953 at optimum dosage.

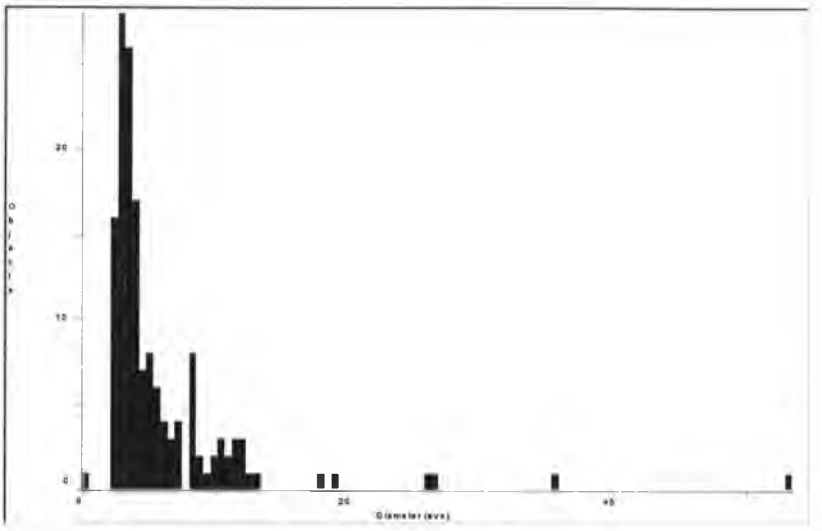

Figure 7.5 Distribution of Decane droplet diameter inside of Cat-Floc 2953 floc at concentration of 500 ppm, for microscopic image 7.1.

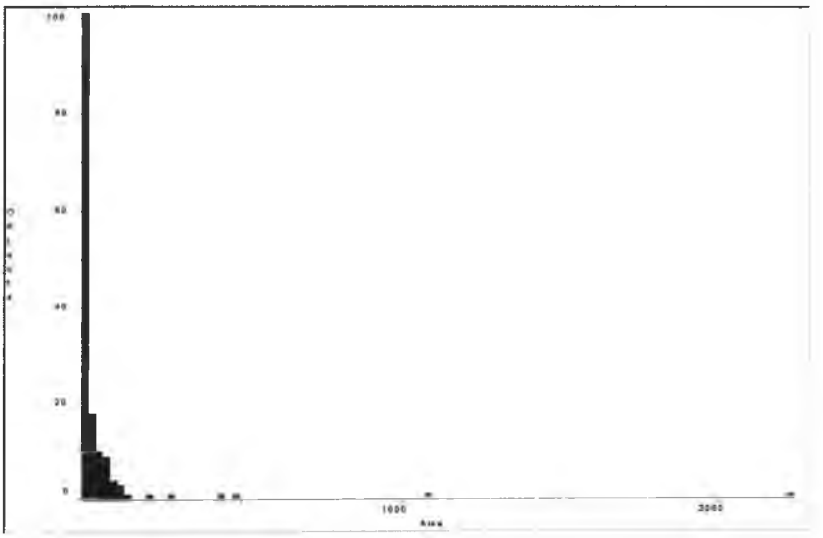

Figure 7.6 Distribution of Decane droplet area inside of Cat-Floc 2953 floc at concentration of 500 ppm, for macroscopic image 7.1.

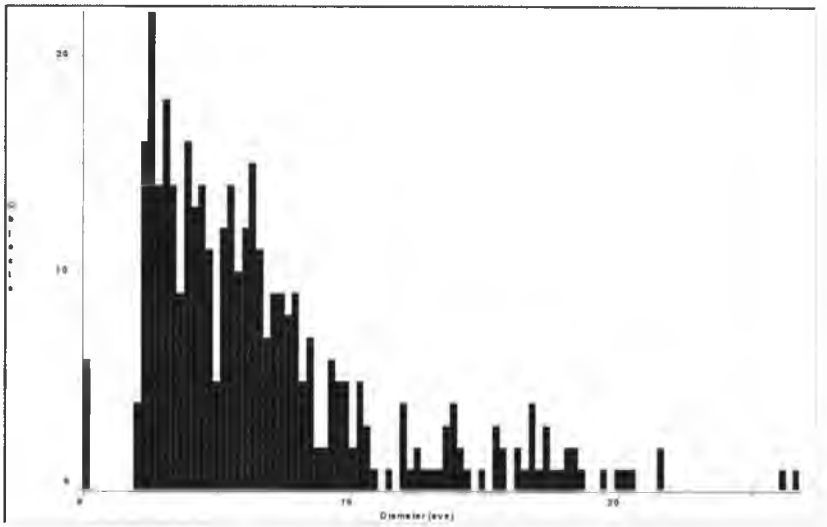

Figure 7.7 Distribution of Decane droplet diameter inside of Cat-Floc 2953 floc at concentration of 500 ppm, for microscopic image 7.2.

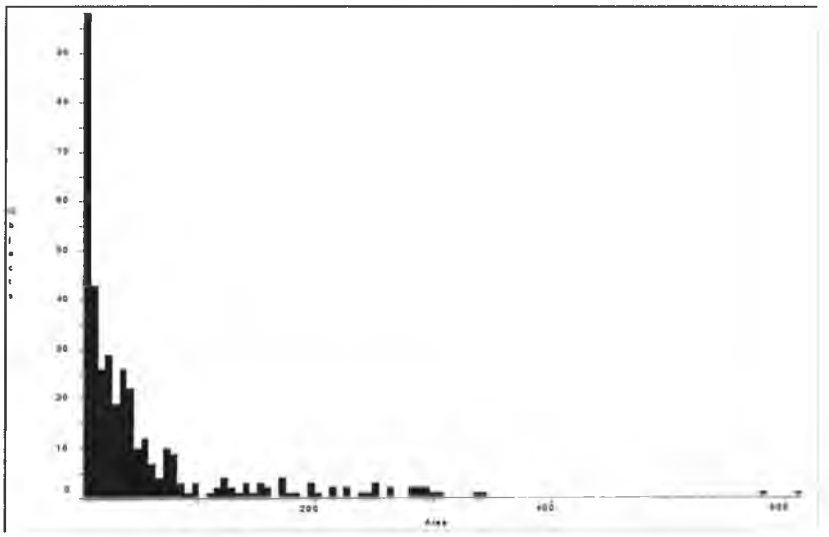

Figure 7.8 Distribution of Decane droplet area inside of Cat-Floc 2953 floc at concentration of 500 ppm, for microscopic image 7.2.

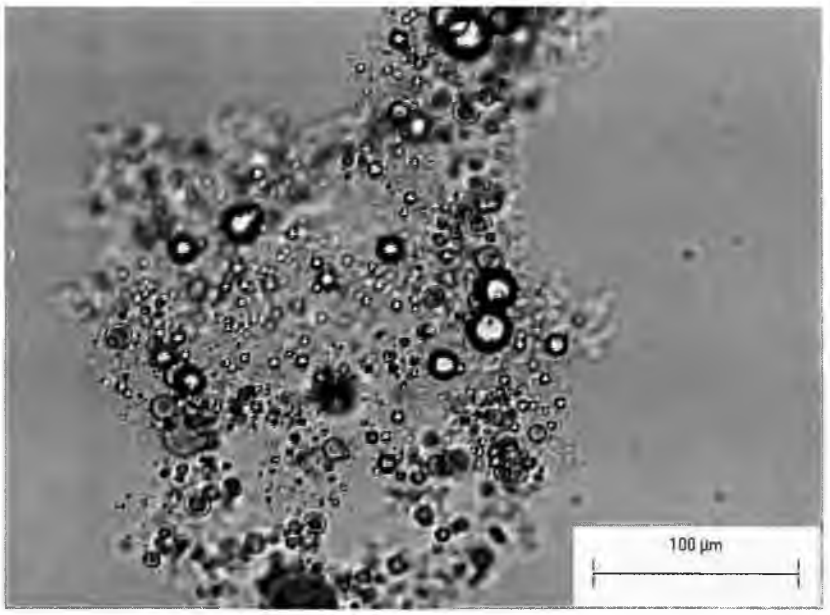

Figure 7.9 Microscopic image of Decane floc at concentration of 500 ppm with EB-5000 at optimum dosage.

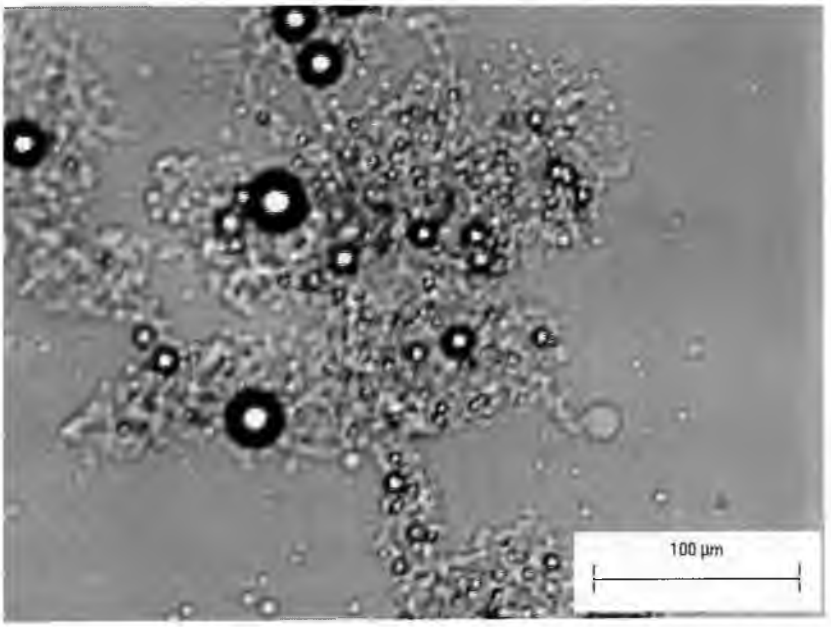

Figure 7.10 Microscopic image of Decane floc at concentration of 500 ppm with EB-5000 at optimum dosage.

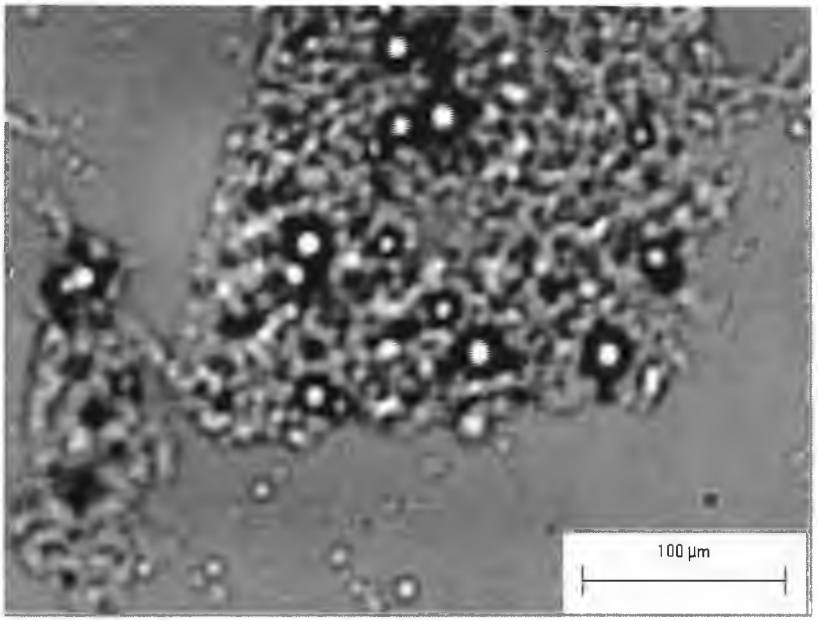

Figure 7.11 Microscopic image of Decane floc at concentration of 500 ppm with EB-5000 at optimum dosage.

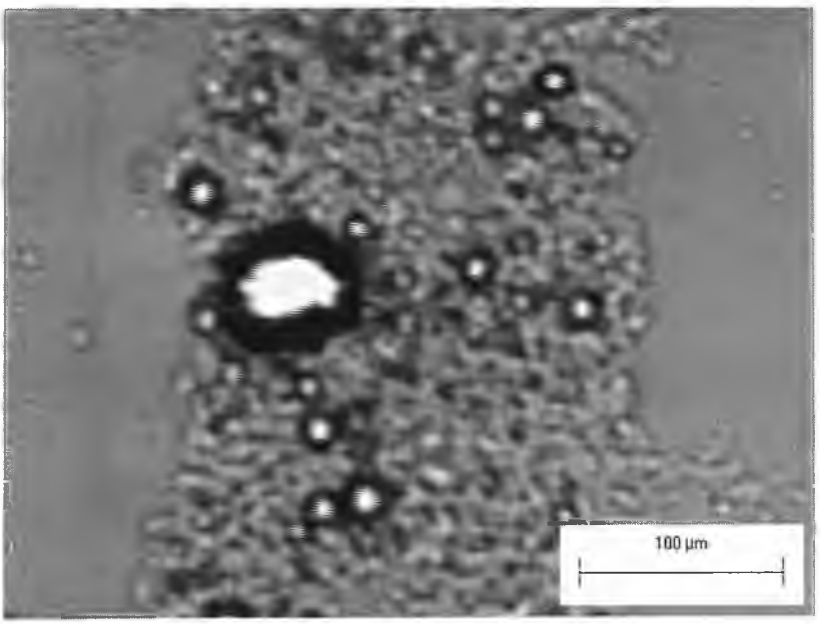

Figure 7.12 Microscopic image of Decane floc at concentration of 500 ppm with EB-5000 at optimum dosage.

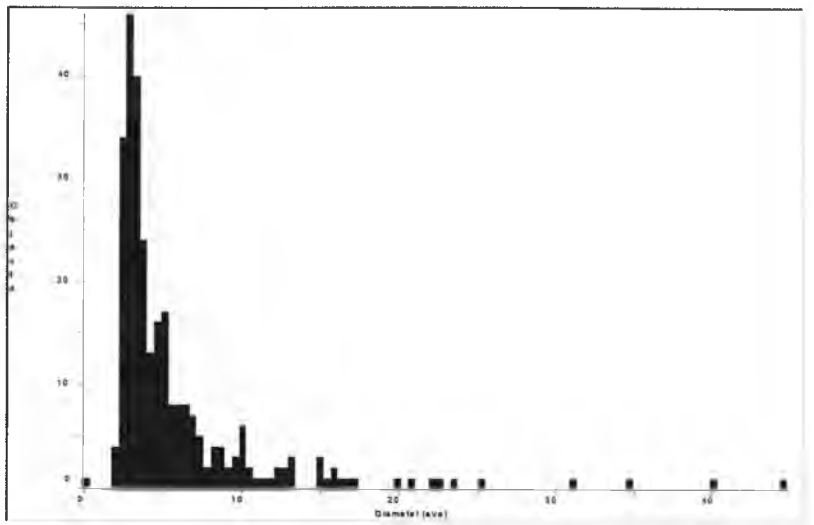

Figure 7.13 Distribution of Decane droplet diameter inside of EB-5000 floc at concentration of 500 ppm, for microscopic image 7.9.

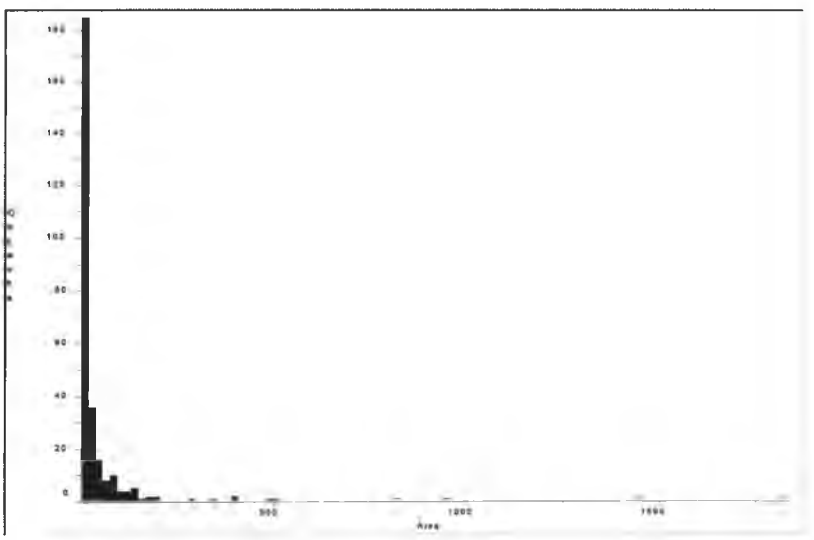

Figure 7.14 Distribution of Decane droplet area inside of EB-5000 floc at concentration of 500 ppm, for microscopic image 7.9.

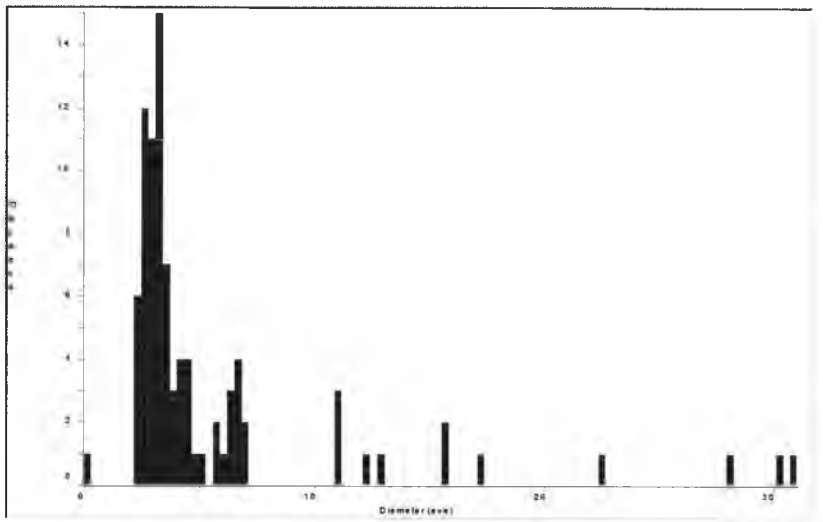

Figure 7.15 Distribution of Decane droplet diameter inside of EB-5000 floc at concentration of 500 ppm, for microscopic image 7.10.

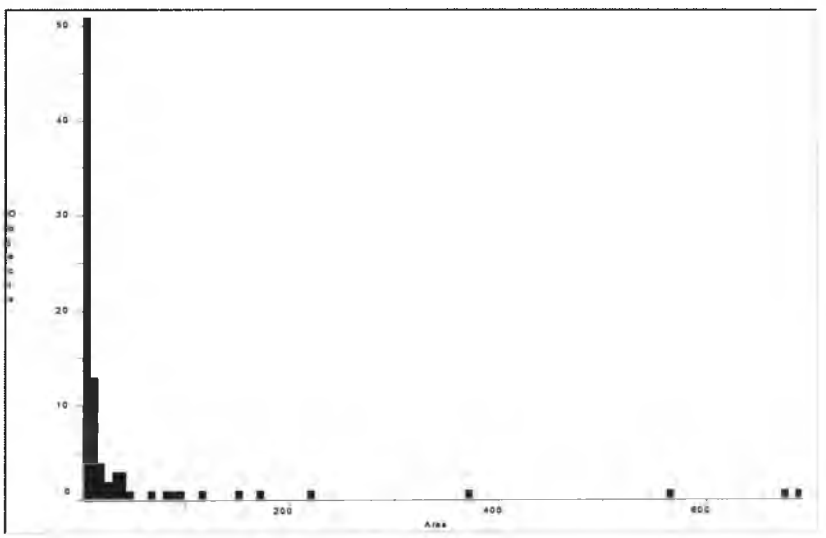

Figure 7.16 Distribution of Decane droplet area inside of EB-5000 floc at concentration of 500 ppm, for microscopic image 7.10.

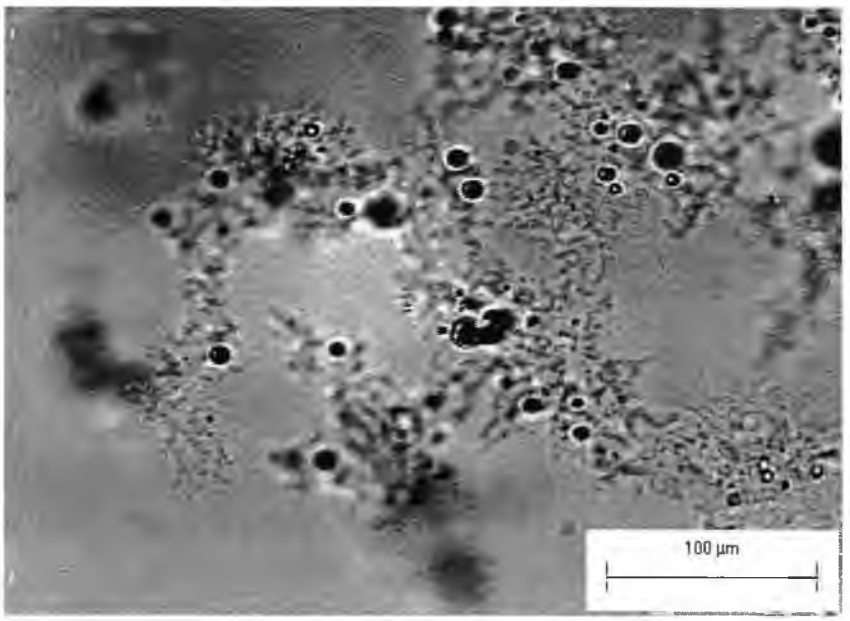

Figure 7.17 Microscopic image of Decane floc at concentration of 300 ppm with Cat-Floc 2953 at optimum dosage.

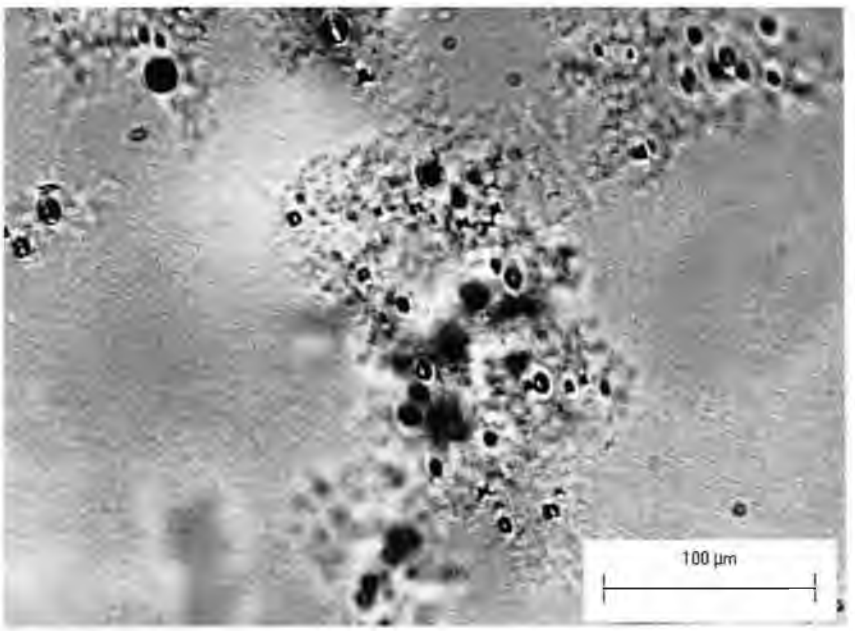

Figure 7.18 Microscopic image of Decane floc at concentration of 300 ppm with Cat-Floc 2953 at optimum dosage.

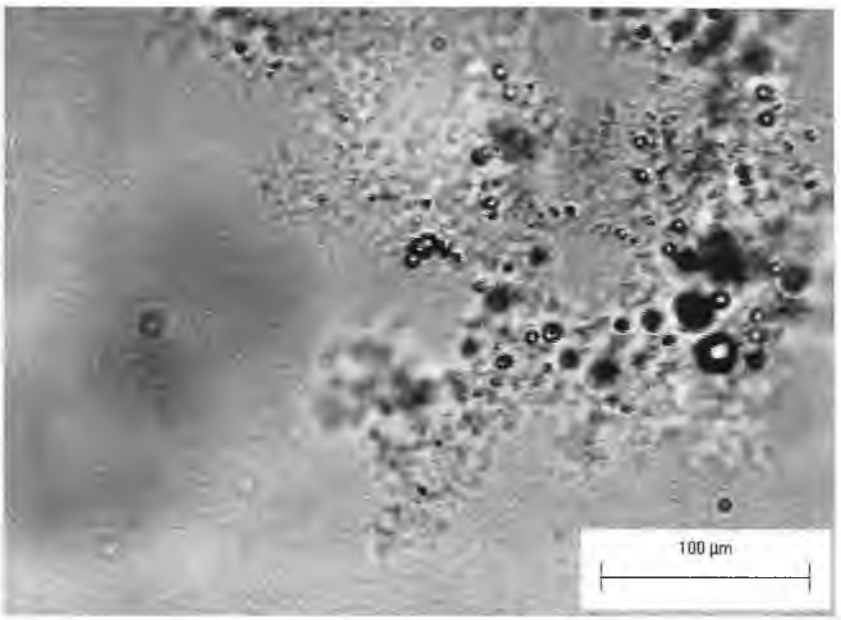

Figure 7.19 Microscopic image of Decane floc at concentration of 300 ppm with Cat-Floc 2953 at optimum dosage.

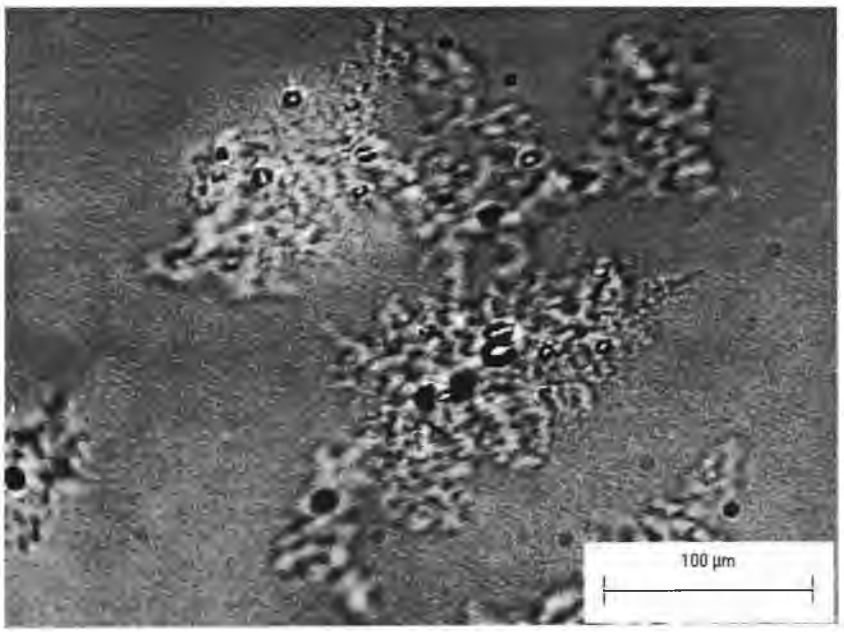

Figure 7.20 Microscopic image of Decane floc at concentration of 300 ppm with Cat-Floc 2953 at optimum dosage.

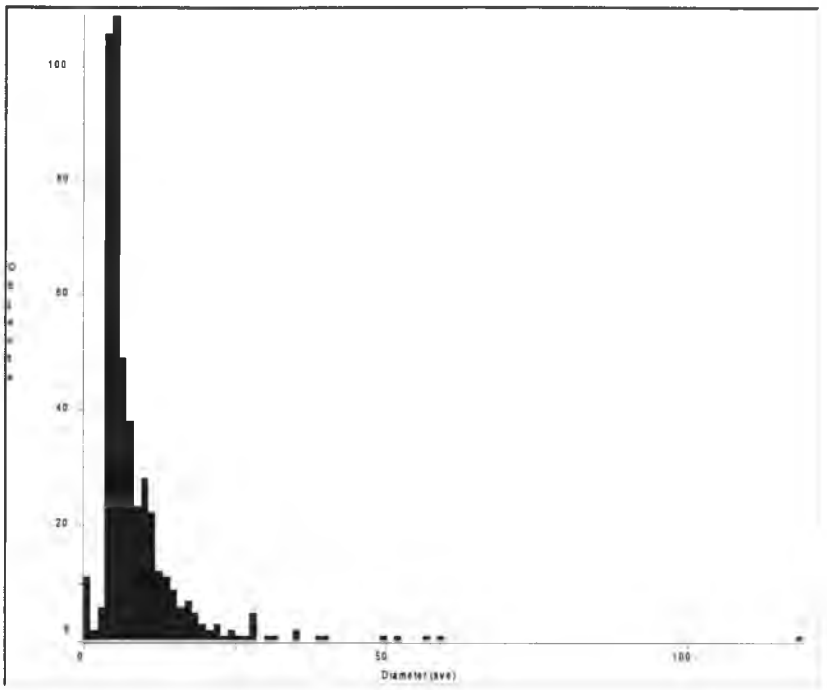

Figure 7.21 Distribution of Decane droplet diameter inside of Cat-Floc 2953 floc at concentration of 300 ppm, for microscopic image 7.17.

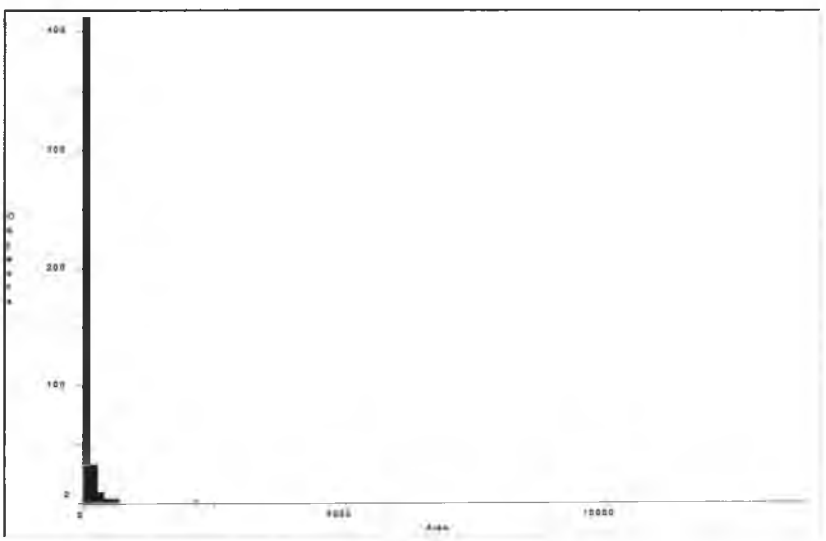

Figure 7.22 Distribution of Decane droplet area inside of Cat-Floc 2953 floc at concentration of 300 ppm, for microscopic image 7.17.

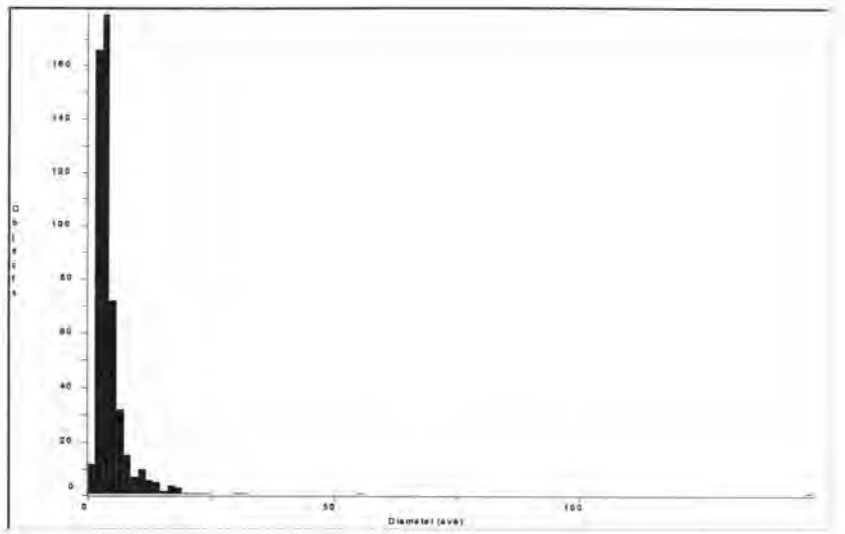

Figure 7.23 Distribution of Decane droplet diameter inside of Cat-Floc 2953 floc at concentration of 300 ppm, for microscopic image 7.18.

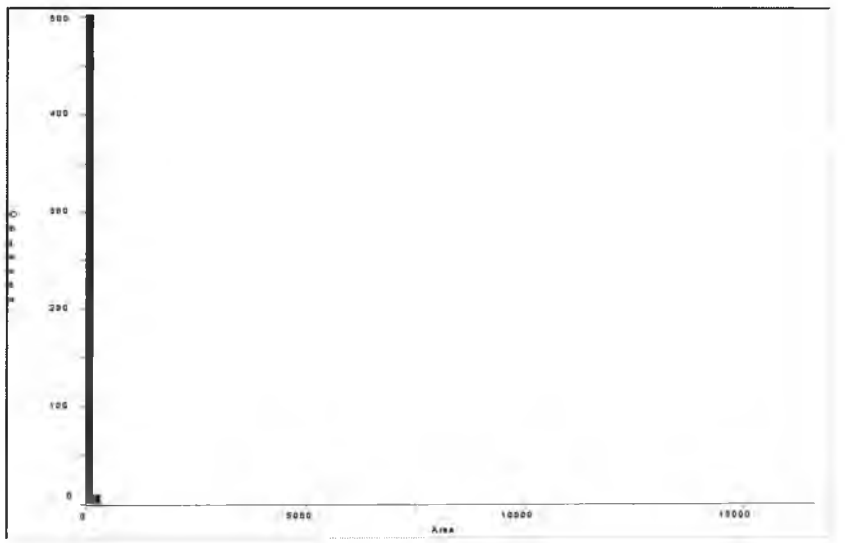

Figure 7.24 Distribution of Decane droplet area inside of Cat-Floc 2953 floc at concentration of 300 ppm, for microscopic image 7.18.

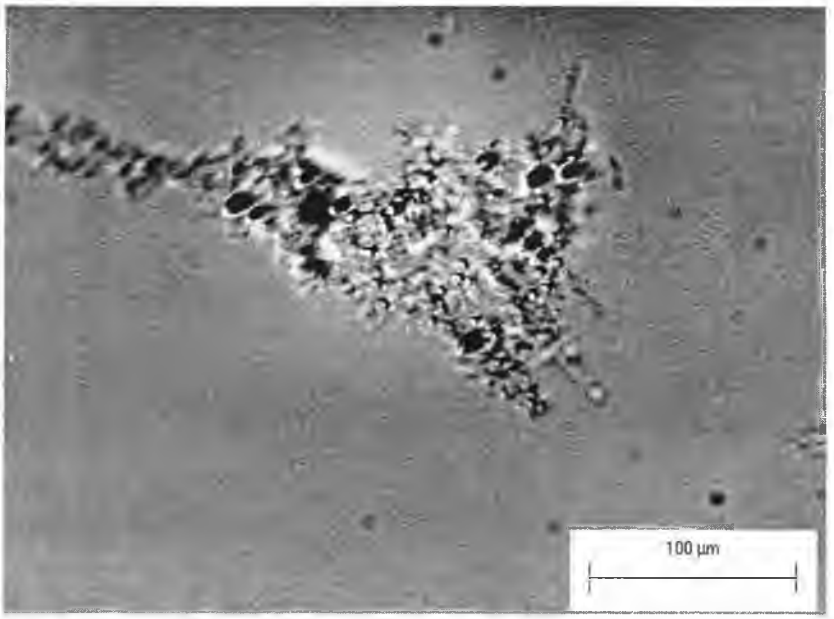

Figure 7.25 Microscopic image of Decane floc at concentration of 300 ppm with EB-5000 at optimum dosage.

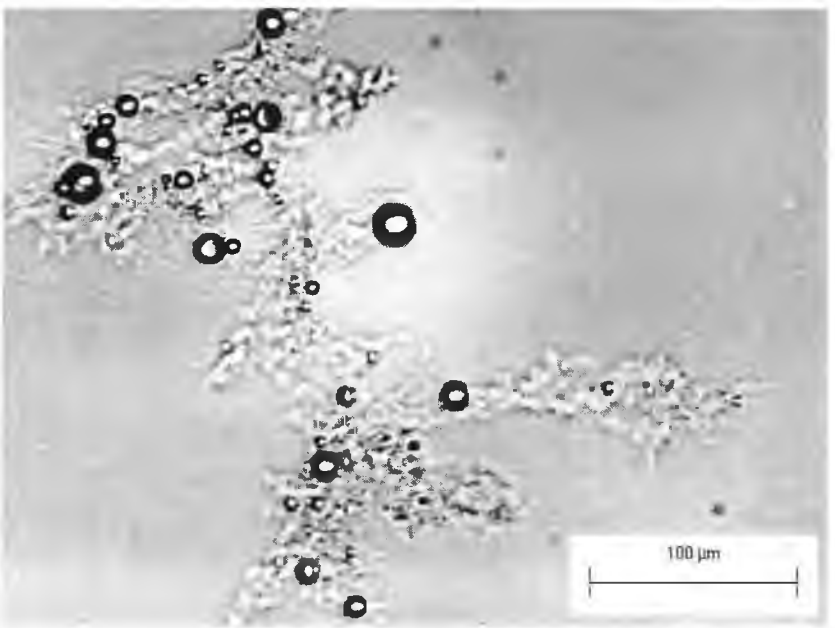

Figure 7.26 Microscopic image of Decane floc at concentration of 300 ppm with EB-5000 at optimum dosage.

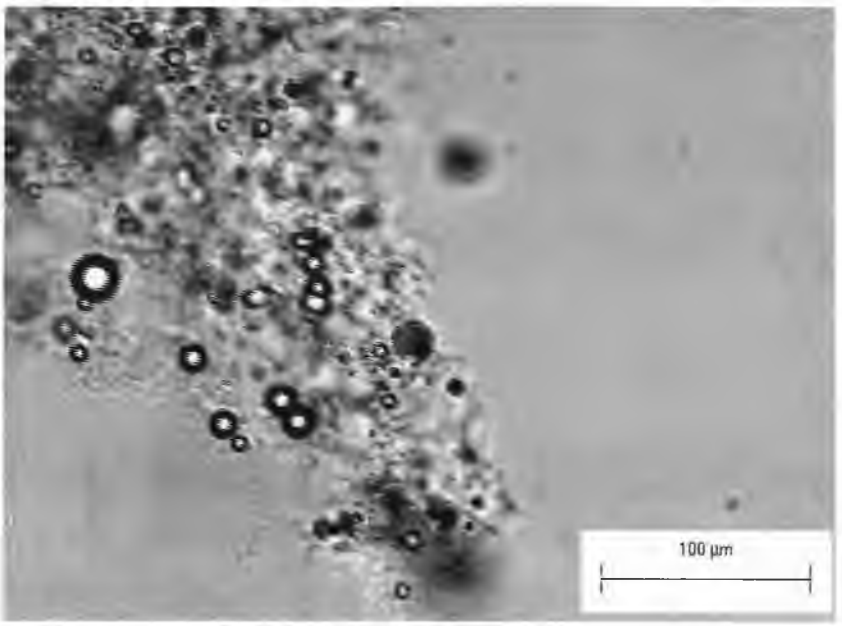

Figure 7.27 Microscopic image of Decane floc at concentration of 300 ppm with EB-5000 at optimum dosage.

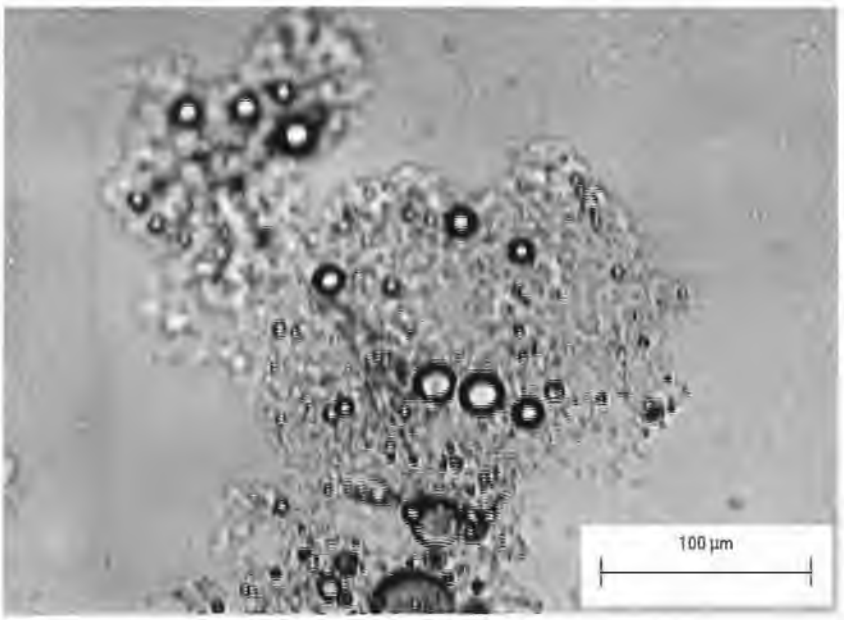

Figure 7.28 Microscopic image of Decane floc at concentration of 300 ppm with EB-5000 at optimum dosage.

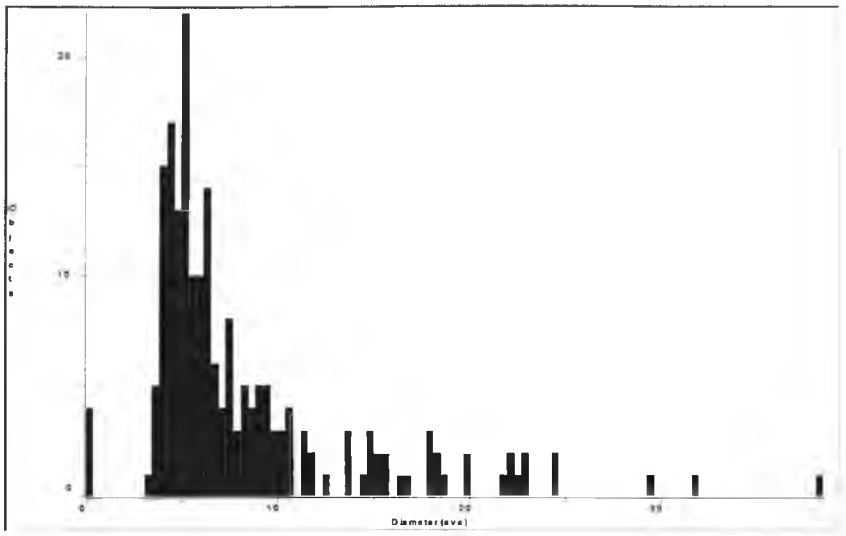

Figure 7.29 Distribution of Decane droplet diameter inside of EB-5000 floc at concentration of 300 ppm, for microscopic image 7.25.

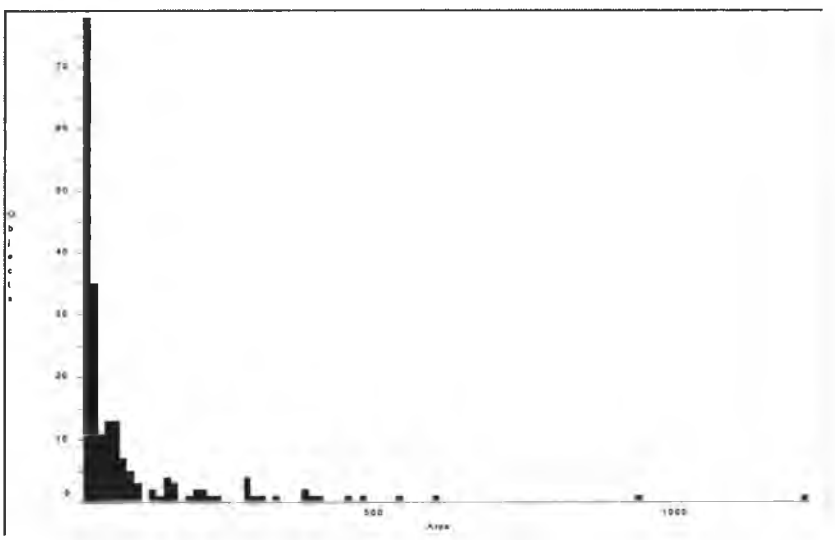

Figure 7.30 Distribution of Decane droplet area inside of EB-5000 floc at concentration of 300 ppm, for microscopic image 7.25.

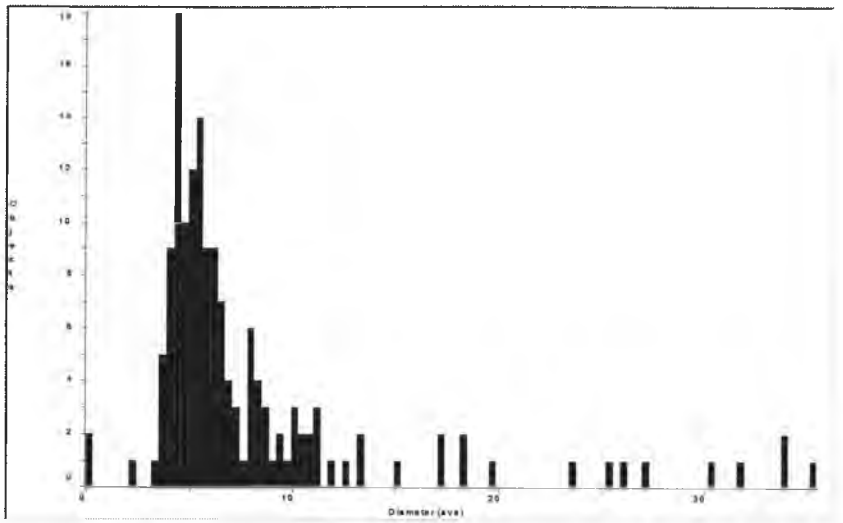

Figure 7.31 Distribution of Decane droplet diameter inside of EB-5000 floc at concentration of 300 ppm, for microscopic image 7.26.

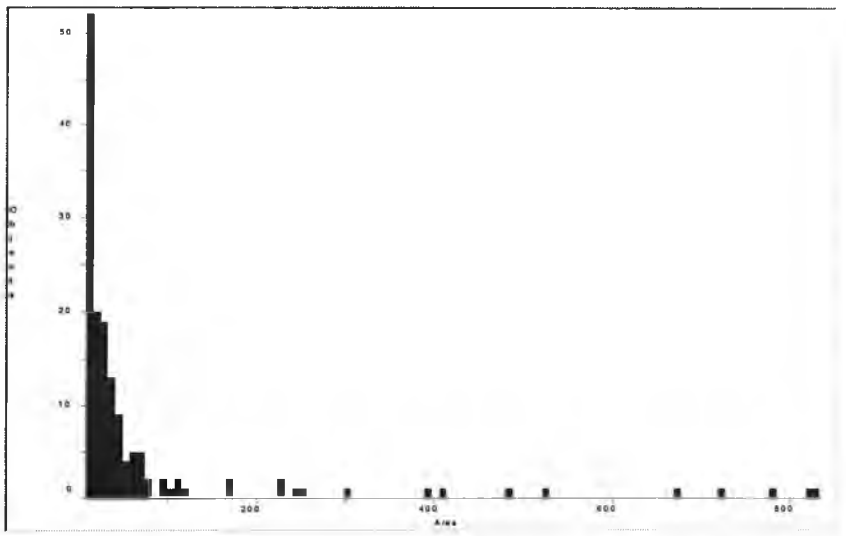

Figure 7.32 Distribution of Decane droplet area inside of EB-5000 floc at concentration of 300 ppm, for microscopic image 7.26.

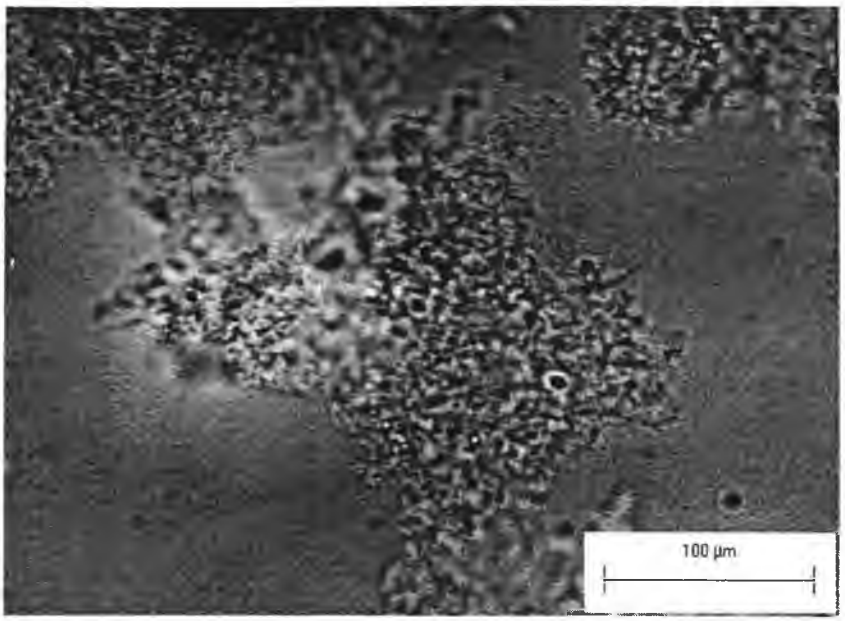

Figure 7.33 Microscopic image of Toluene floc at concentration 500 ppm with Cat-Floc 2952 at optimum dosage.

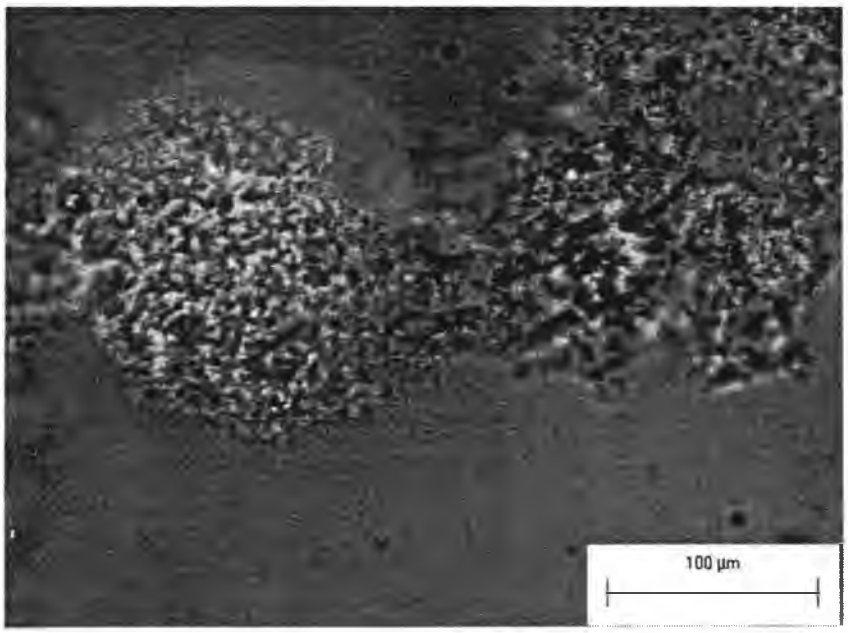

Figure 7.34 Microscopic image of Toluene floc at concentration 500 ppm with Cat-Floc 2952 at optimum dosage.

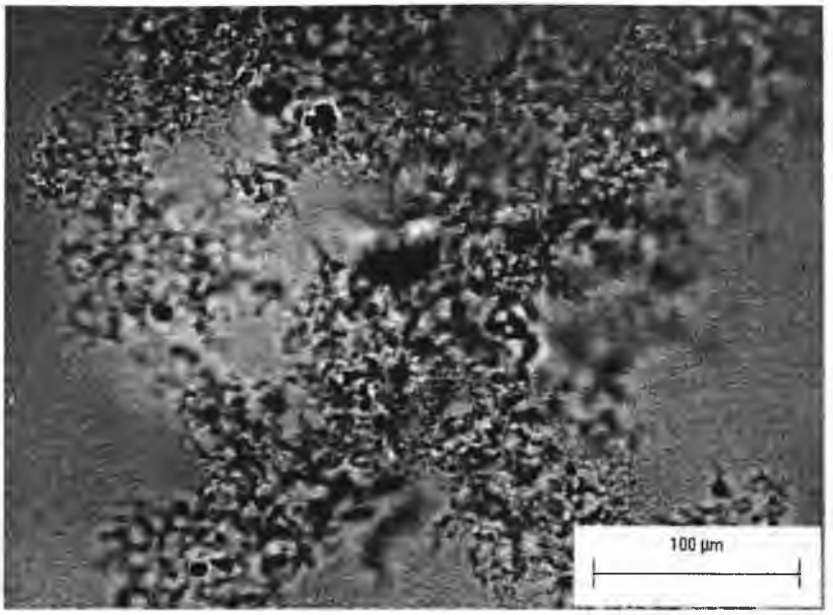

Figure 7.35 Microscopic image of Toluene floc at concentration 500 ppm with Cat-Floc 2952 at optimum dosage.

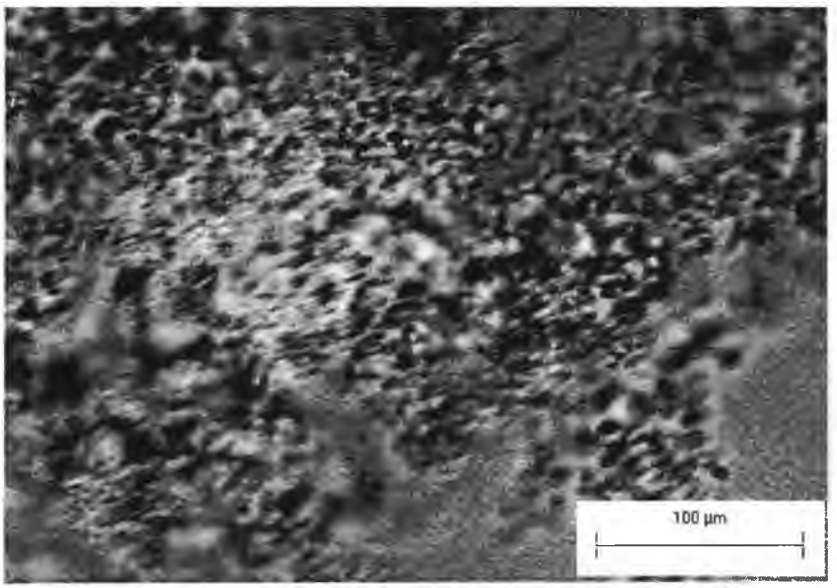

Figure 7.36 Microscopic image of Toluene floc at concentration 500 ppm with Cat-Floc 2952 at optimum dosage.

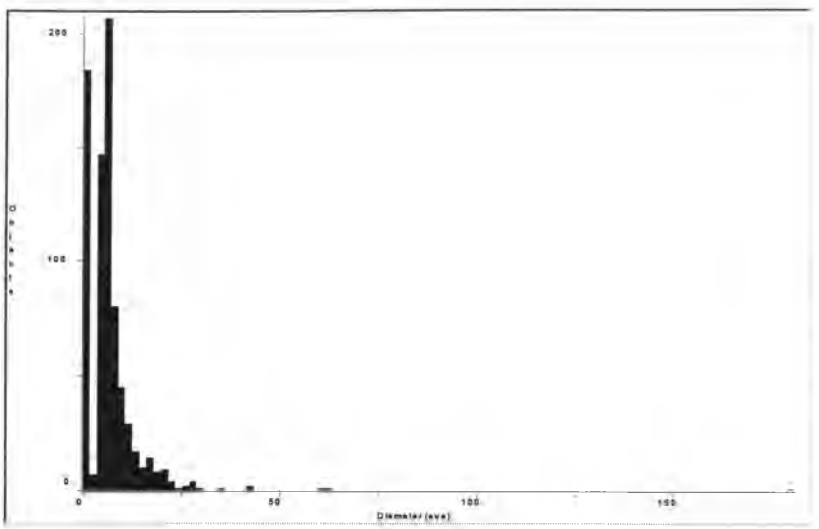

Figure 7.37 Distribution of Toluene droplet diameter inside Cat-Floc 2953 at concentration of 500 ppm, for microscopic image 7.33.

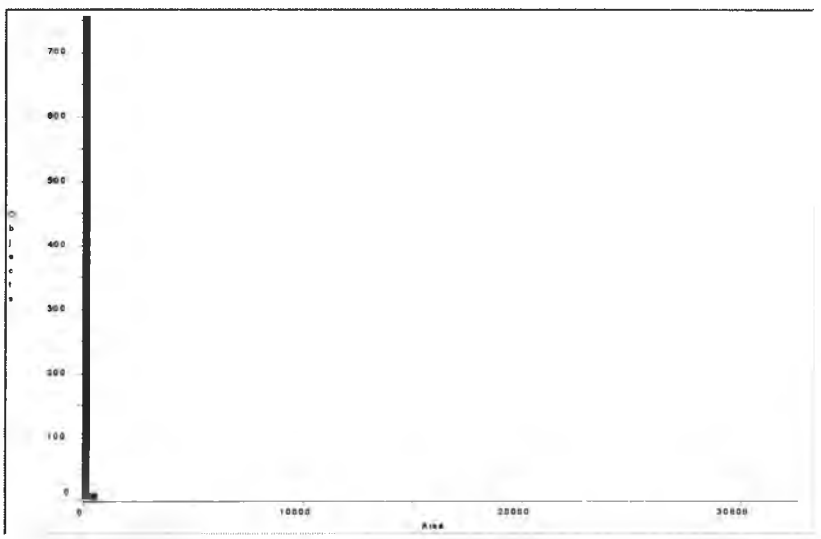

Figure 7.38 Distribution of Toluene droplet area inside Cat-Floc 2953 at concentration of 500 ppm, for microscopic image 7.33.

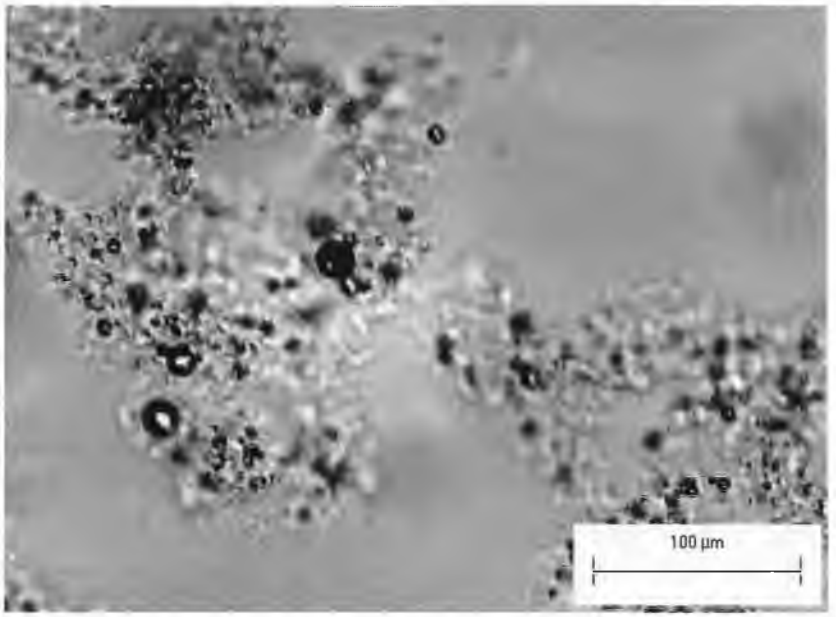

Figure 7.39 Microscopic image of Toluene floc at concentration 500 ppm with EB-5000 at optimum dosage.

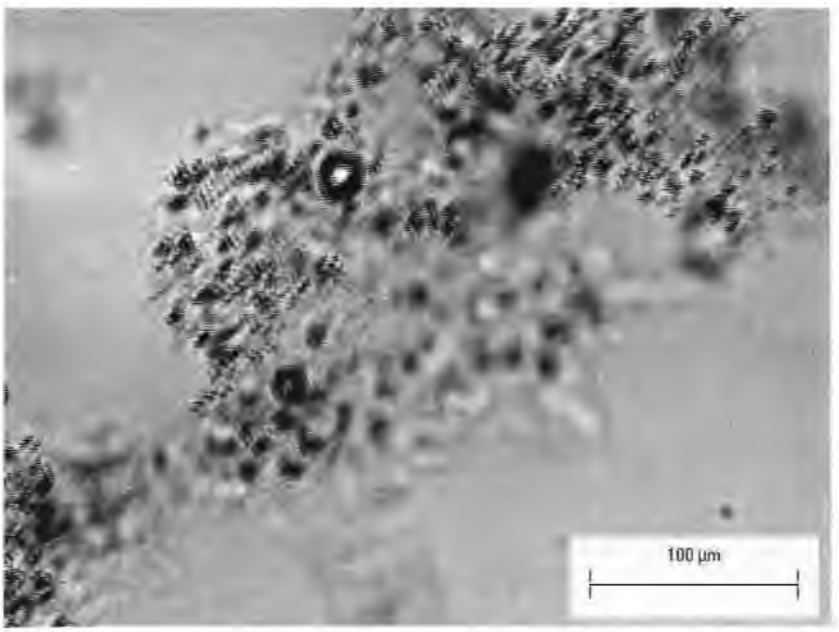

Figure 7.40 Microscopic image of Toluene floc at concentration 500 ppm with EB-5000 at optimum dosage.

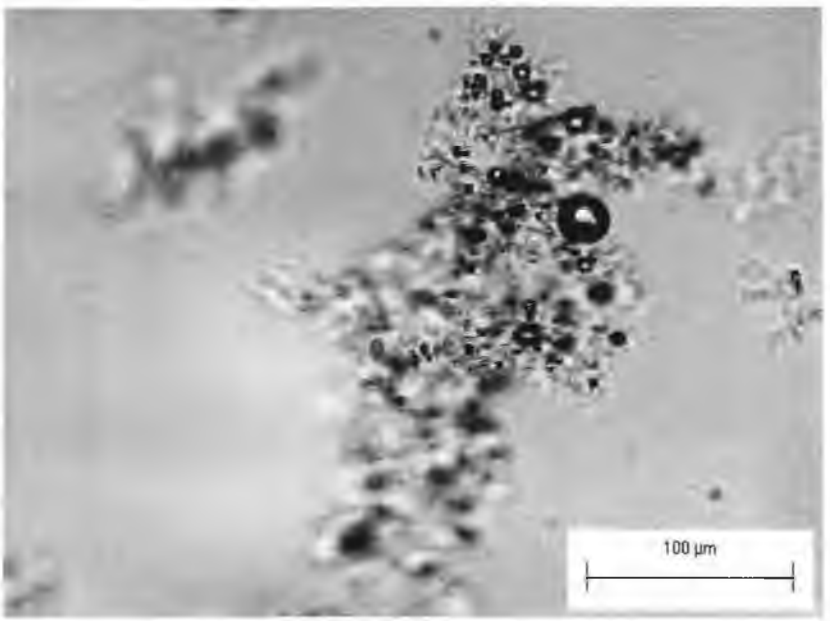

Figure 7.41 Microscopic image of Toluene floc at concentration 500 ppm with EB-5000 at optimum dosage.

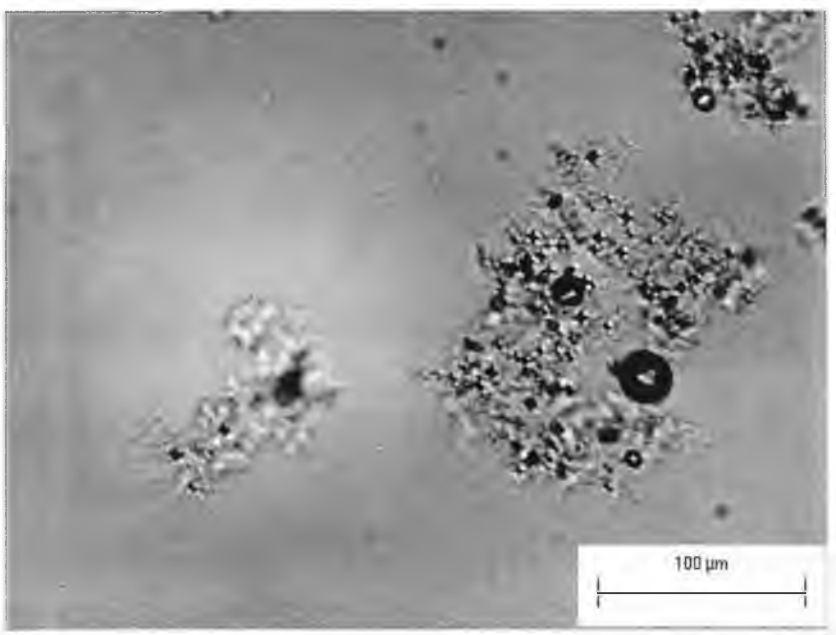

Figure 7.42 Microscopic image of Toluene floc at concentration 500 ppm with EB-5000 at optimum dosage.

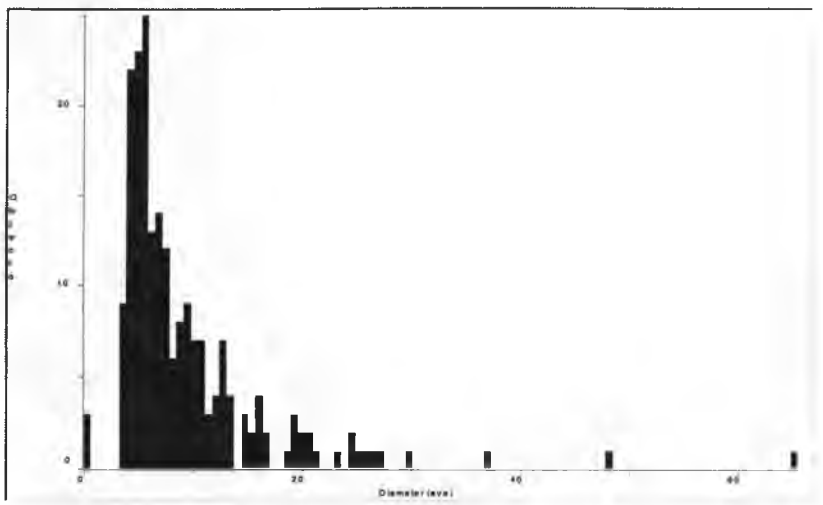

Figure 7.43 Distribution of Toluene droplet diameter insideEB-5000 at concentration of 500 ppm, for microscopic image 7.39.

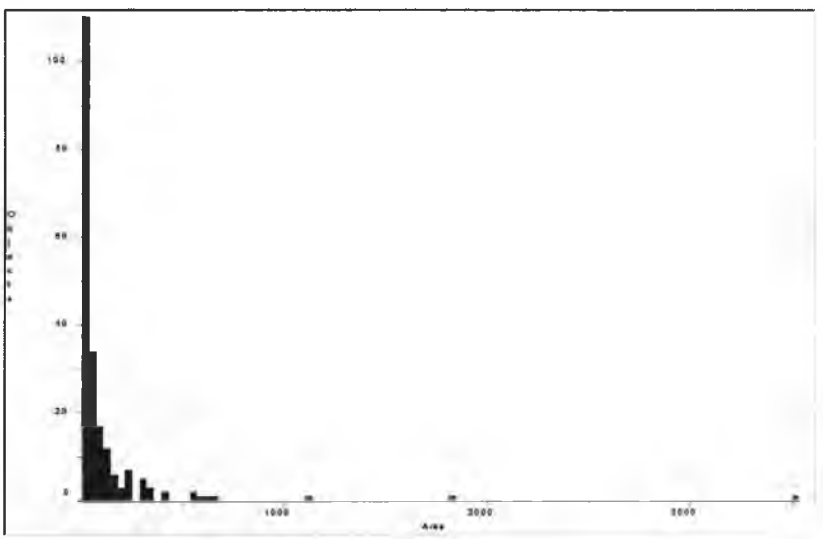

Figure 7.44 Distribution of Toluene droplet area insideEB-5000 at concentration of 500 ppm, for microscopic image 7.39.

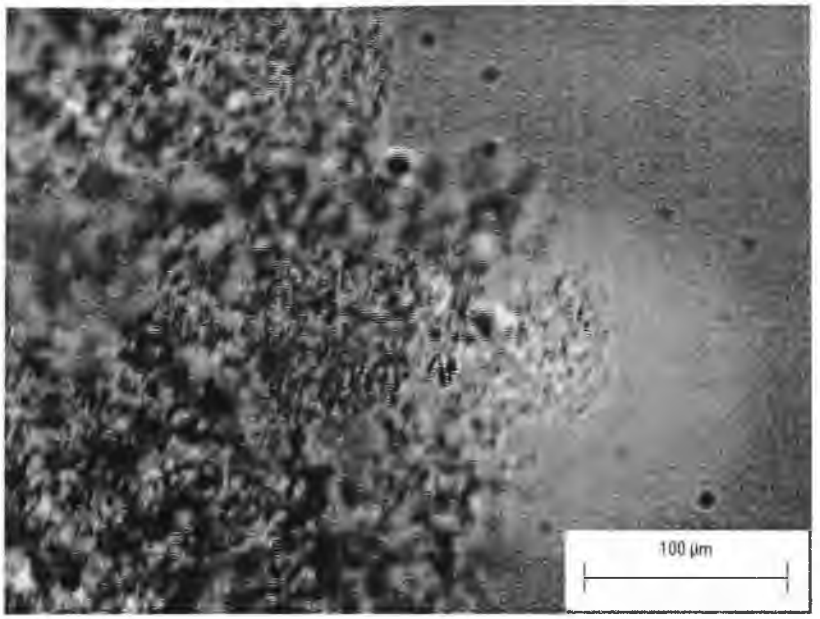

Figure 7.45 Microscopic image of Toluene floc at concentration 300 ppm with Cat-Floc 2953 at optimum dosage.

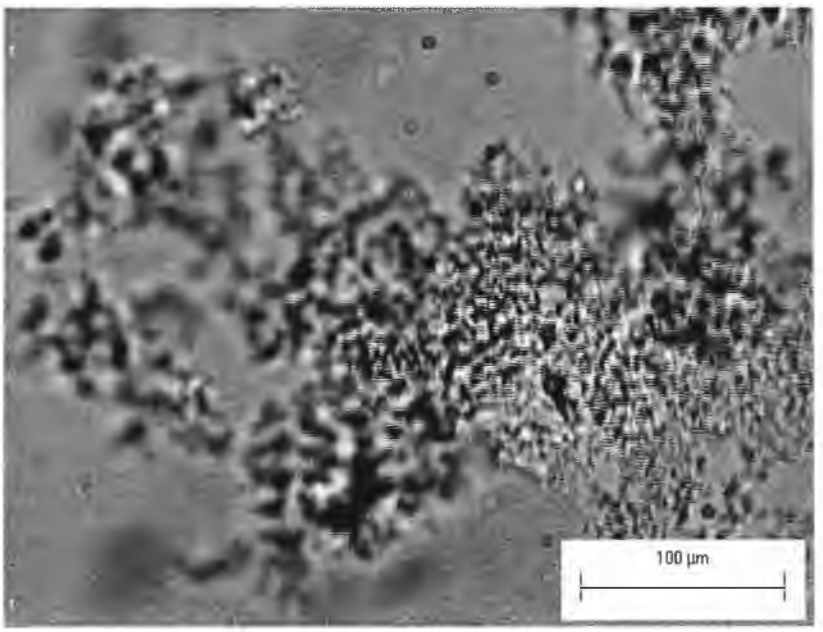

Figure 7.46 Microscopic image of Toluene floc at concentration 300 ppm with Cat-Floc 2953 at optimum dosage.

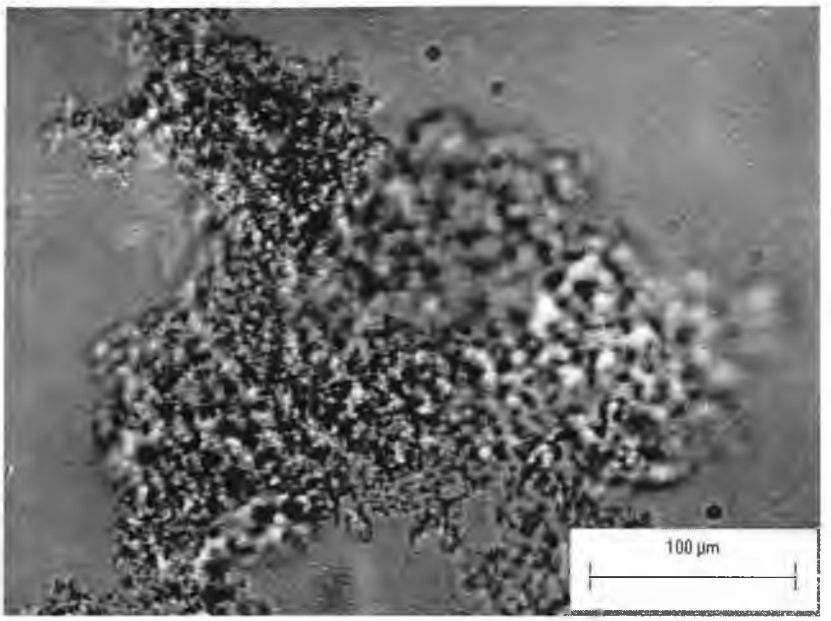

Figure 7.47 Microscopic image of Toluene floc at concentration 300 ppm with Cat-Floc 2953 at optimum dosage.

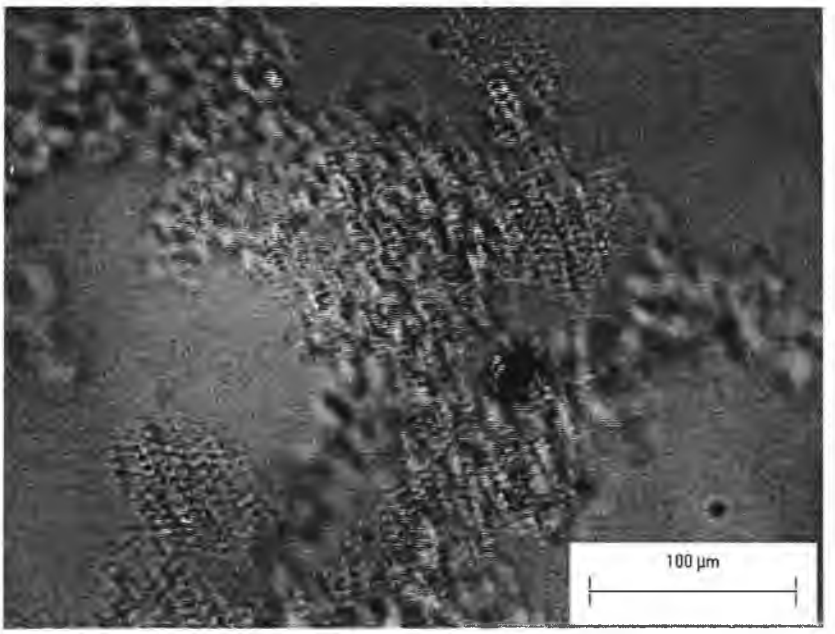

Figure 7.48 Microscopic image of Toluene floc at concentration 300 ppm with Cat-Floc 2953 at optimum dosage.

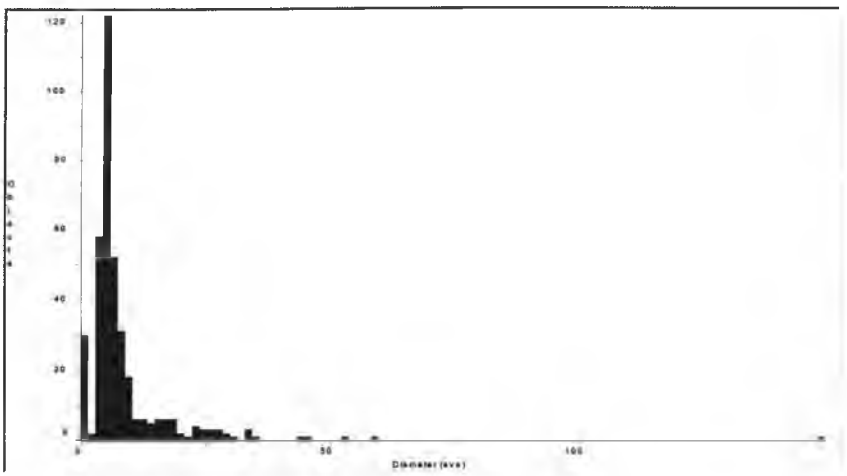

Figure 7.49 Distribution of Toluene droplet diameter inside Cat-Floc 2953 at concentration of 300 ppm, for microscopic image 7.45.

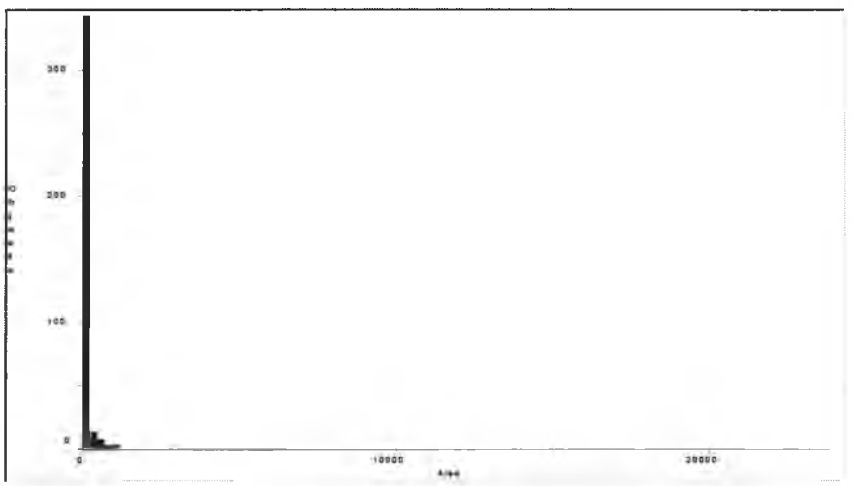

Figure 7.50 Distribution of Toluene droplet area inside Cat-Floc 2953 at concentration of 300 ppm, for microscopic image 7.45.

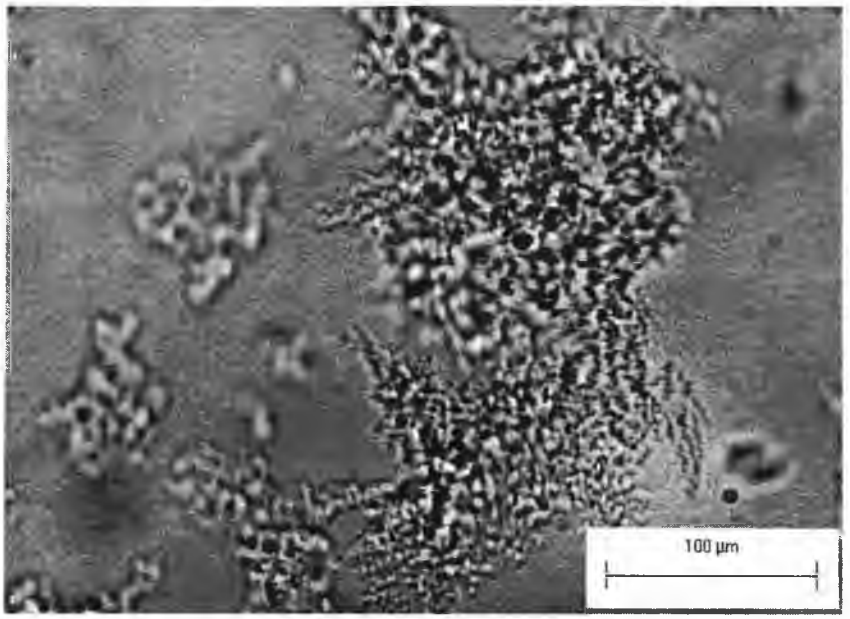

Figure 7.51 Microscopic image of Toluene floc at concentration 300 ppm with EB-5000 at optimum dosage.

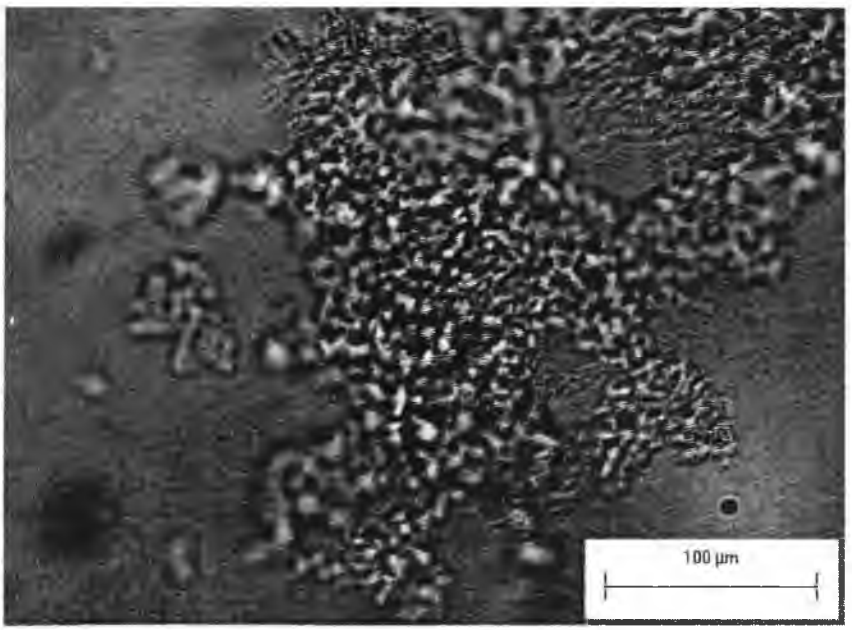

Figure 7.52 Microscopic image of Toluene floc at concentration 300 ppm with EB-5000 at optimum dosage.

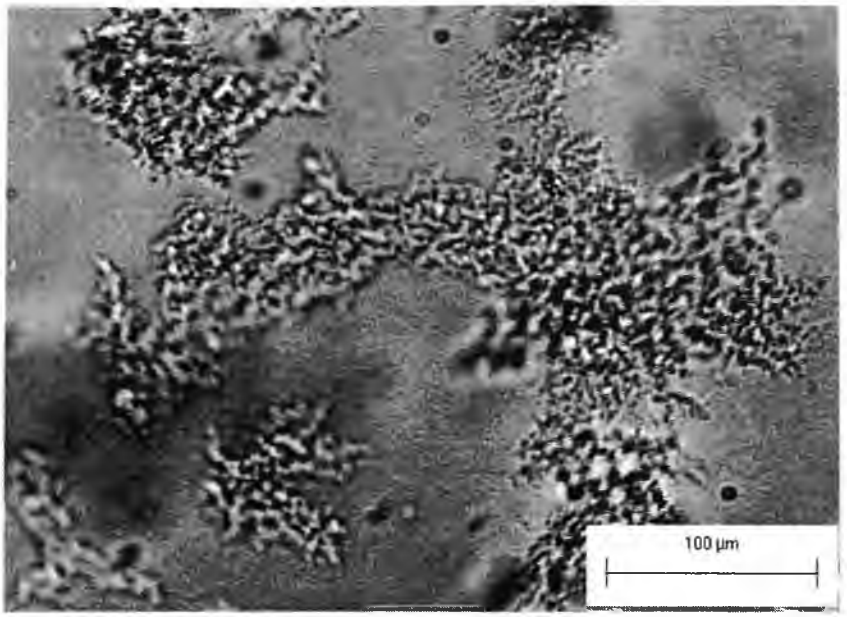

Figure 7.53 Microscopic image of Toluene floc at concentration 300 ppm with EB-5000 at optimum dosage.

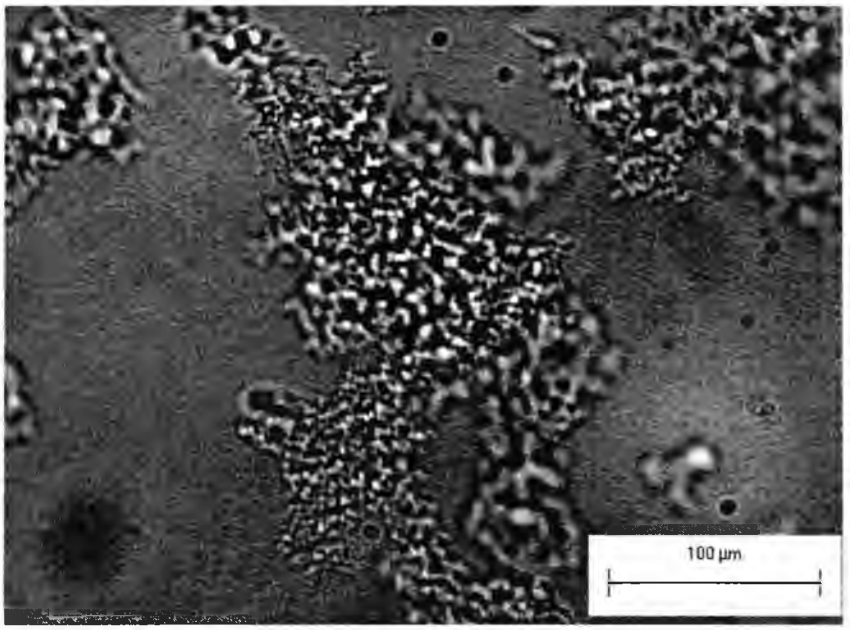

Figure 7.54 Microscopic image of Toluene floc at concentration 300 ppm with EB-5000 at optimum dosage.

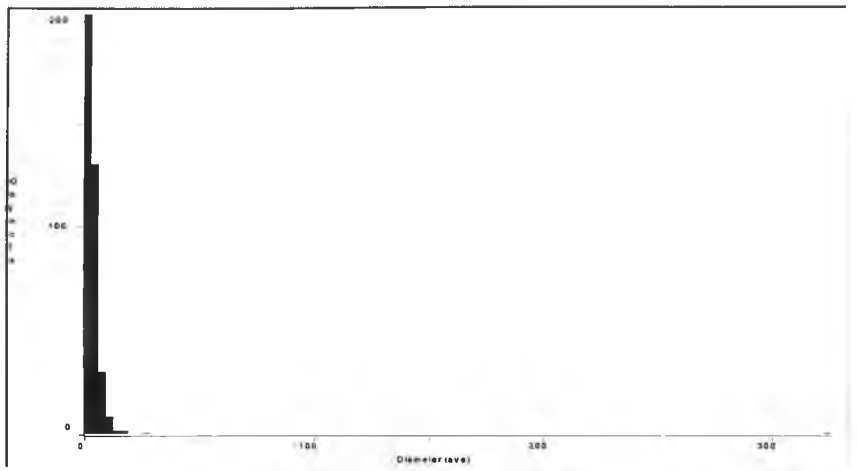

Figure 7.55 Distribution of Toluene droplet diameter inside EB-5000 at concentration of 300 ppm, for microscopic image 7.51.

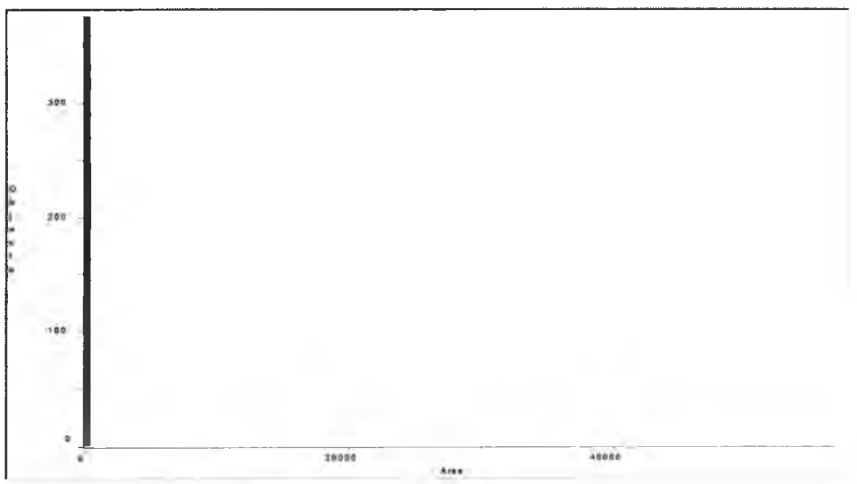

Figure 7.56 Distribution of Toluene droplet area inside EB-5000 at concentration of 300 ppm, for microscopic image 7.51.

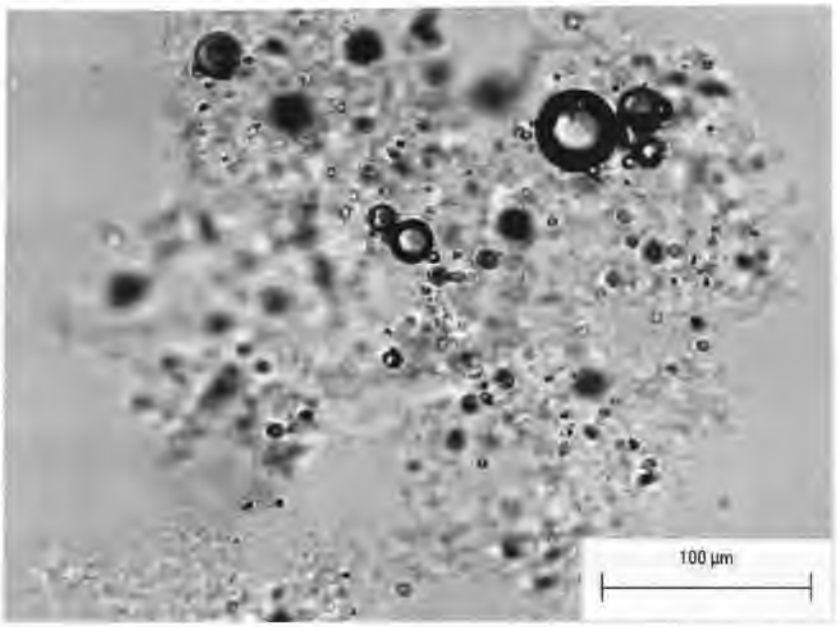

Figure 7.57 Microscopic image of m-xylene floc at concentration of 500 ppm with Cat-Floc 2953 at optimum dosage.

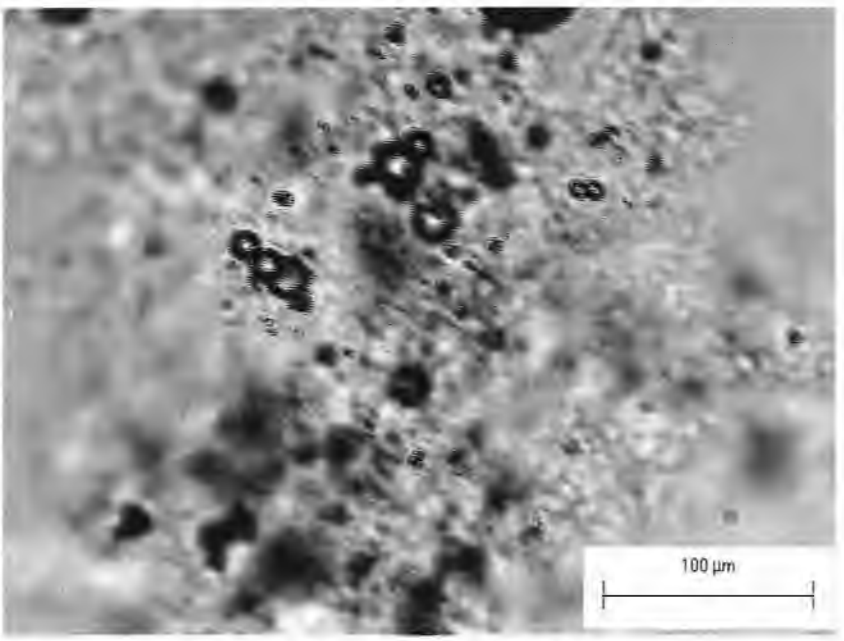

Figure 7.58 Microscopic image of m-xylene floc at concentration of 500 ppm with Cat-Floc 2953 at optimum dosage.

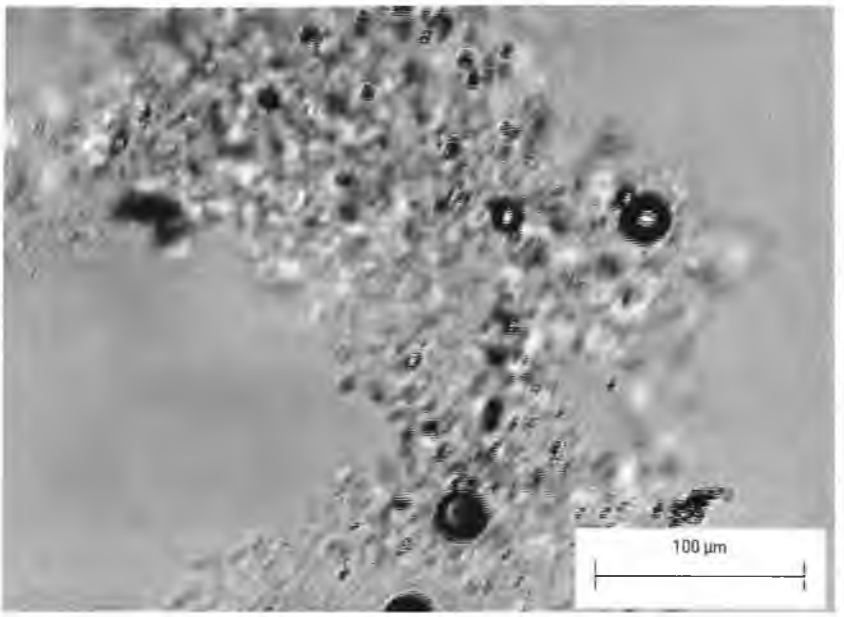

Figure 7.59 Microscopic image of m-xylene floc at concentration of 500 ppm with Cat-Floc 2953 at optimum dosage.

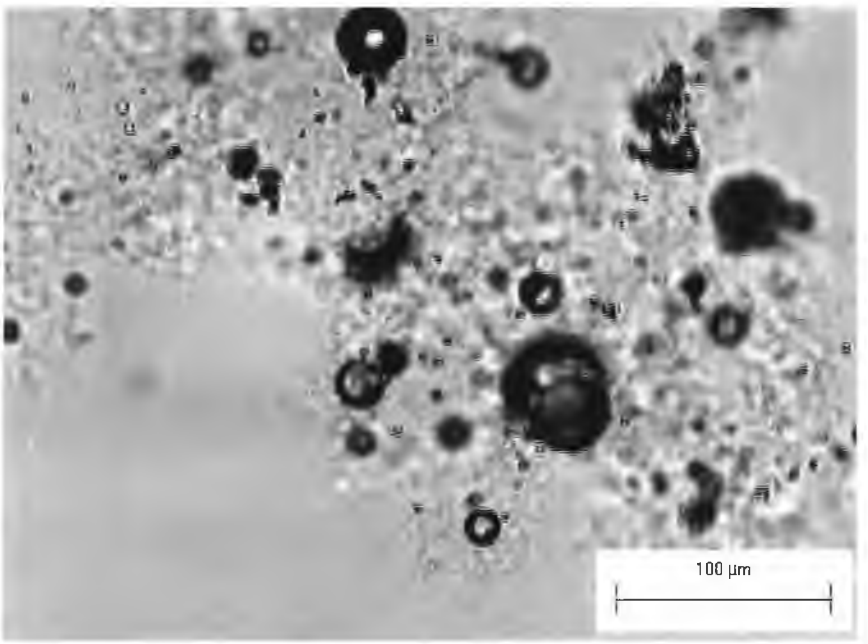

Figure 7.60 Microscopic image of m-xylene floc at concentration of 500 ppm with Cat-Floc 2953 at optimum dosage.

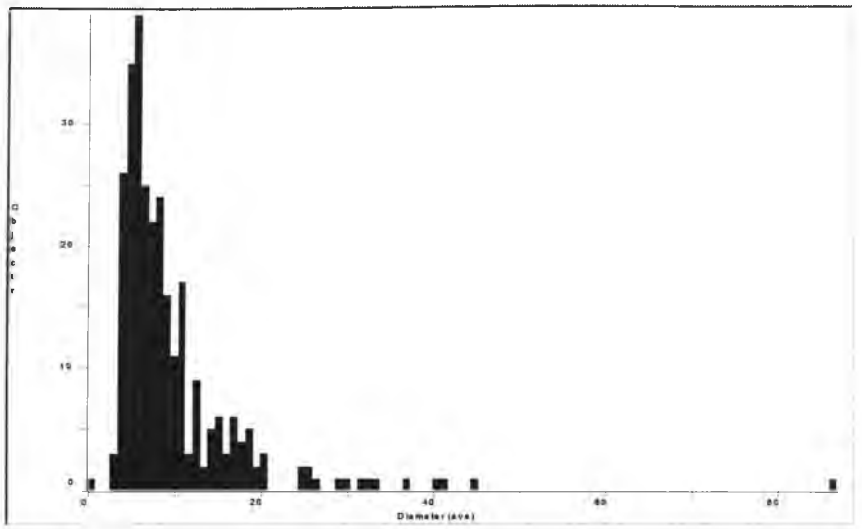

Figure 7.61 Distribution of m-xylene droplet diameter inside of Cat-Floc 2953 floc at concentration of 500 ppm, for microscopic image 7.57.

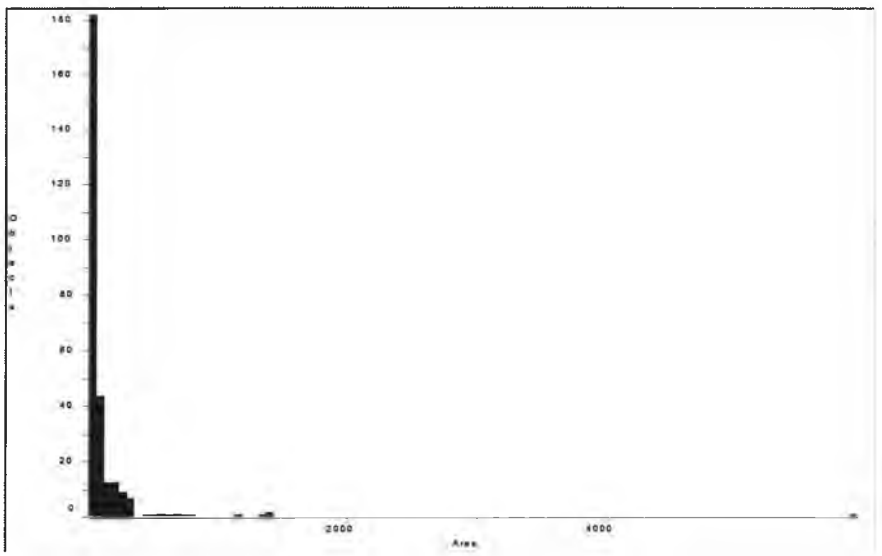

Figure 7.62 Distribution of m-xylene droplet area inside of Cat-Floc 2953 floc at concentration of 500 ppm, for micrscopic image 7.57.

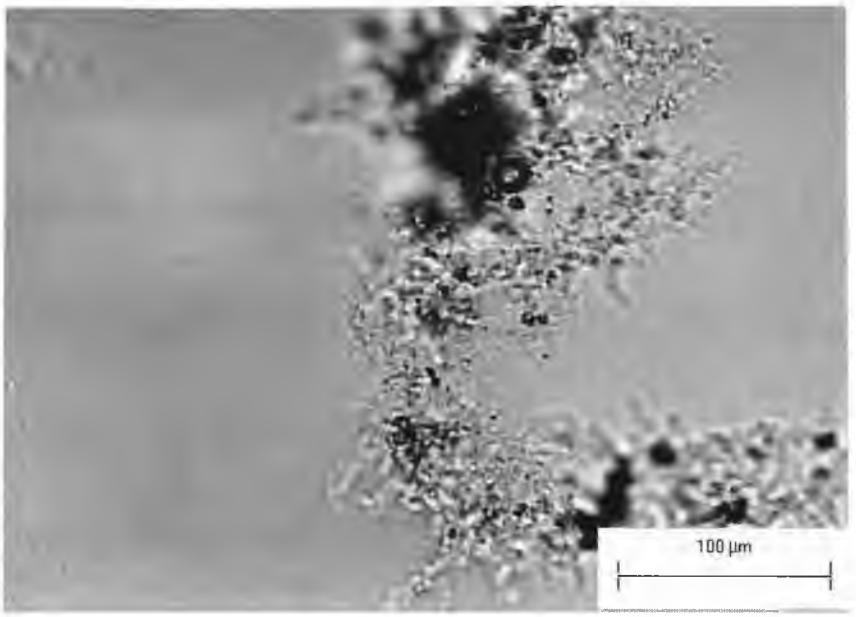

Figure 7.63 Microscopic image of m-xylene floc at concentration of 500 ppm with EB-5000 at optimum dosage.

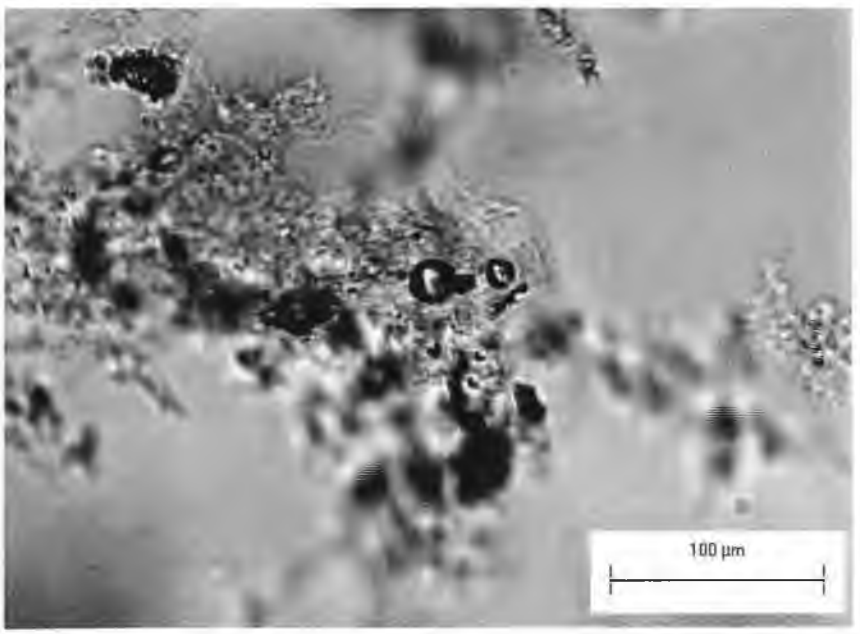

Figure 7.64 Microscopic image of m-xylene floc at concentration of 500 ppm with EB-5000 at optimum dosage.

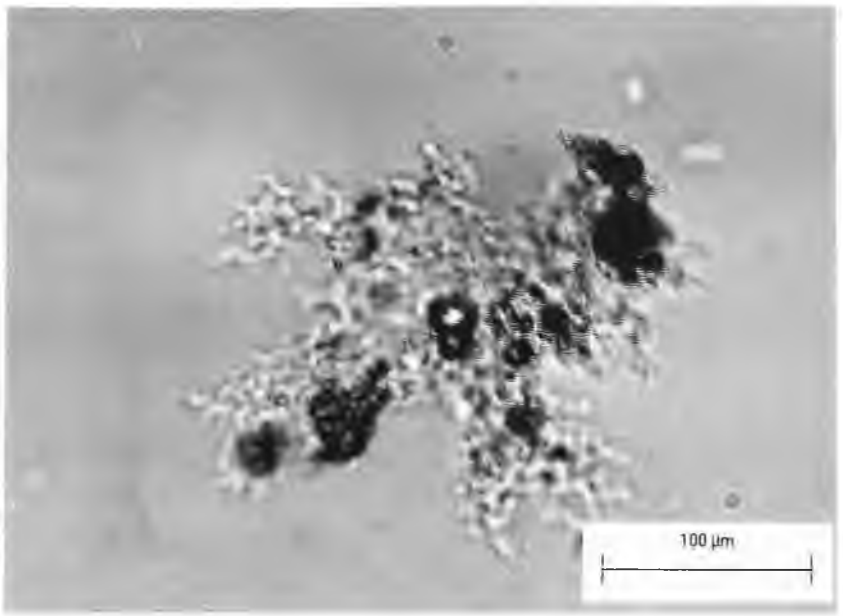

Figure 7.65 Microscopic image of m-xylene floc at concentration of 500 ppm with EB-5000 at optimum dosage.

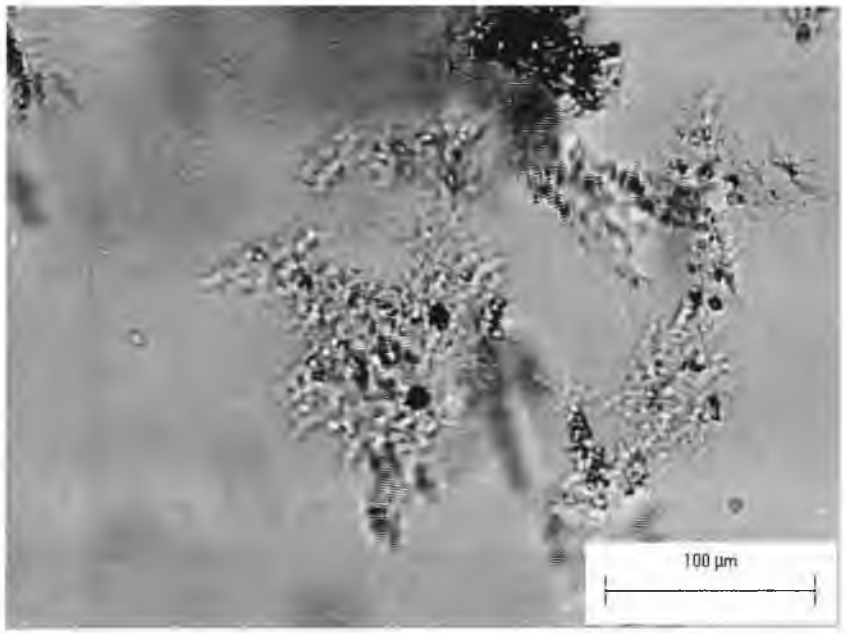

Figure 7.66 Microscopic image of m-xylene floc at concentration of 500 ppm with EB-5000 at optimum dosage.

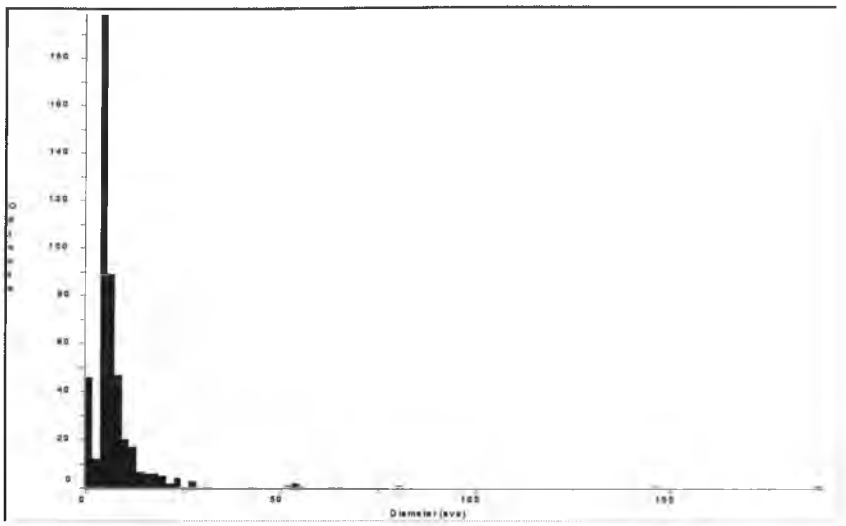

Figure 7.67 Distribution of m-xylene droplet diameter inside of EB-5000 floc at concentration of 500 ppm, for microscopic image 7.63.

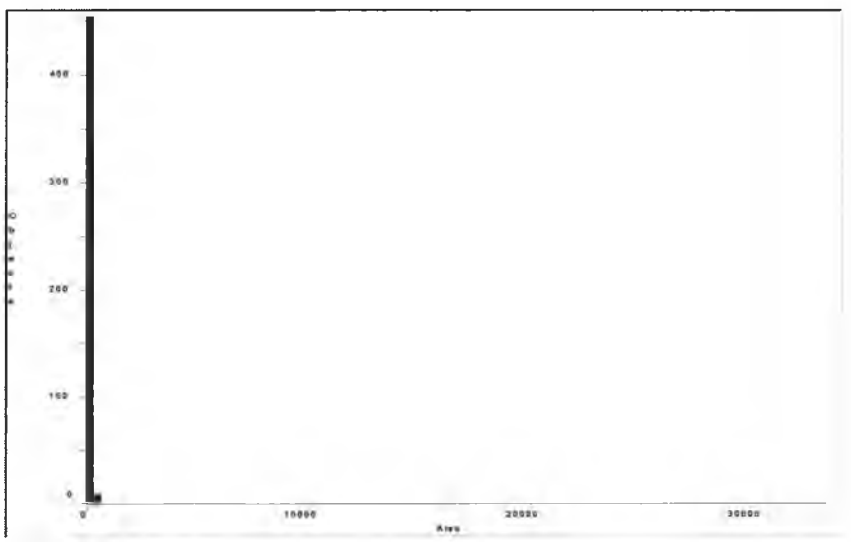

Figure 7.68 Distribution of m-xylene droplet area inside of EB-5000 floc at concentration of 500 ppm, for microscopic image 7.63.

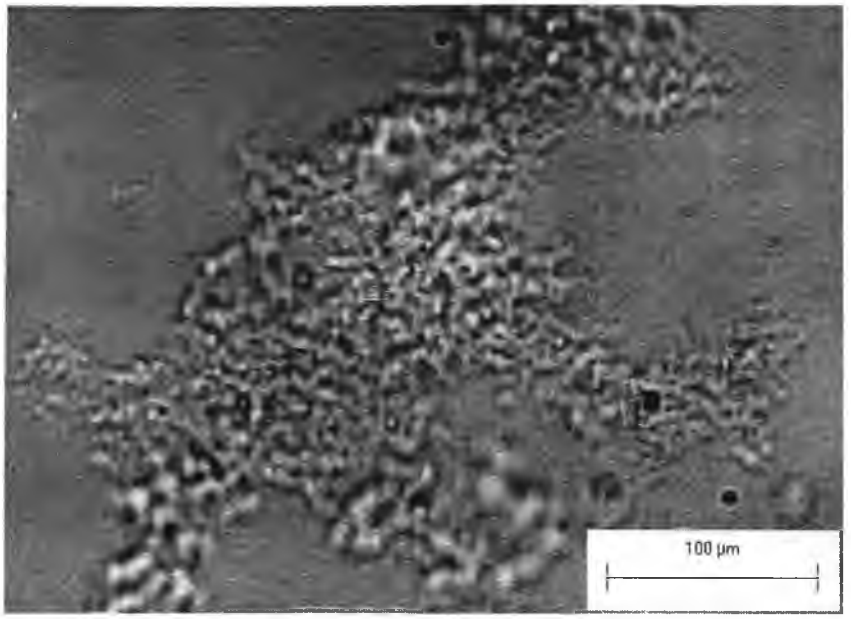

Figure 7.69 Microscopic image of m-xylene floc at concentration of 300 ppm with Cat-Floc at optimum dosage.

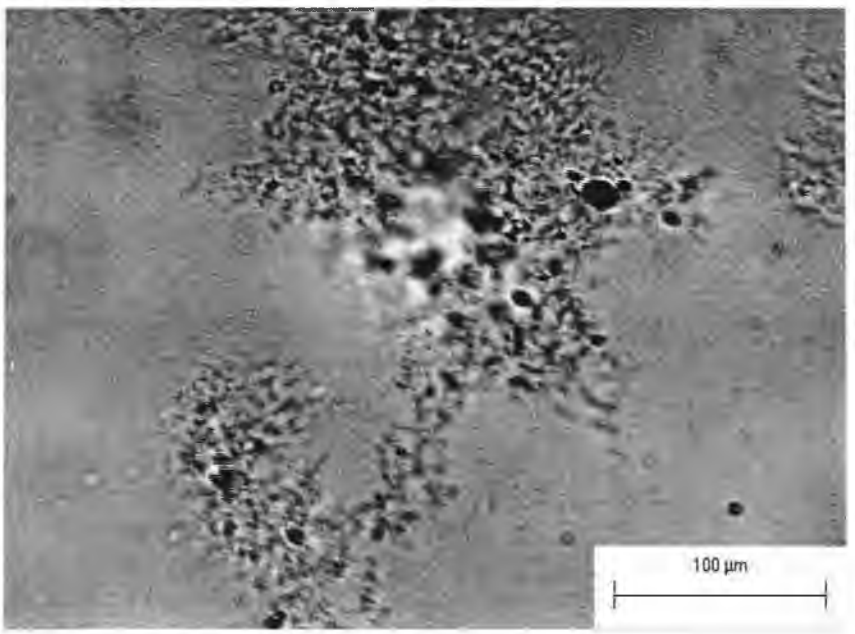

Figure 7.70 Microscopic image of m-xylene floc at concentration of 300 ppm with Cat-Floc at optimum dosage.

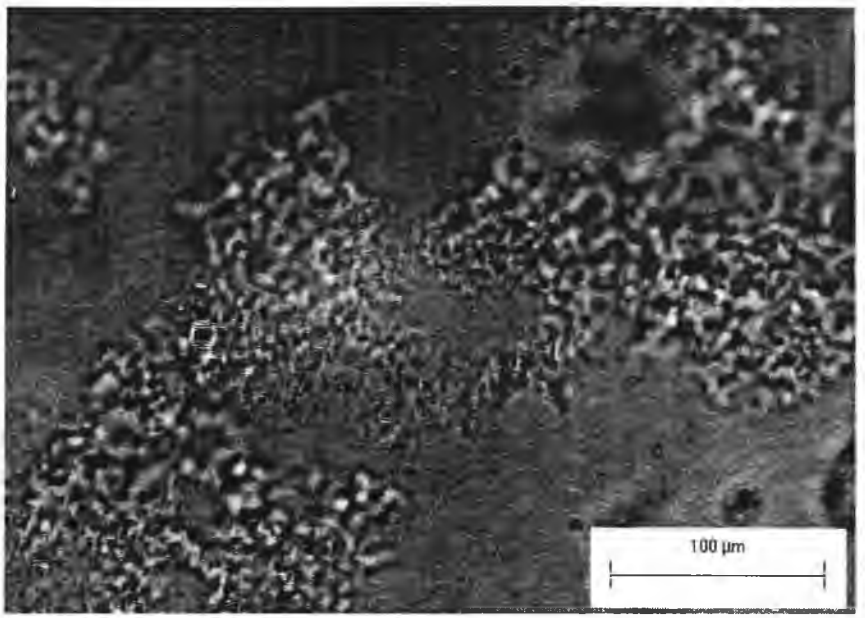

Figure 7.71 Microscopic image of m-xylene floc at concentration of 300 ppm with Cat-Floc at optimum dosage.

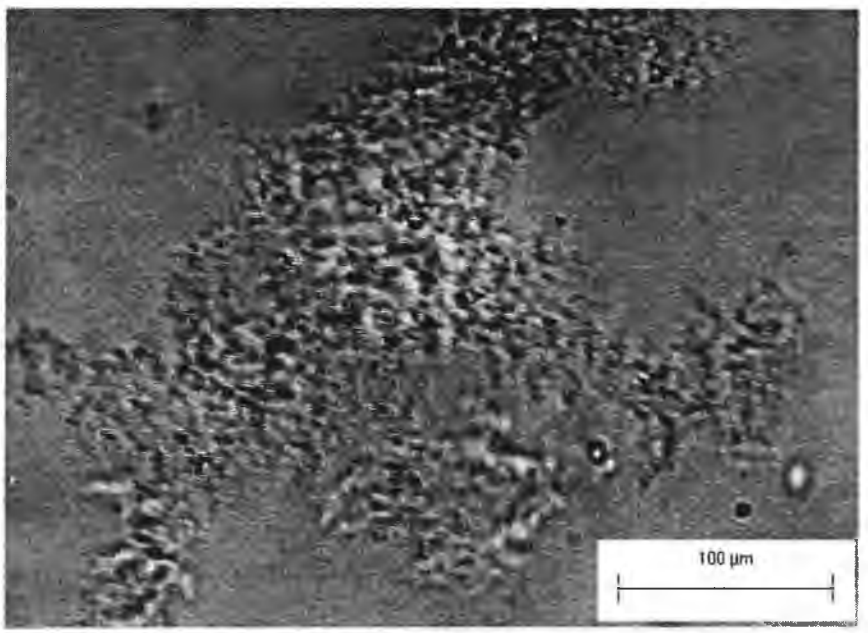

Figure 7.72 Microscopic image of m-xylene floc at concentration of 300 ppm with Cat-Floc at optimum dosage.

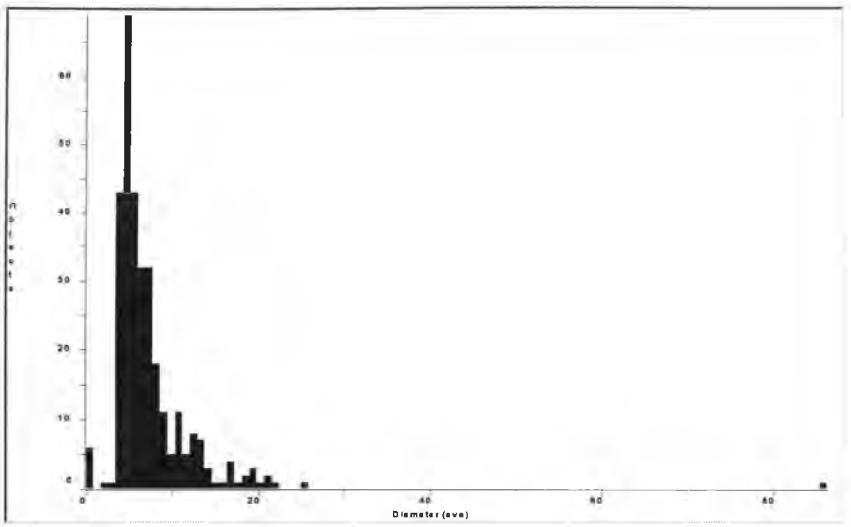

Figure 7.73 Distribution of m-xylene droplet diameter inside of Cat-Floc floc at concentration of 300 ppm, for microscopic image 7.69.

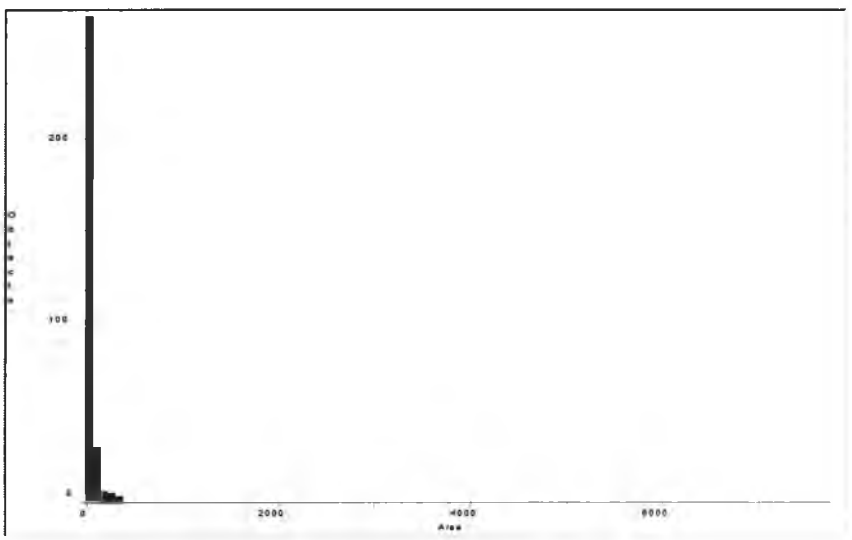

Figure 7.74 Distribution of m-xylene droplet area inside of Cat-Floc floc at concentration of 300 ppm, for microscopic image 7.69.

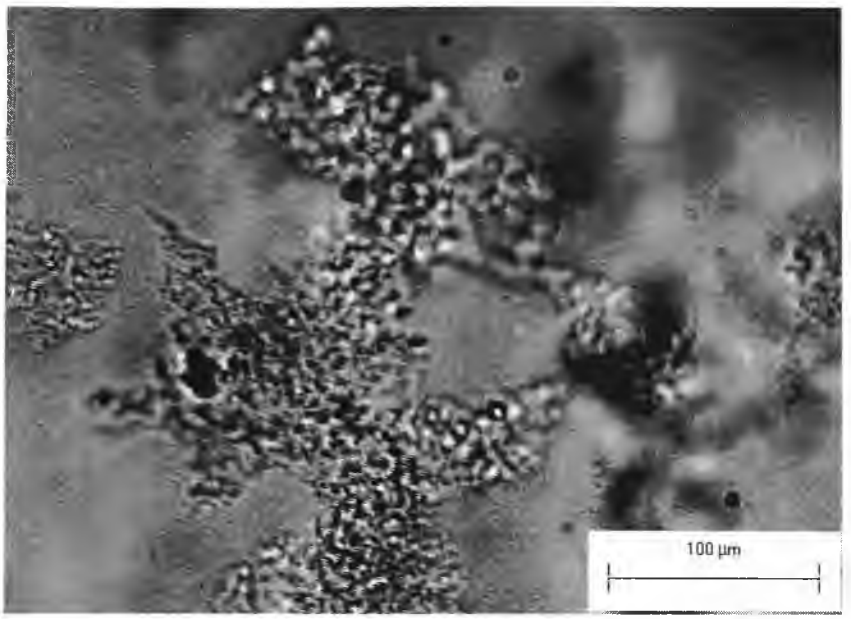

Figure 7.75 Microscopic image of m-xylene floc at concentration of 300 ppm with EB-5000 at optimum dosage.

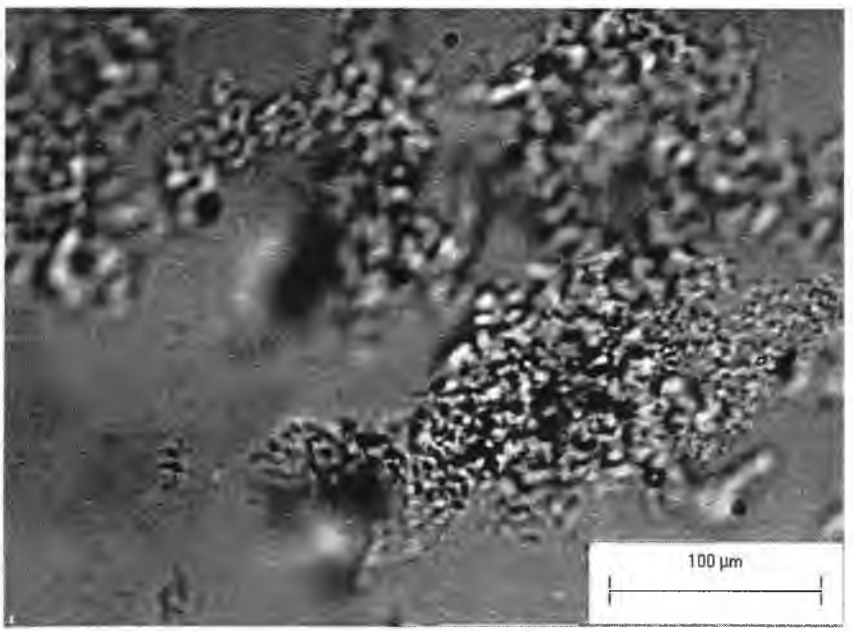

Figure 7.76 Microscopic image of m-xylene floc at concentration of 300 ppm with EB-5000 at optimum dosage.

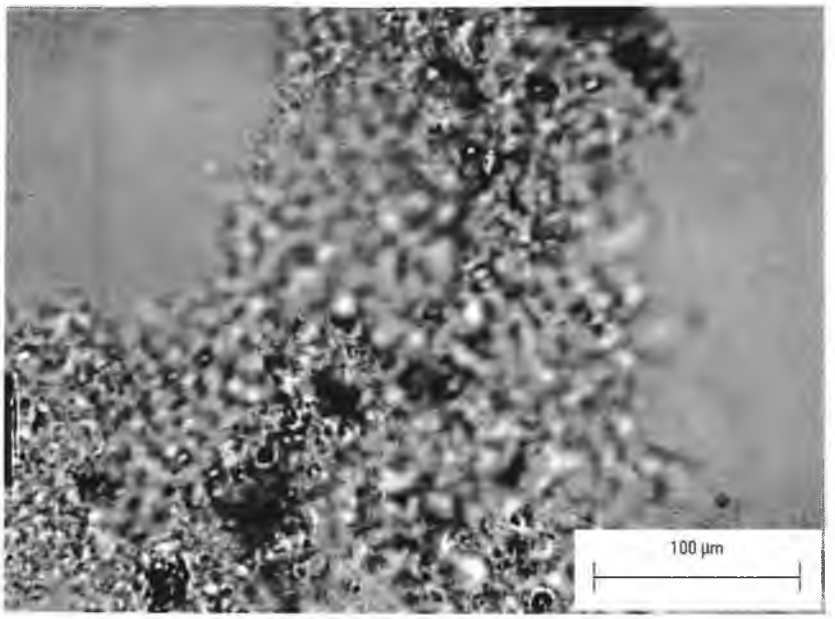

Figure 7.77 Microscopic image of m-xylene floc at concentration of 300 ppm with EB-5000 at optimum dosage.

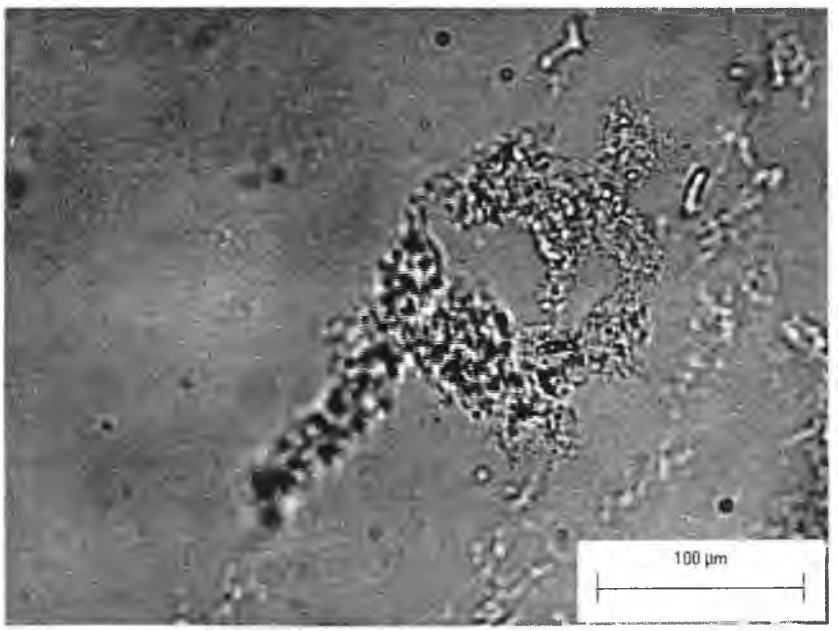

Figure 7.78 Microscopic image of m-xylene floc at concentration of 300 ppm with EB-5000 at optimum dosage.

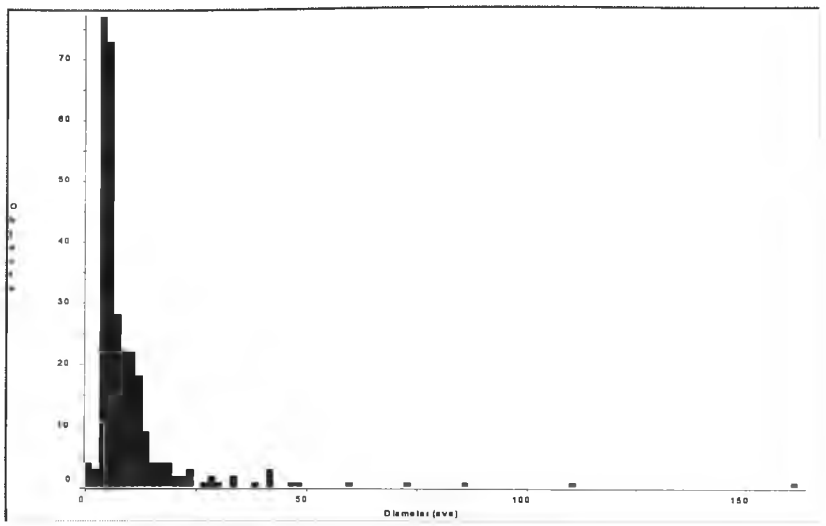

Figure 7.79 Distribution of m-xylene droplet diameter inside of EB-5000 floc at concentration of 300 ppm, for microsscopic image 7.75.

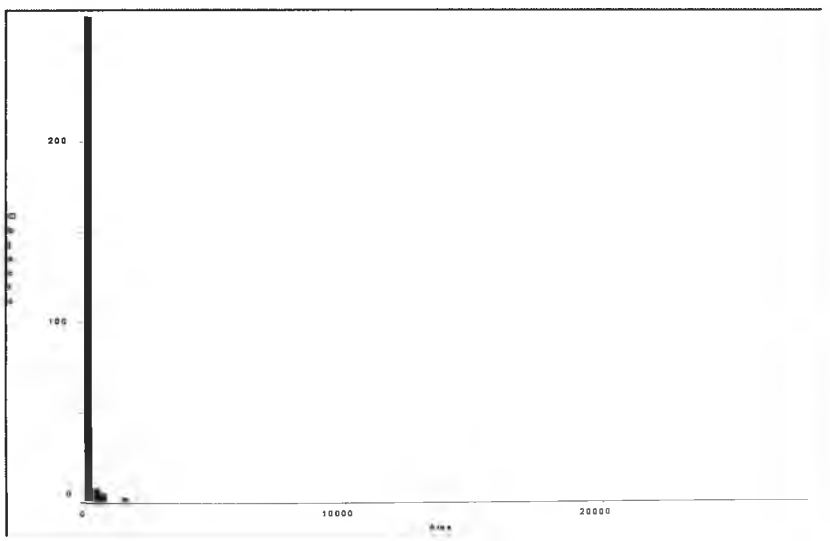

Figure 7.80 Distribution of m-xylene droplet area inside of EB-5000 floc at concentration of 300 ppm, for microscopic image 7.75.

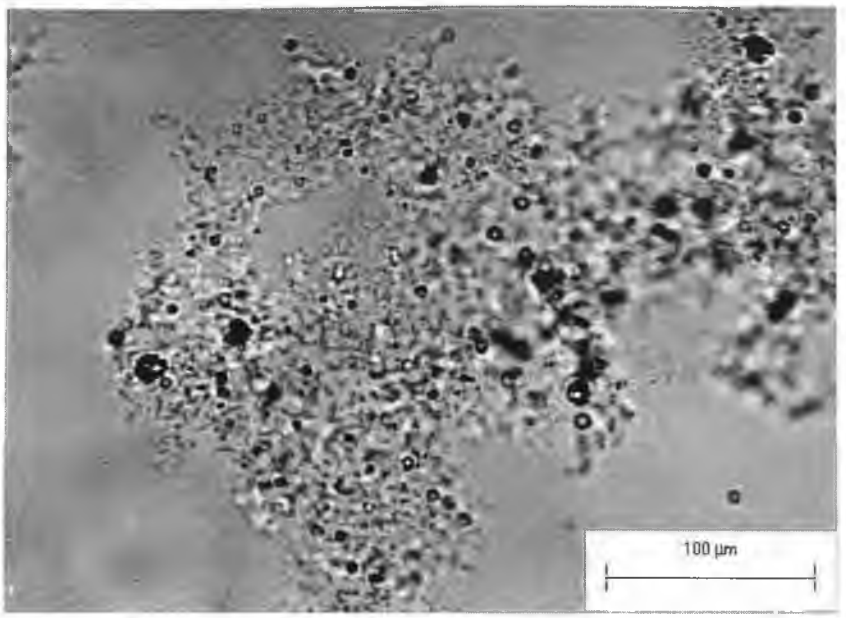

Figure 7.81 Microscopic image of Styrene floc at concentration of 500 ppm with Cat-Floc 2953 at optimum dosage.

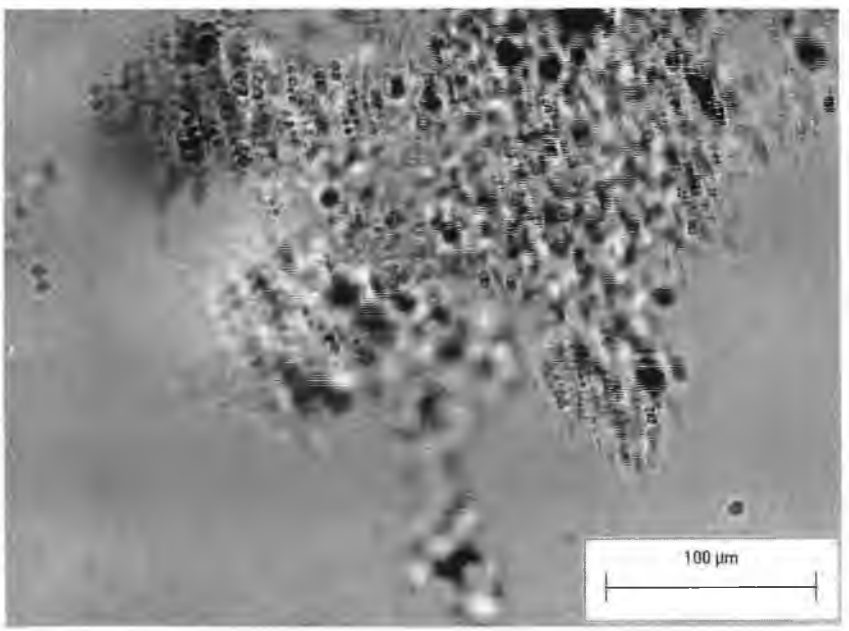

Figure 7.82 Microscopic image of Styrene floc at concentration of 500 ppm with Cat-Floc 2953 at optimum dosage.

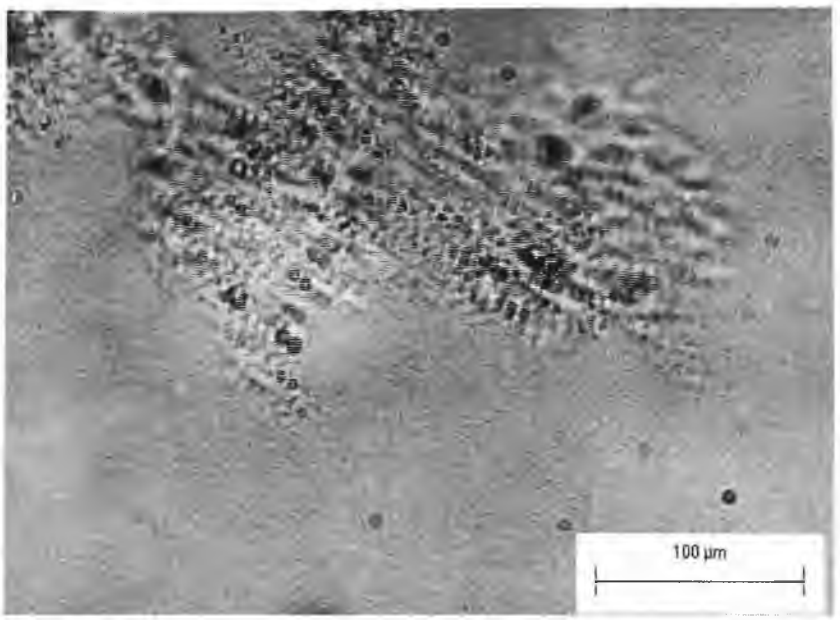

Figure 7.83 Microscopic image of Styrene floc at concentration of 500 ppm with Cat-Floc 2953 at optimum dosage.

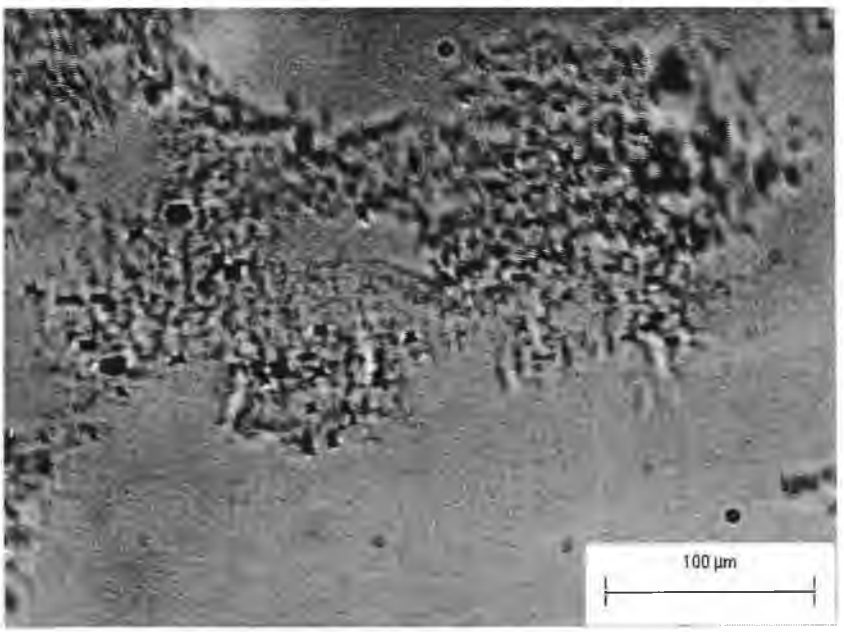

Figure 7.84 Microscopic image of Styrene floc at concentration of 500 ppm with Cat-Floc 2953 at optimum dosage.

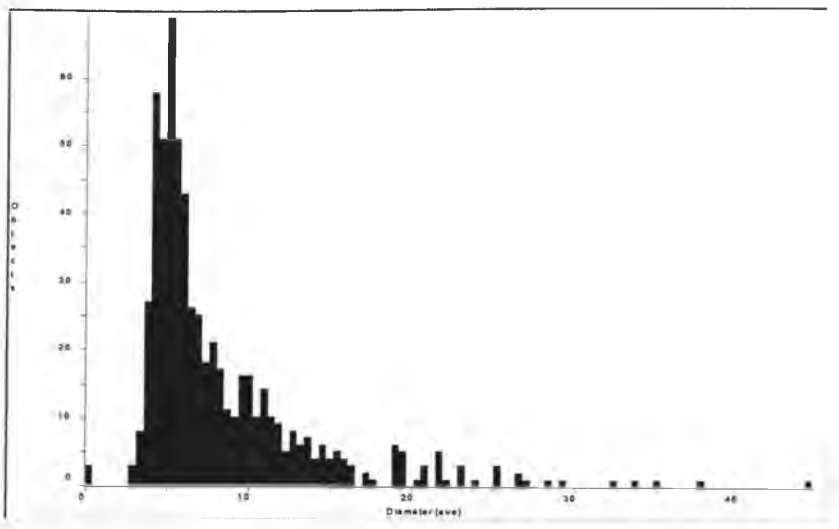

Figure 7.85 Distribution of Styrene droplet diameter inside of Cat-Floc floc at concentration of 500 ppm, for microscopic image 7.81.

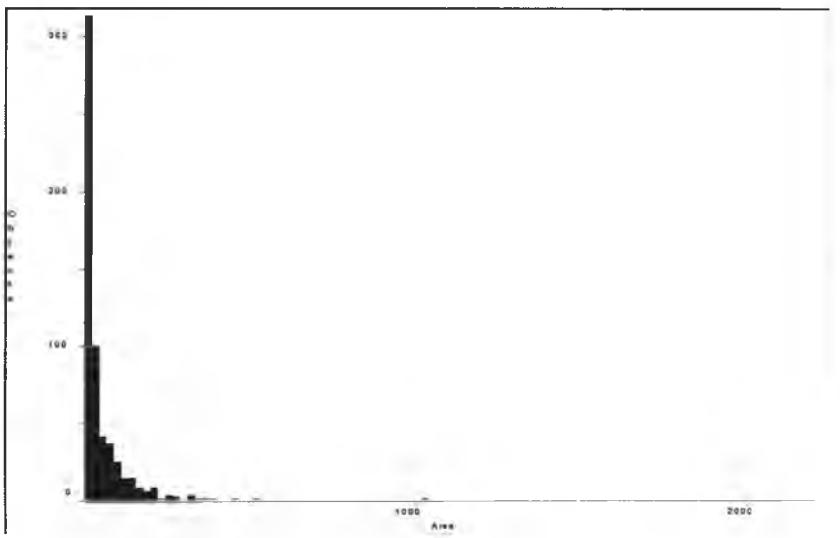

Figure 7.86 Distribution of Styrene droplet area inside of Cat-Floc floc at concentration of 500 ppm, microscopic image 7.81.

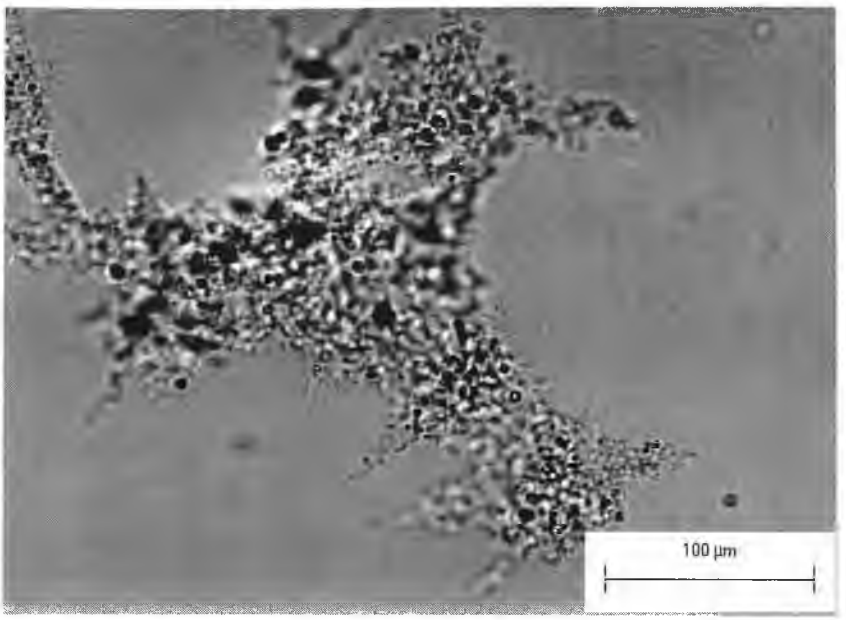

Figure 7.87 Microscopic image of Styrene floc at concentration of 500 ppm with EB-5000 at optimum dosage.

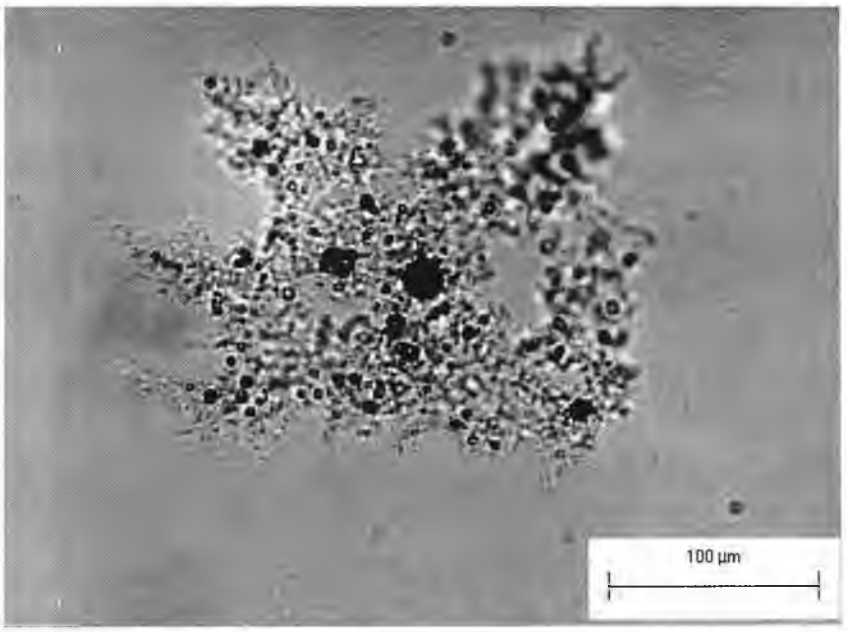

Figure 7.88 Microscopic image of Styrene floc at concentration of 500 ppm with EB-5000 at optimum dosage.

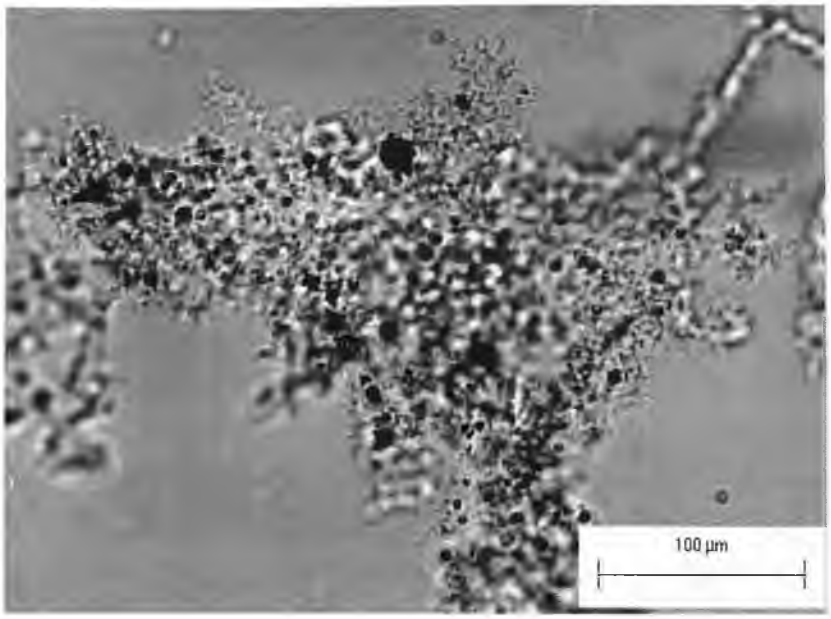

Figure 7.89 Microscopic image of Styrene floc at concentration of 500 ppm with EB-5000 at optimum dosage.

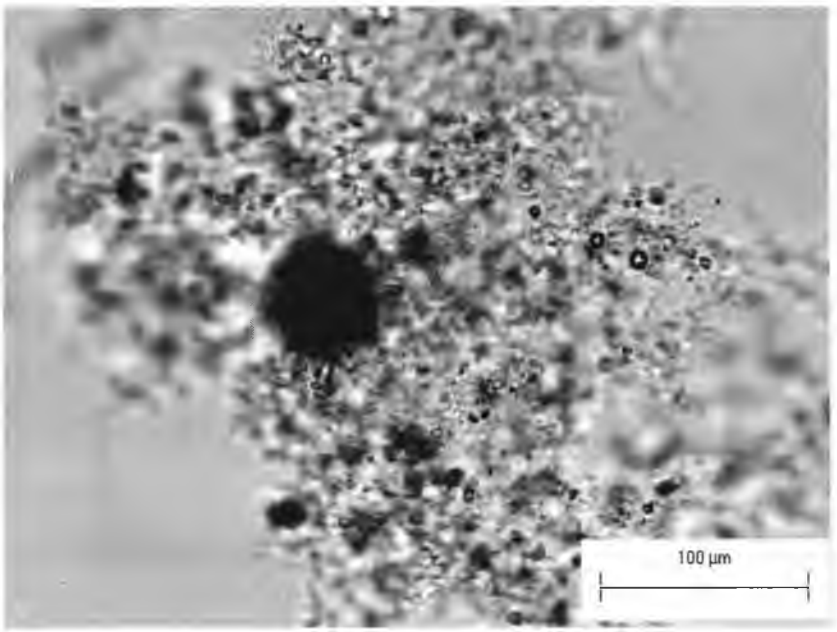

Figure 7.90 Microscopic image of Styrene floc at concentration of 500 ppm with EB-5000 at optimum dosage.

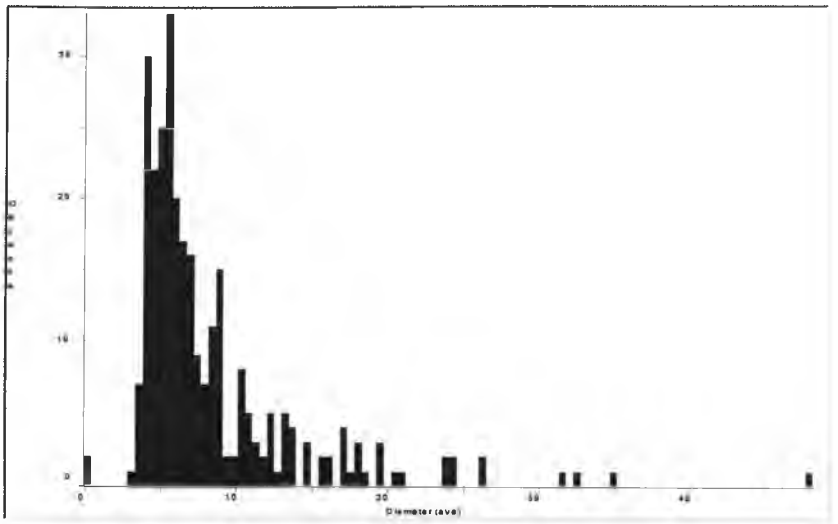

Figure 7.91 Distribution of Styrene droplet diameter inside of EB-5000 floc at concentration of 500 ppm, for microscopic image 7.87.

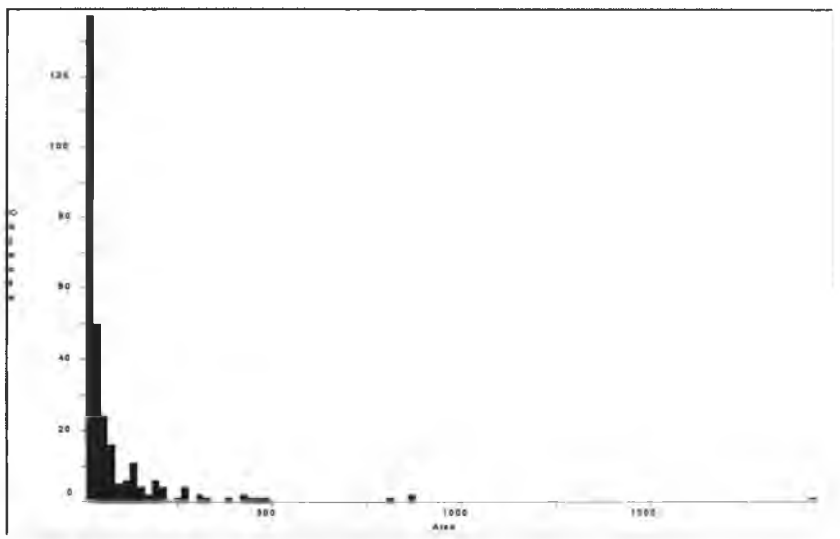

Figure 7.92 Distribution of Styrene droplet area inside of EB-5000 floc at concentration of 500 ppm, for microscopic image 7.87.

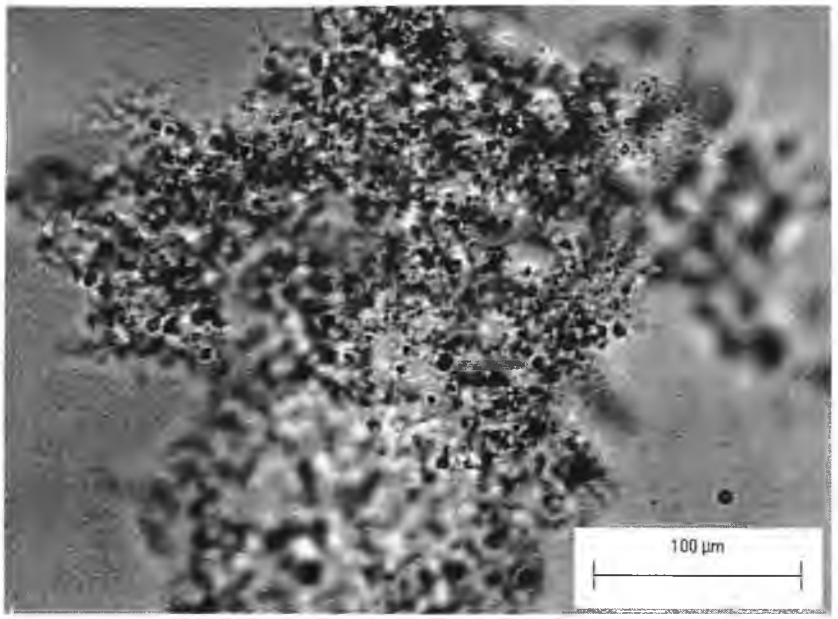

Figure 7.93 Microscopic image of Styrene floc at concentration of 300 ppm with Cat-Floc at optimum dosage.

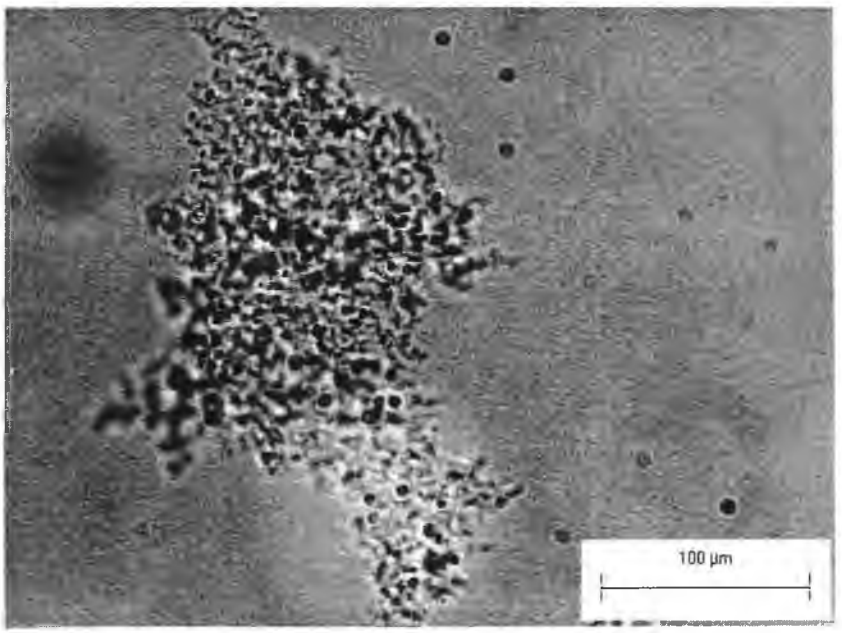

Figure 7.94 Microscopic image of Styrene floc at concentration of 300 ppm with Cat-Floc at optimum dosage.

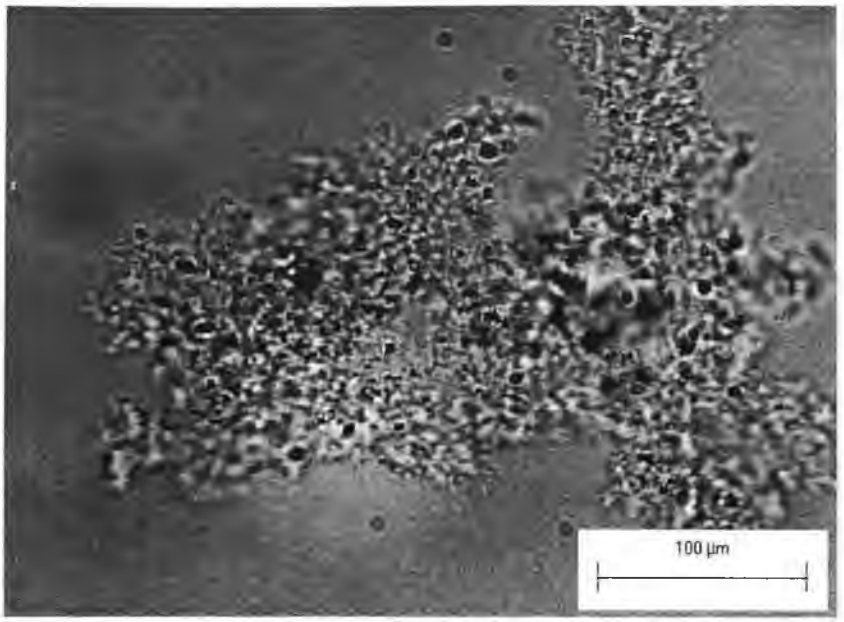

Figure 7.95 Microscopic image of Styrene floc at concentration of 300 ppm with Cat-Floc at optimum dosage.

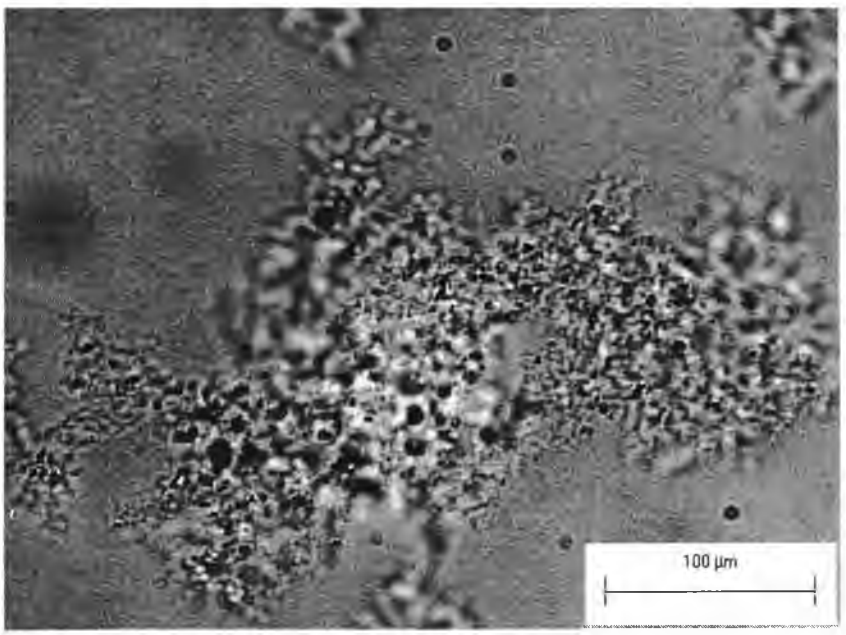

Figure 7.96 Microscopic image of Styrene floc at concentration of 300 ppm with Cat-Floc at optimum dosage.

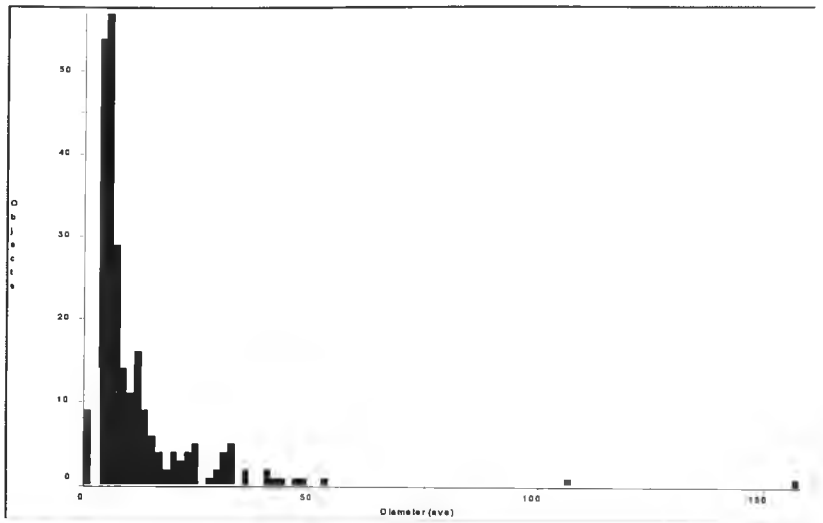

Figure 7.97 Distribution of Styrene droplet diameter inside of Cat-Floc at concentration of 300 ppm, for microscopic image 7.93.

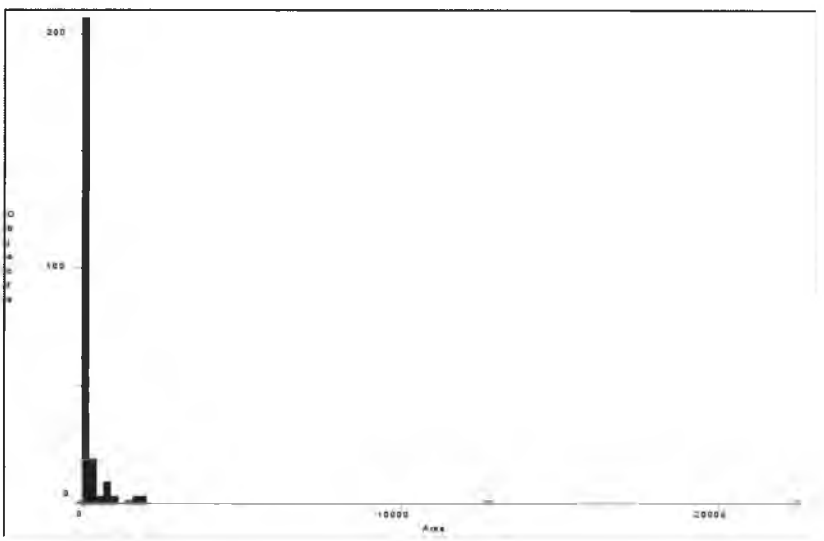

Figure 7.98 Distribution of Styrene droplet area inside of Cat-Floc at concentration of 300 ppm, for microscopic image 7.93.

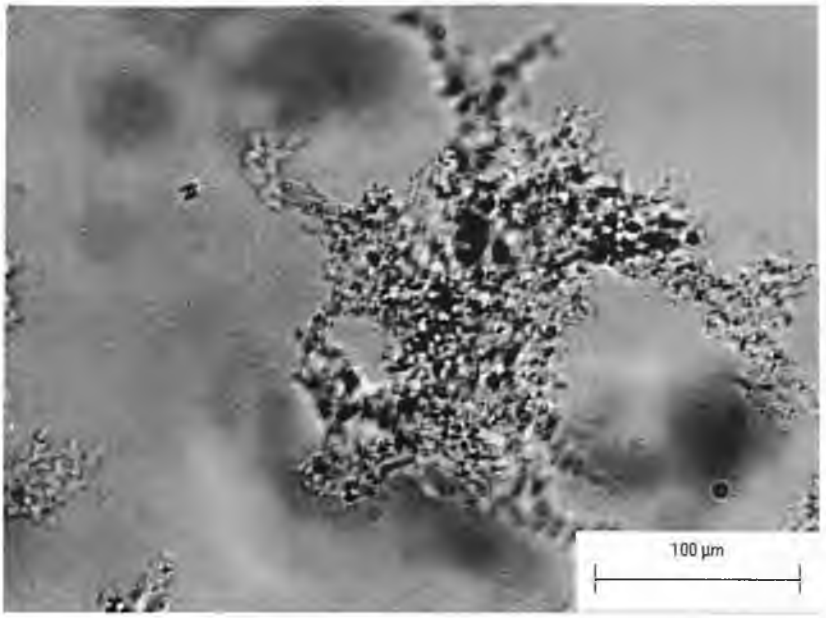

Figure 7.99 Microscopic image of Styrene floc at concentration of 300 ppm with EB-5000 at optimum dosage.

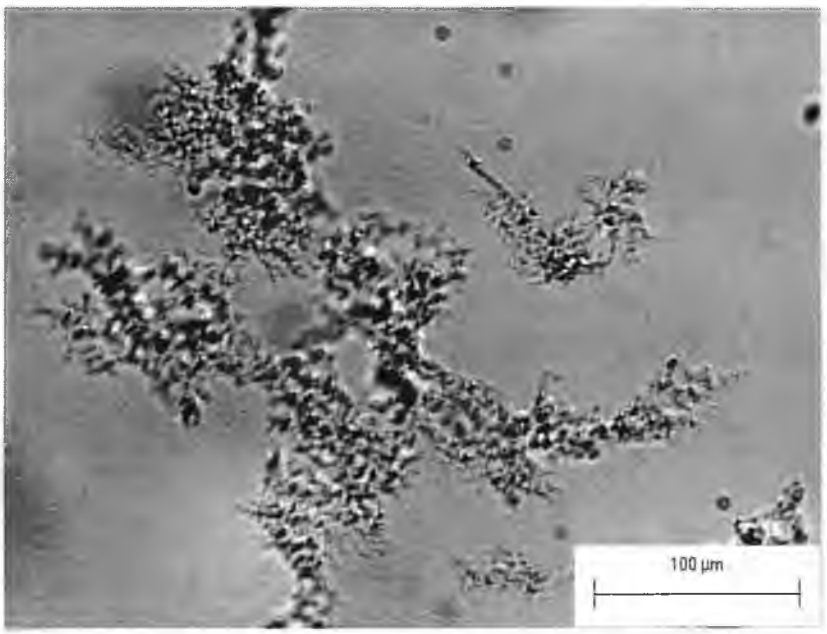

Figure 7.100 Microscopic image of Styrene floc at concentration of 300 ppm with EB-5000 at optimum dosage.

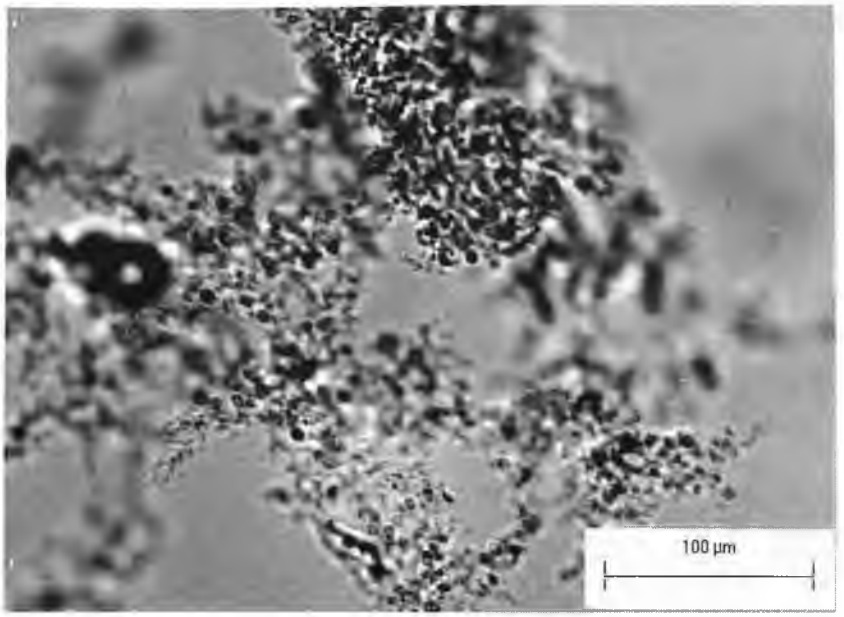

Figure 7.101 Microscopic image of Styrene floc at concentration of 300 ppm with EB-5000 at optimum dosage.

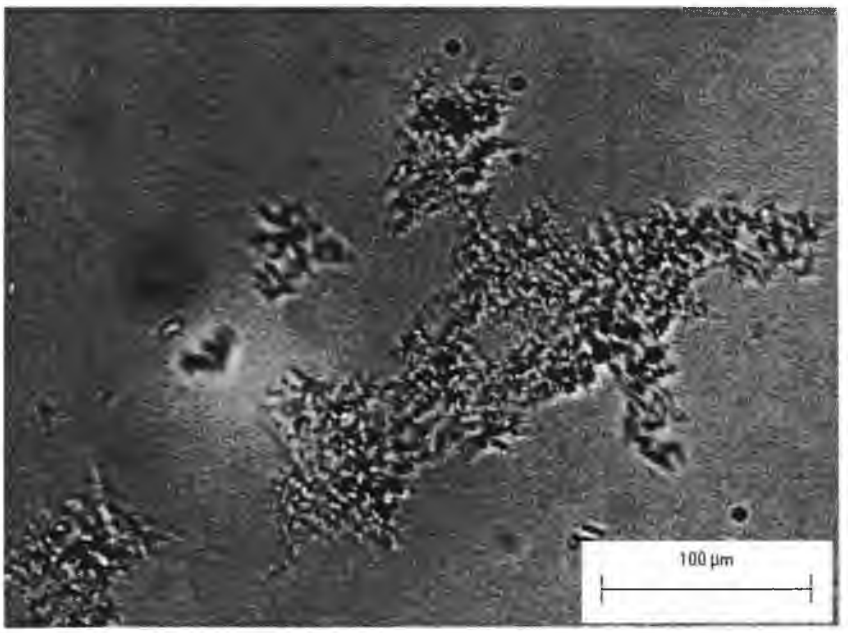

Figure 7.102 Microscopic image of Styrene floc at concentration of 300 ppm with EB-5000 at optimum dosage.

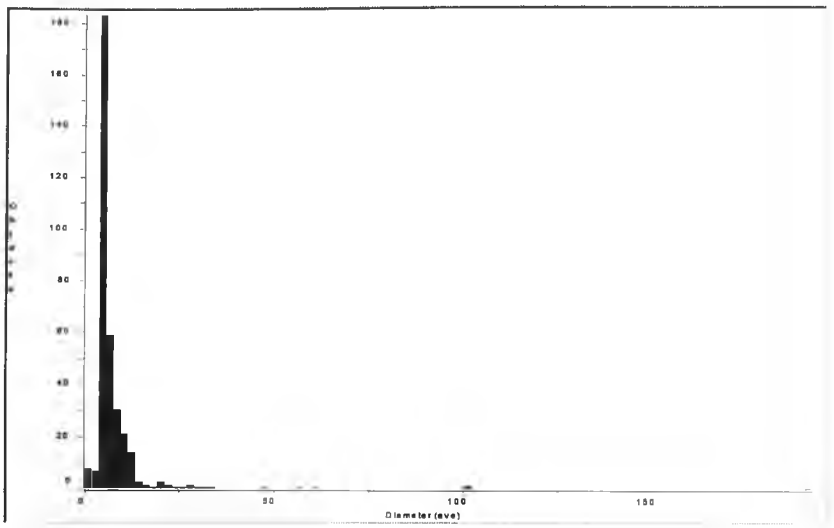

Figure 7.103 Distribution of Styrene droplet diameter inside of EB-5000 floc at concentration of 300 ppm, for microscopic image 7.99.

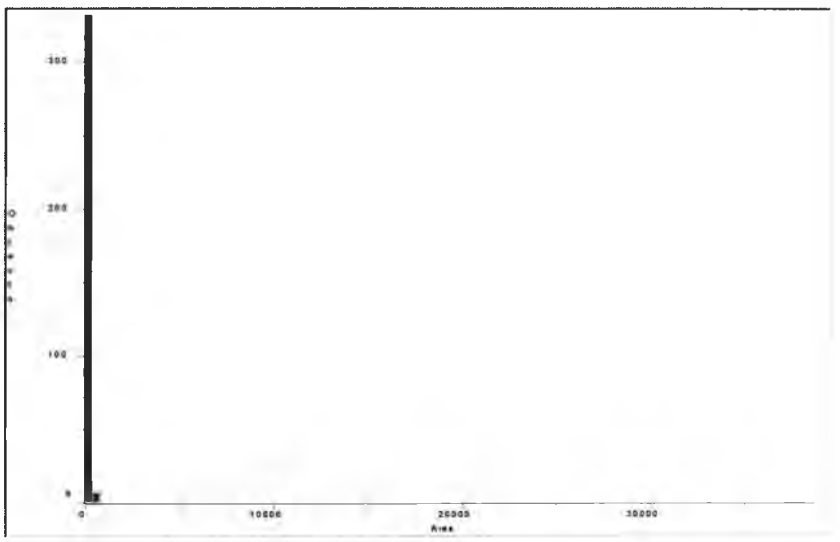

Figure 7.104 Distribution of Styrene droplet are inside of EB-5000 floc at concentration of 300 ppm, for microscopic image 7.99.

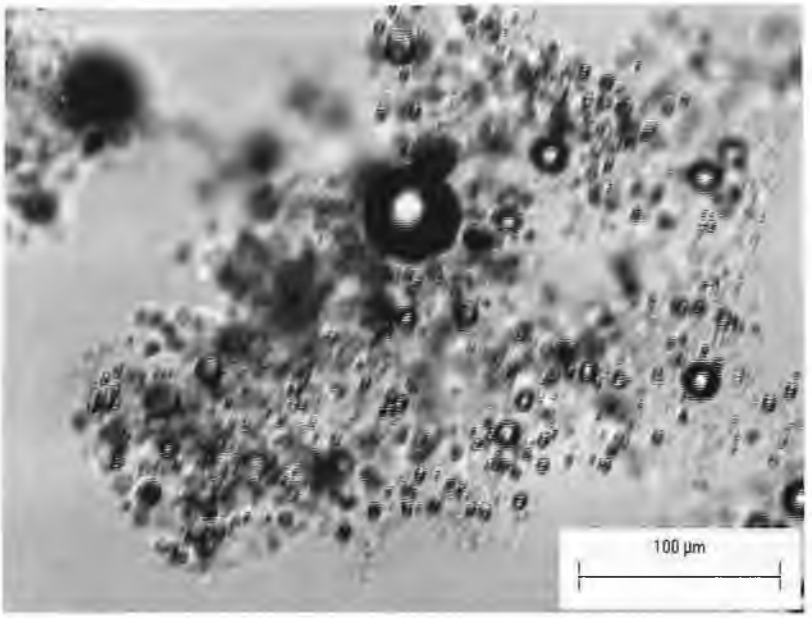

Figure 7.105 Microscopic image of Gasoline floc at concentration of 500 ppm with Cat-Floc 2953 at optimum dosage.

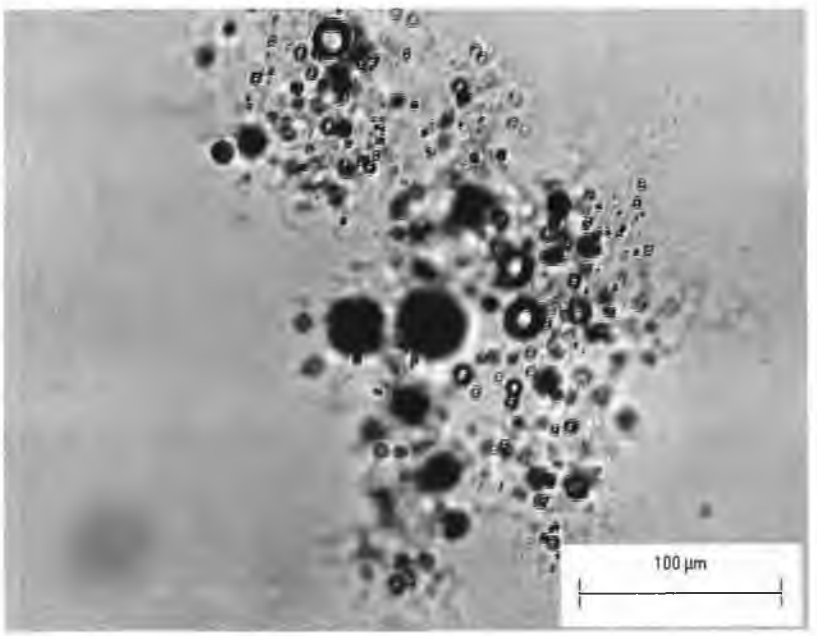

Figure 7.106 Microscopic image of Gasoline floc at concentration of 500 ppm with Cat-Floc 2953 at optimum dosage.

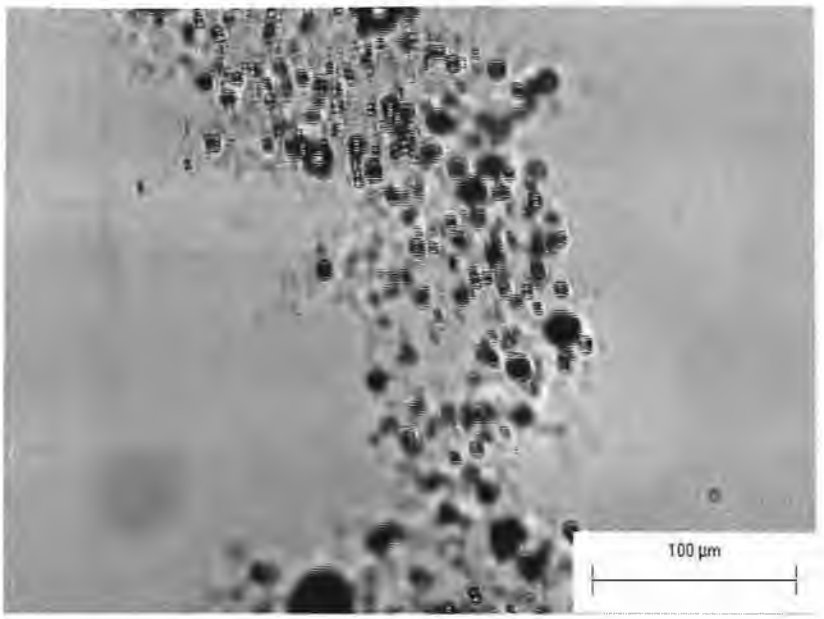

Figure 7.107 Microscopic image of gasoline floc at concentration of 500 ppm with Cat-Floc 2953 at optimum dosage.

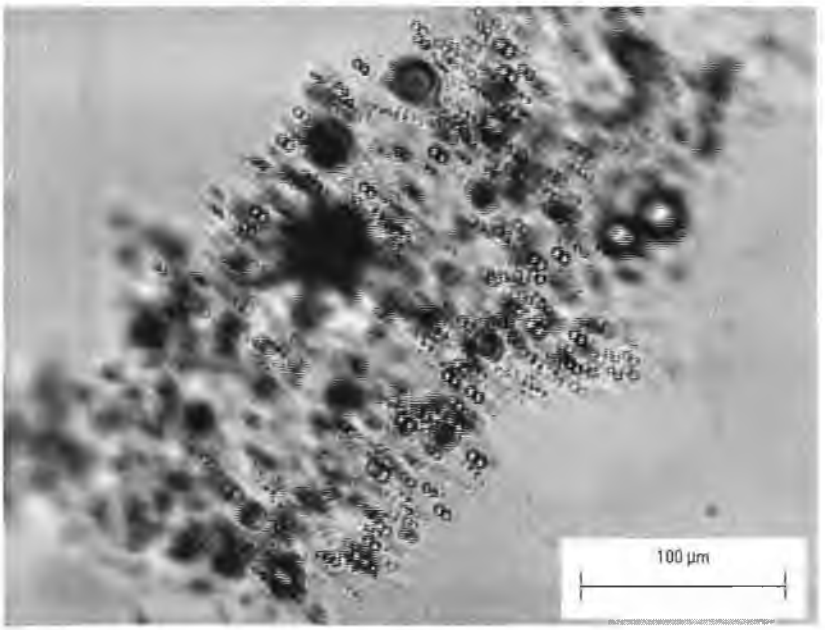

Figure 7.108 Microscopic image of gasoline floc at concentration of 500 ppm with Cat-Floc 2953 at optimum dosage.

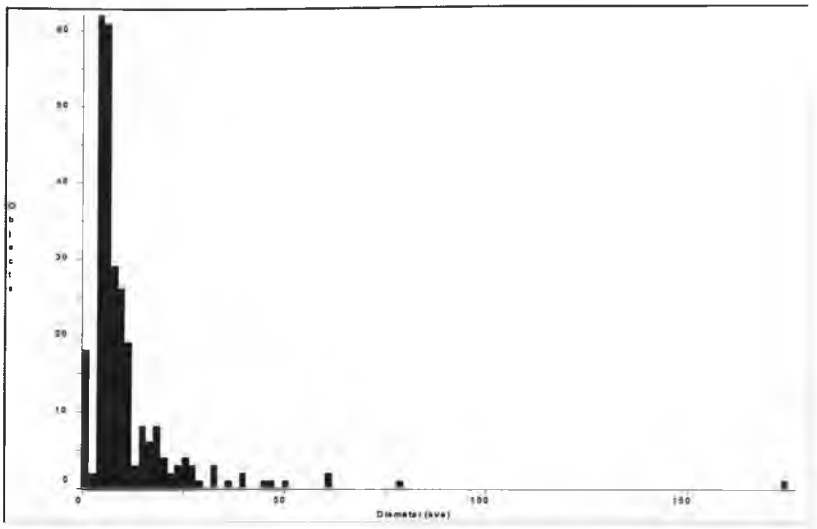

Figure 7.109 Distribution of Gasoline droplet diameter inside of Cat-Floc floc at concentration of 500 ppm, for microscopic image 7.105.

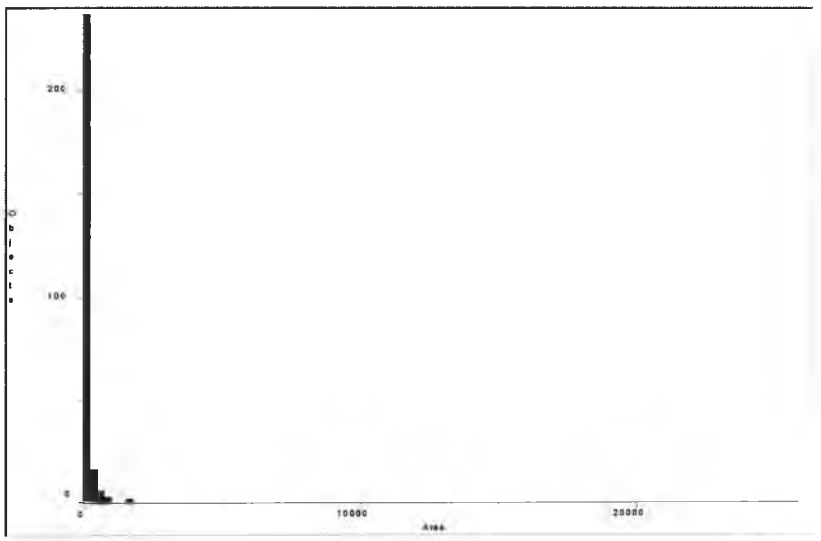

Figure 7.110 Distribution of Gasoline droplet area inside of Cat-Floc floc at concentration of 500 ppm, for microscopic image 7.105.

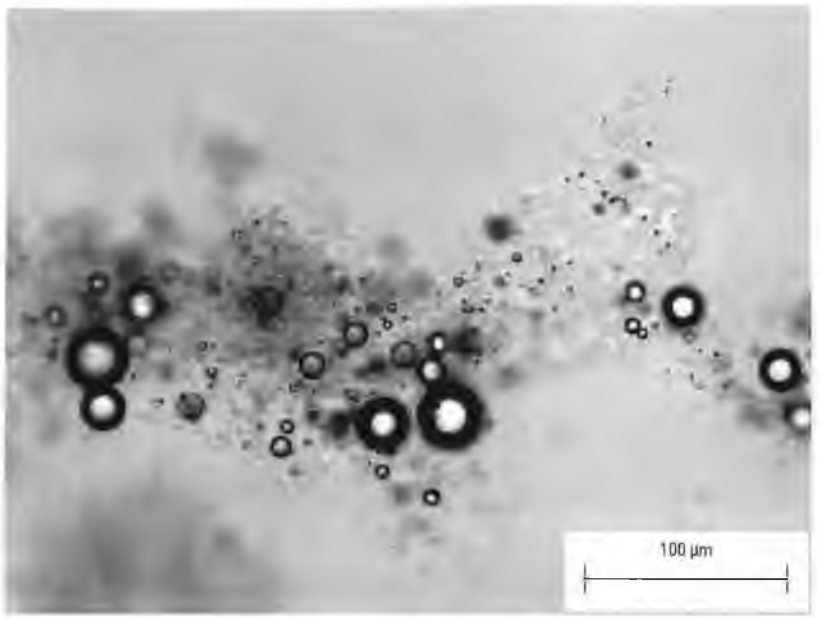

Figure 7.111 Microscopic image of Gasoline floc at concentration of 500 ppm with EB-5000 at optimum dosage.

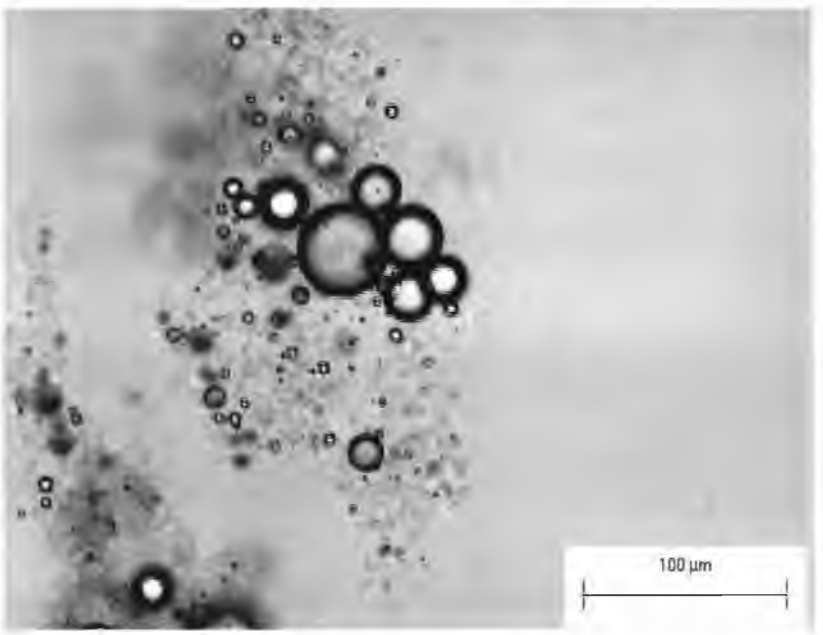

Figure 7.112 Microscopic image of gasoline floc at concentration of 500 ppm with EB-5000 at optimum dosage.

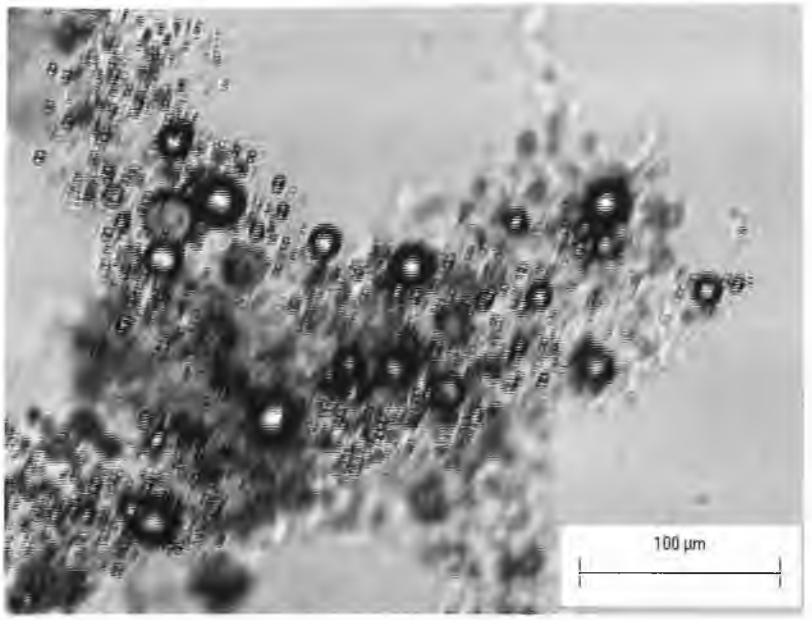

Figure 7.113 Microscopic image of gasoline floc at concentration of 500 ppm with EB-5000 at optimum dosage.

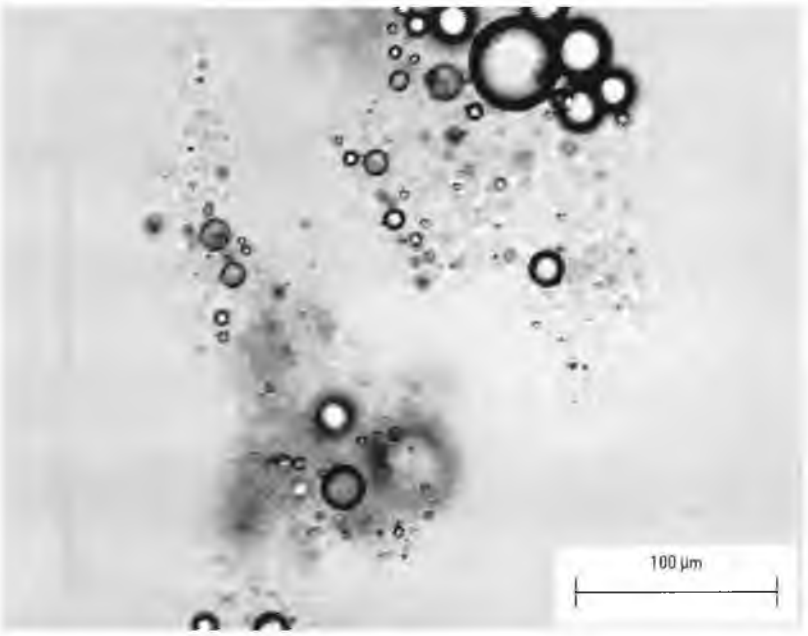

Figure 7.114 Microscopic image of gasoline floc at concentration of 500 ppm with EB-5000 at optimum dosage.

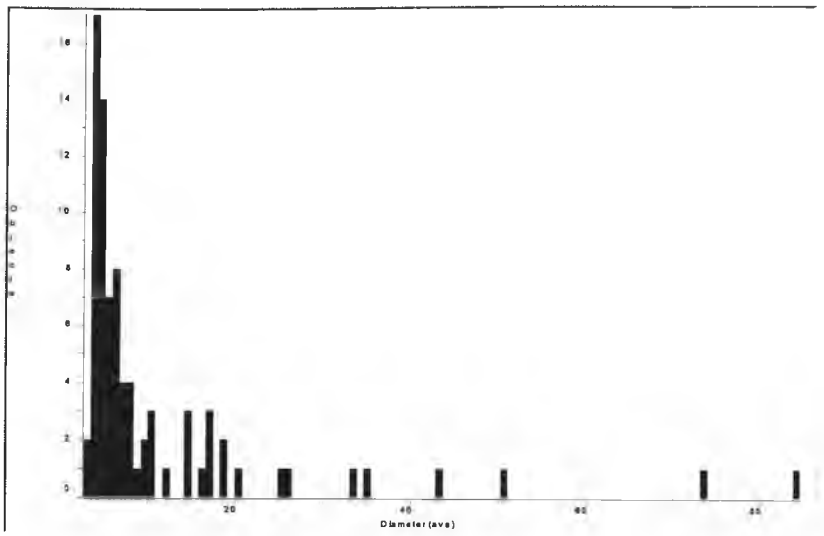

Figure 7.115 Distribution of Gasoline droplet diameter inside of EB-5000 floc at concentration of 500 ppm, for microscopic image 7.111.

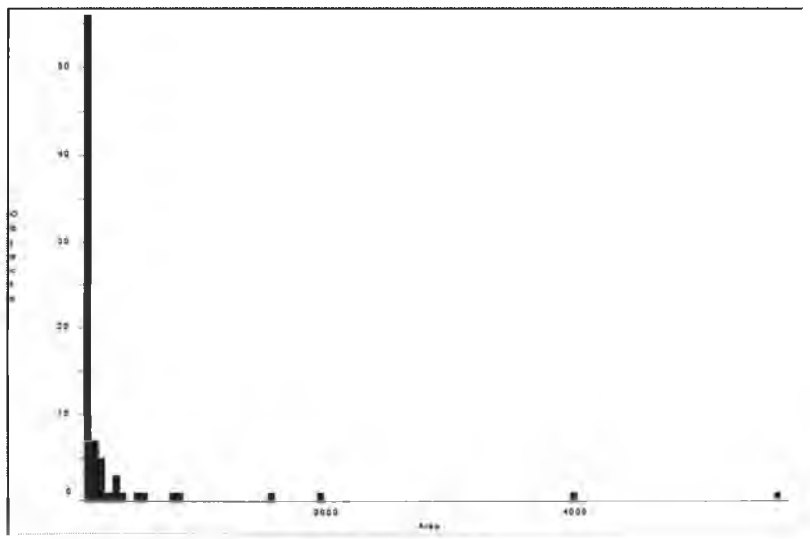

Figure 7.116 Distribution of Gasoline droplet area inside of EB-5000 floc at concentration of 500 ppm, for microscopic image 7.111.

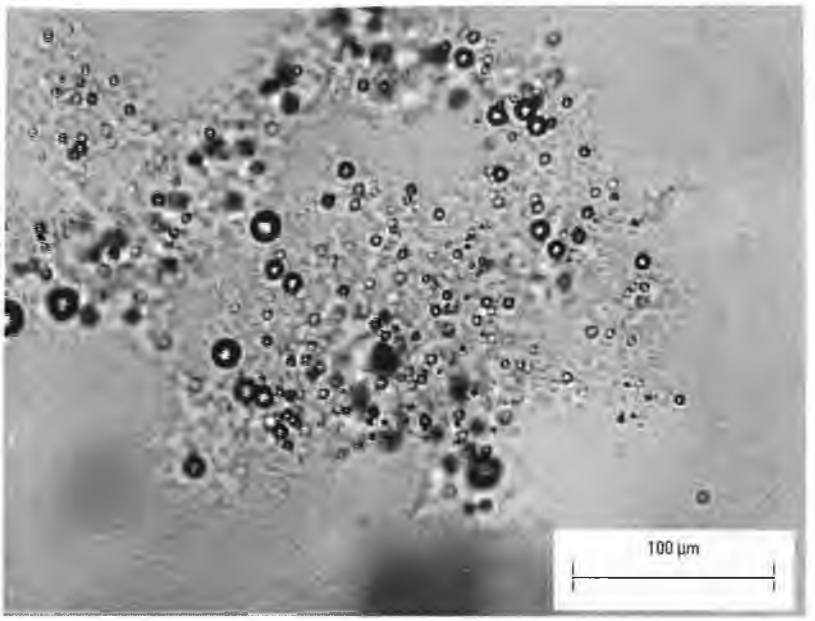

Figure 7.117 Microscopic image of Gasoline floc at concentration of 300 ppm with Cat-Floc 2953 at optimum dosage.

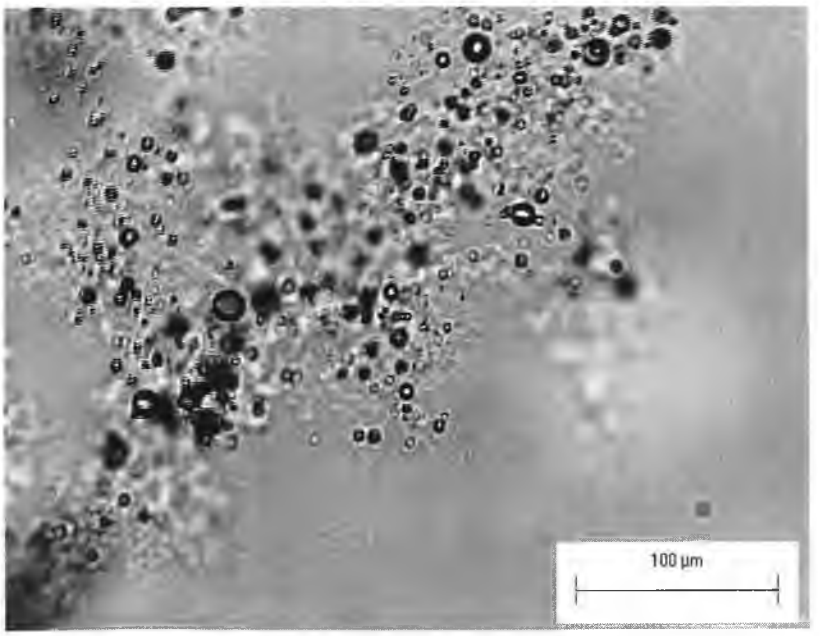

Figure 7.118 Microscopic image of Gasoline floc at concentration of 300 ppm with Cat-Floc 2953 at optimum dosage.

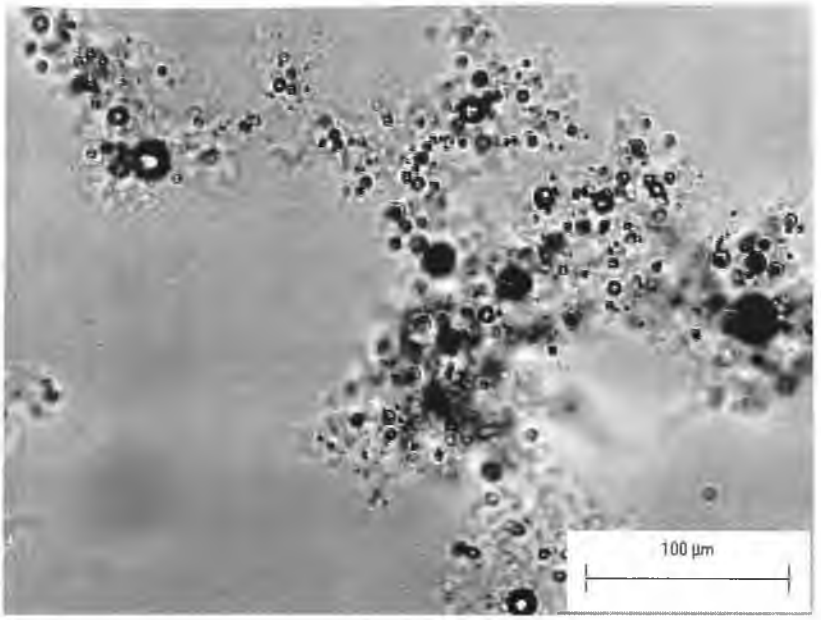

Figure 7.119 Microscopic image of Gasoline floc at concentration of 300 ppm with Cat-Floc 2953 at optimum dosage.

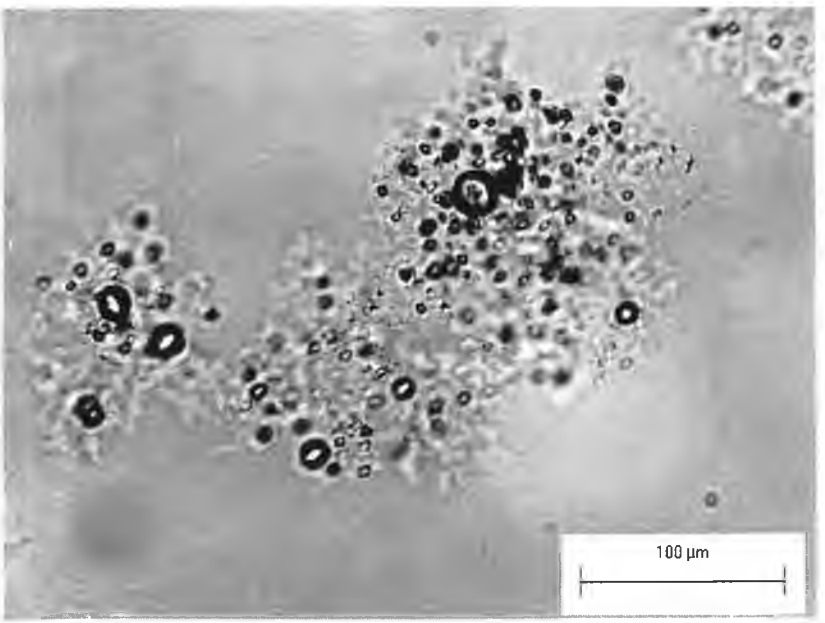

Figure 7.120 Microscopic image of Gasoline floc at concentration of 300 ppm with Cat-Floc 2953 at optimum dosage.

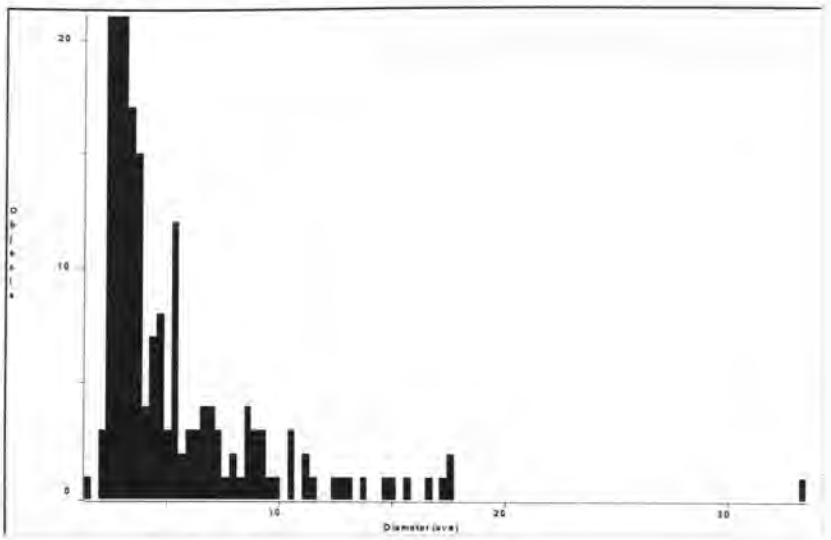

Figure 7.121 Distribution of Gasoline droplet diameter inside of Cat-Floc floc at concentration of 300 ppm, for microscopic image 7.117.

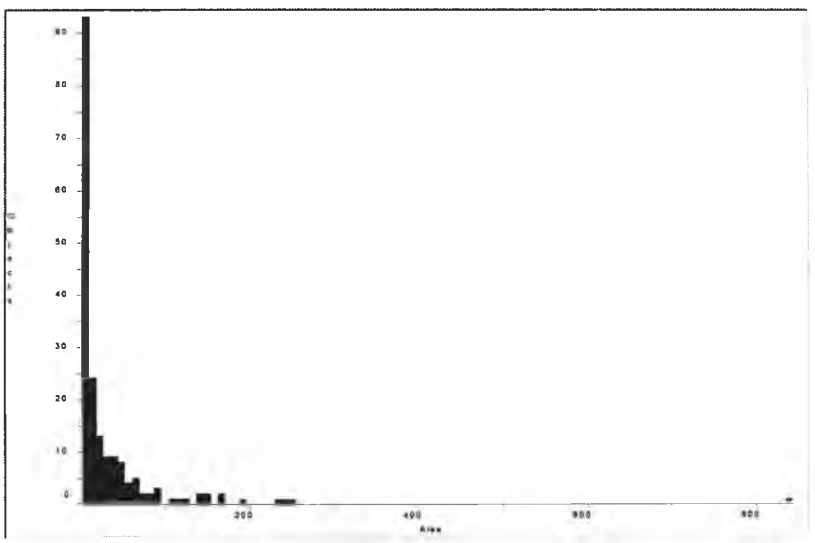

Figure 7.122 Distribution of Gasoline droplet area inside of Cat-Floc floc at concentration of 300 ppm, for microscopic image 7.117.

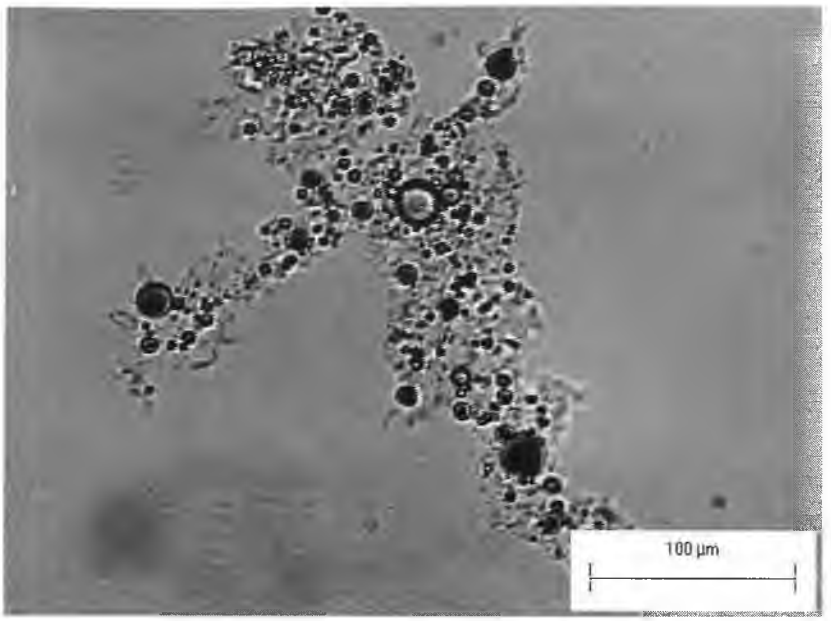

Figure 7.123 Microscopic image of Gasoline floc at concentration of 300 ppm with EB-5000 at optimum dosage.

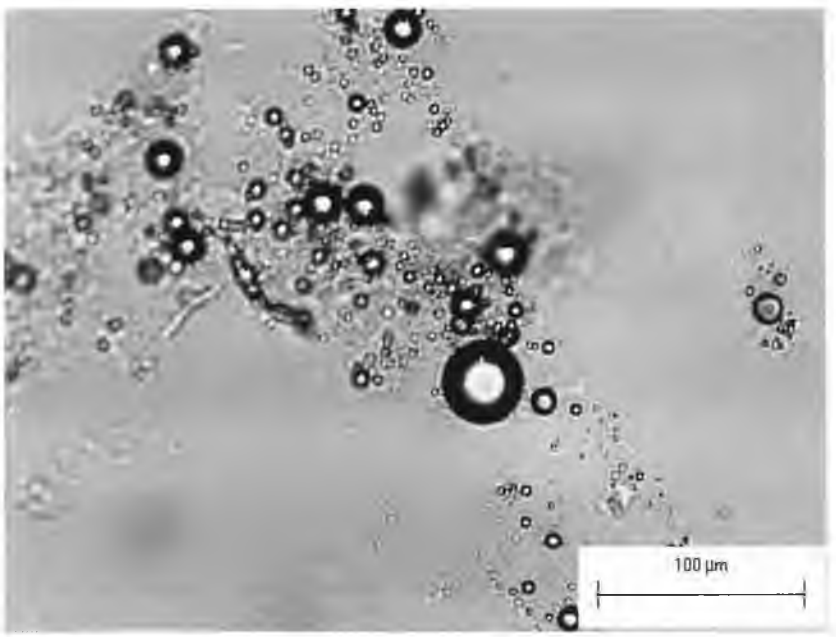

Figure 7.124 Microscopic image of Gasoline floc at concentration of 300 ppm with EB-5000 at optimum dosage.

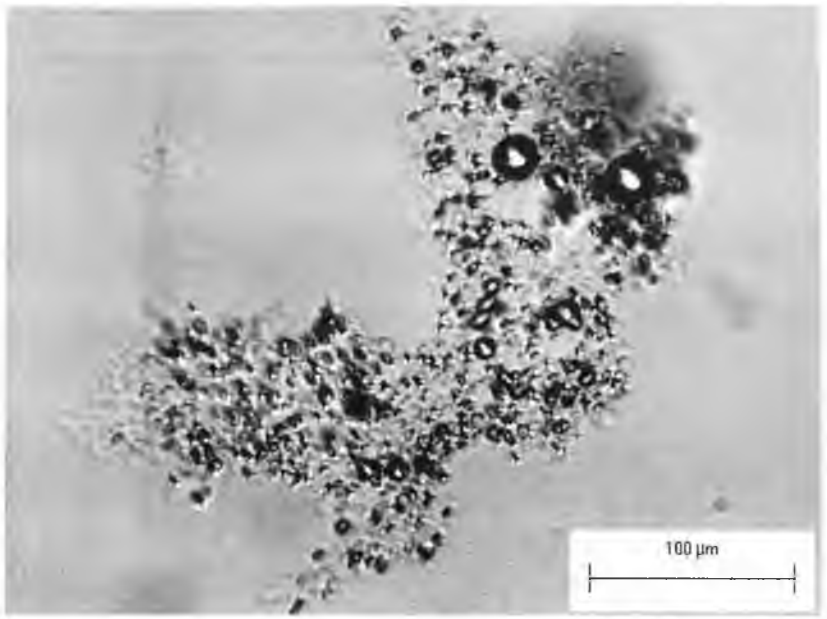

Figure 7.125 Microscopic image of Gasoline floc at concentration of 300 ppm with EB-5000 at optimum dosage.

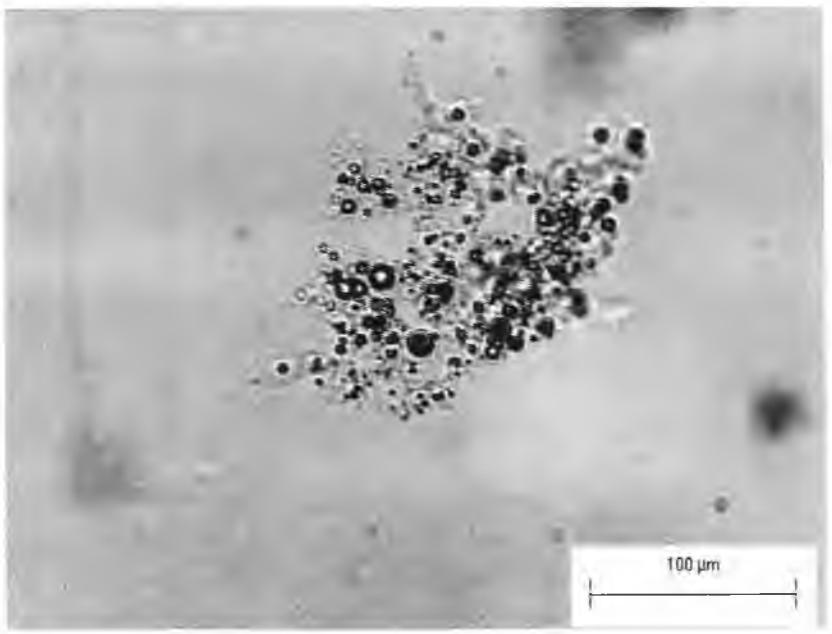

Figure 7.126 Microscopic image of Gasoline floc at concentration of 300 ppm with EB-5000 at optimum dosage.

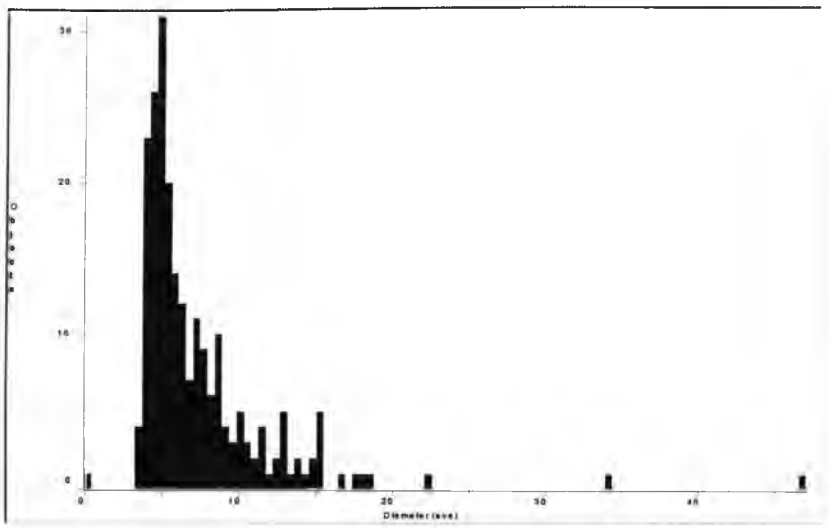

Figure 7.127 Distribution of Gasoline droplet diameter inside of EB-5000 floc at concentration of 300 ppm, for microscopic image 7.123.

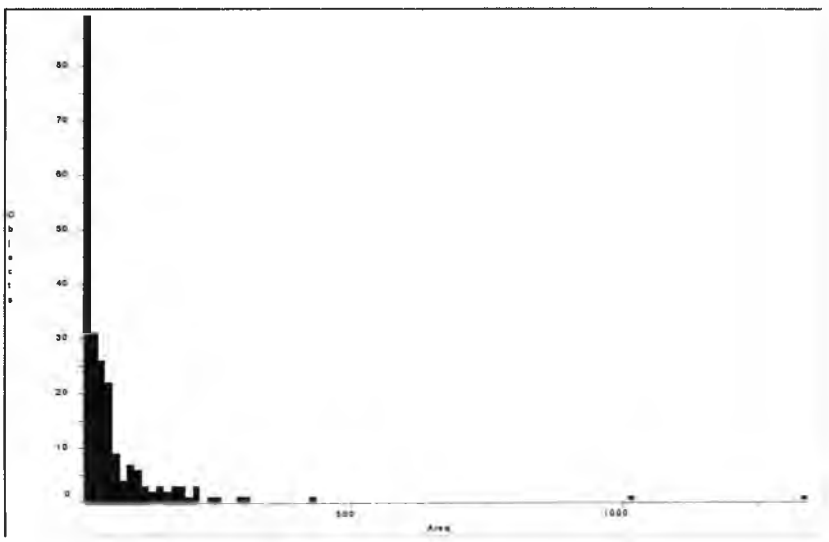

Figure 7.128 Distribution of Gasoline droplet area inside of EB-5000 floc at concentration of 300 ppm, for microscopic image 7.123

7.2. Chemical Analysis

The chemical data analysis consisted of utilizing concentration (peak area) from the GC printouts and measurements before and after the coagulation process, for each hydrocarbon. Removal efficiency was defined as:

Hydrocarbon Removal Efficiency (%)

Where:

C_i = initial concentration of hydrocarbon

C_f = final concentration of hydrocarbon

Prior to GC analysis, coagulated hydrocarbon and noncoagulated samples were diluted. Table 7.1. displays concentrations prior and after the coagulation process was accomplished and efficiency of hydrocarbon removal, for both Cat-Floc 2953 and EB-5000 polyelectrolytes. Figure 7.129 and Figure 7.132 exhibited the noncoagulated sample concentration peaks at 500 ppm and 300 ppm concentrations of hydrocarbon mixtures including toluene, m-xylene, styrene and decane. Hydrocarbon peak areas after removal by Cat-Floc 2953 are presented in Figure 7.130, 7.133, 7.136, and figure 7.139. Hydrocarbon peak areas after removal by EB-5000 are presented in Figure 7.131, 7.134, 7.137, and figure 7.140.

Turbidity results are important due to Drinking Water Standard. Samples were measured for changes in turbidity (to monitor removal of suspended solids). All the coagulated samples showed little increase in turbidity removal by Cat-Floc 2953 due to increased molecular weight and charge of this cationic polymer compare to EB-5000 (turbidity results presented in Appendix). Overall removal of hydrocarbons by Cat-Floc 2953 was more efficient.

M-xylene is the most hydrophobic aromatic hydrocarbon and its removal was the most efficient in comparison to other hydrocarbons. The removal of decane, which is straight chain hydrocarbon, was extremely effective at higher concentration.

Table 7.1. Removal efficiency of different hydrocarbons by polyelectrolytes

Contaminant	Coagulant	C_i (mg/L)	C_f (mg/L)	Removal efficiency,%
Decane 500*	CF-2953	6.417	0.00	100
Decane 500*	EB-5000	6.417	1.542	75.97
Decane 300*	CF-2953	3.337	0.00	100
Decane 300*	EB-5000	3.337	2.279	31.71
Toluene 500*	CF-2953	4.584	2.527	44.87
Toluene 500*	EB-5000	4.584	2.025	55.83
Toluene 300*	CF-2953	5.118	1.897	62.9
Toluene 300*	EB-5000	5.118	2.027	60.39
m-xylene 500*	CF-2953	5.223	1.48	71.66
m-xylene 500*	EB-5000	5.223	1.701	67.4
m-xylene 300*	CF-2953	5.426	1.427	73.7
m-xylene 300*	EB-5000	5.426	2.481	54.28
Styrene 500*	CF-2953	5.996	2.389	60.16
Styrene 500*	EB-5000	5.996	2.202	63.3
Styrene 300*	CF-2953	5.689	2.067	63.67
Styrene 300*	EB-5000	5.689	2.754	51.59

* Concentration of hydrocarbons prior to dilution.

Column:	**DB-5**, 30m x 0.45 mm I.D., 1.27 μm
Carrier:	helium at 6.5 mL/min
Oven:	35°C for 6 min., 35-55 at 4° C/min
	55°C for 3 min., 55-105 at 17° C/min
Injector:	Direct injection liner with two restrictions 250° C
Detector:	FID, 250° C

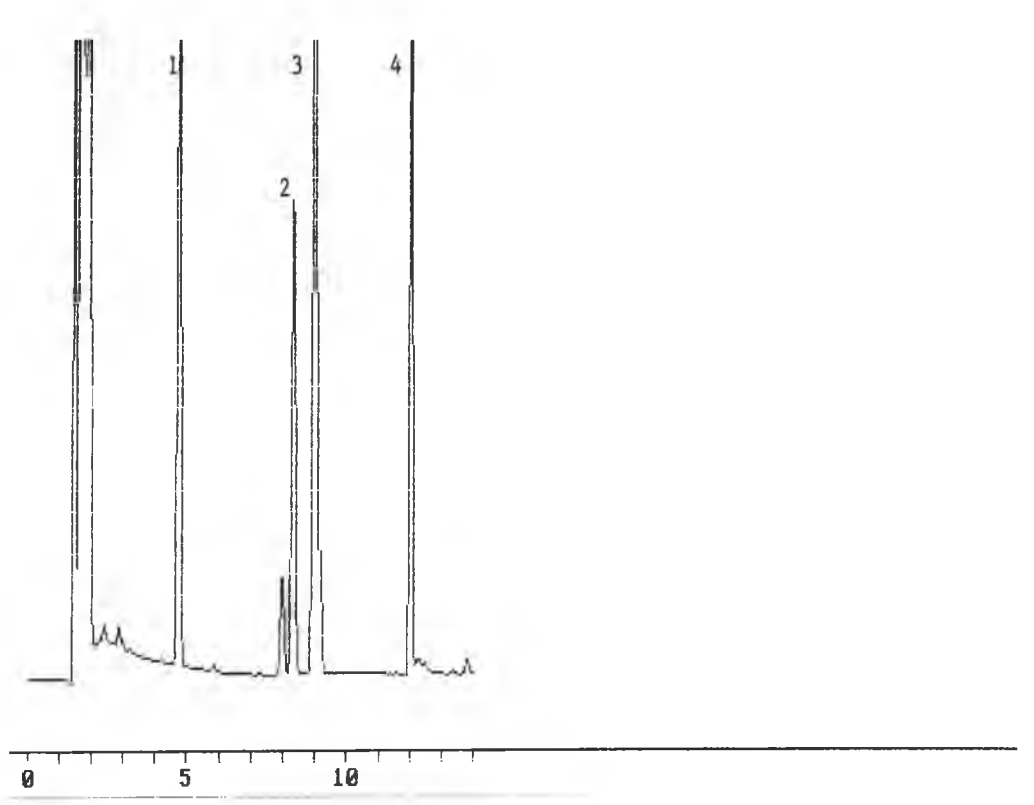

1. **Toluene**
2. **M-xylene**
3. **Styrene**
4. **Decane**

Figure 7.129 GC printout of noncoagulated sample at concentration of 500 ppm, hydrocarbon-water mixture.

Column:	**DB-5**, 30m x 0.45 mm I.D., 1.27 μm
Carrier:	helium at 6.5 mL/min
Oven:	35°C for 6 min., 35-55 at 4° C/min
	55°C for 3 min., 55-105 at 17° C/min
Injector:	Direct injection liner with two restrictions 250° C
Detector:	FID, 250° C

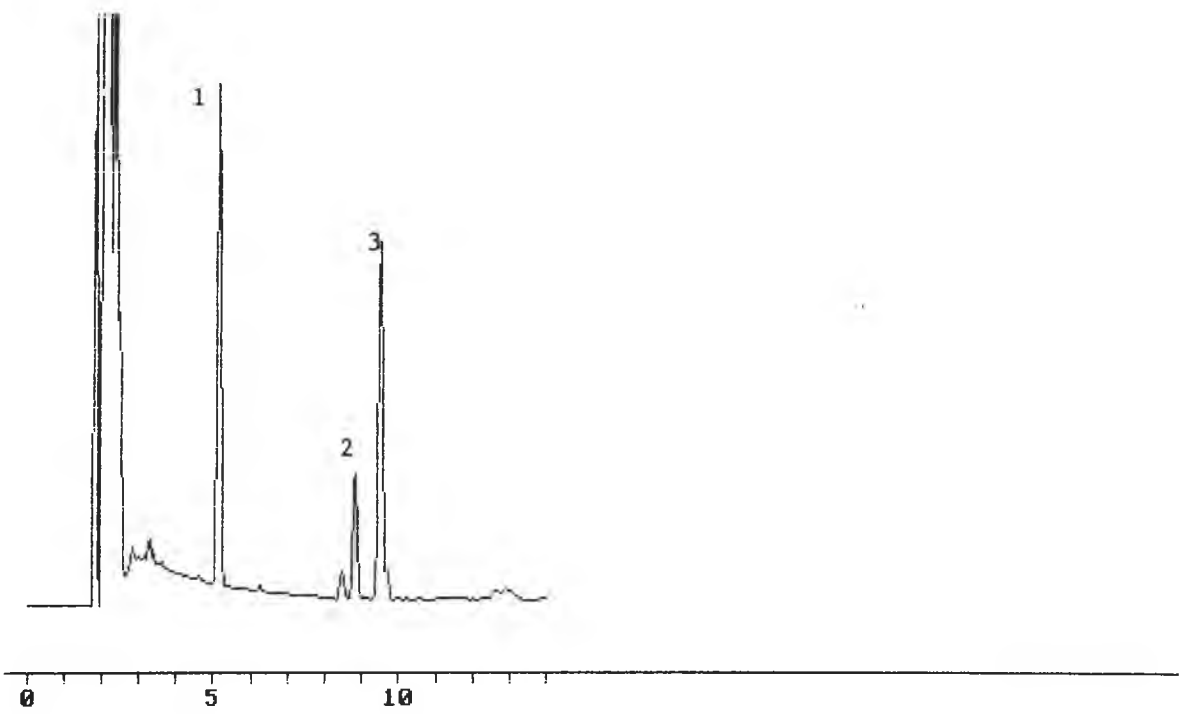

1. **Toluene**
2. **M-xylene**
3. **Styrene**

Figure 7.130 GC printout of Cat-Floc 2953, coagulated sample at 500 ppm hydrocarbon concentrations.

Column:	**DB-5**, 30m x 0.45 mm I.D., 1.27 μm
Carrier:	helium at 6.5 mL/min
Oven:	35°C for 6 min., 35-55 at 4° C/min
	55°C for 3 min., 55-105 at 17° C/min
Injector:	Direct injection liner with two restrictions 250° C
Detector:	FID, 250° C

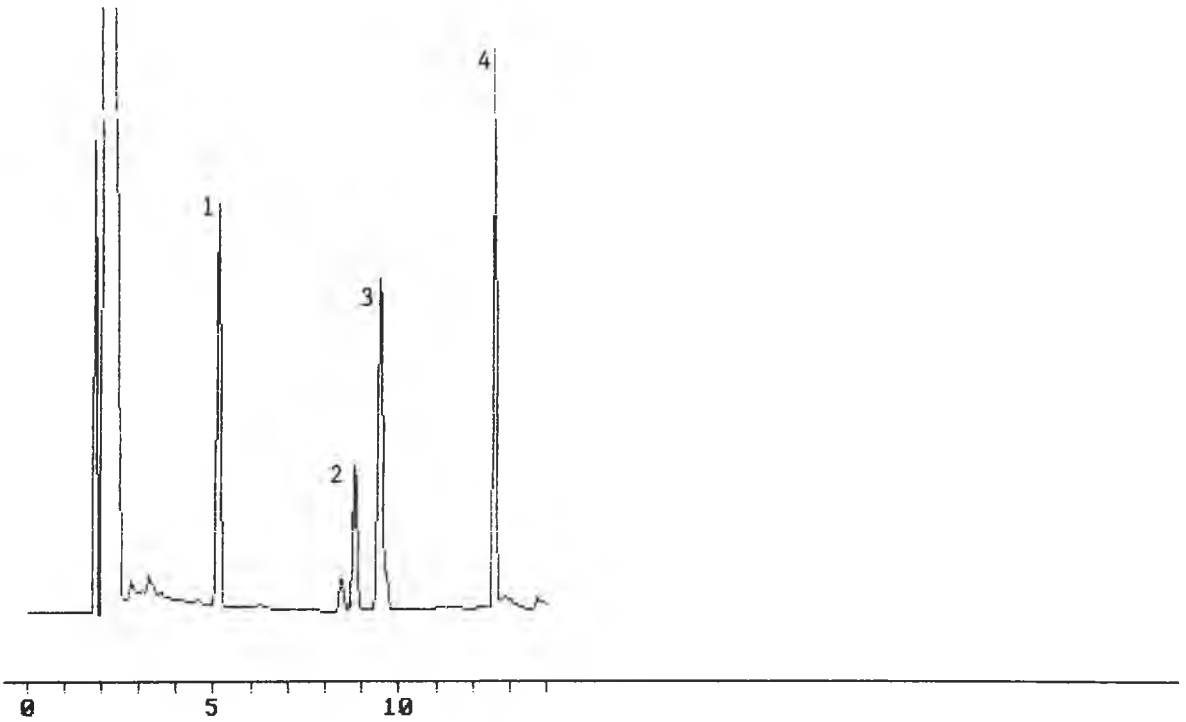

1. **Toluene**
2. **M-xylene**
3. **Styrene**
4. **Decane**

Figure 7.131 GC printout of EB-5000 coagulated sample at 500 ppm hydrocarbon concentrations.

Column:	**DB-5**, 30m x 0.45 mm I.D., 1.27 μm
Carrier:	helium at 6.5 mL/min
Oven:	35°C for 6 min., 35-55 at 4° C/min
	55°C for 3 min., 55-105 at 17° C/min
Injector:	Direct injection liner with two restrictions 250° C
Detector:	FID, 250° C

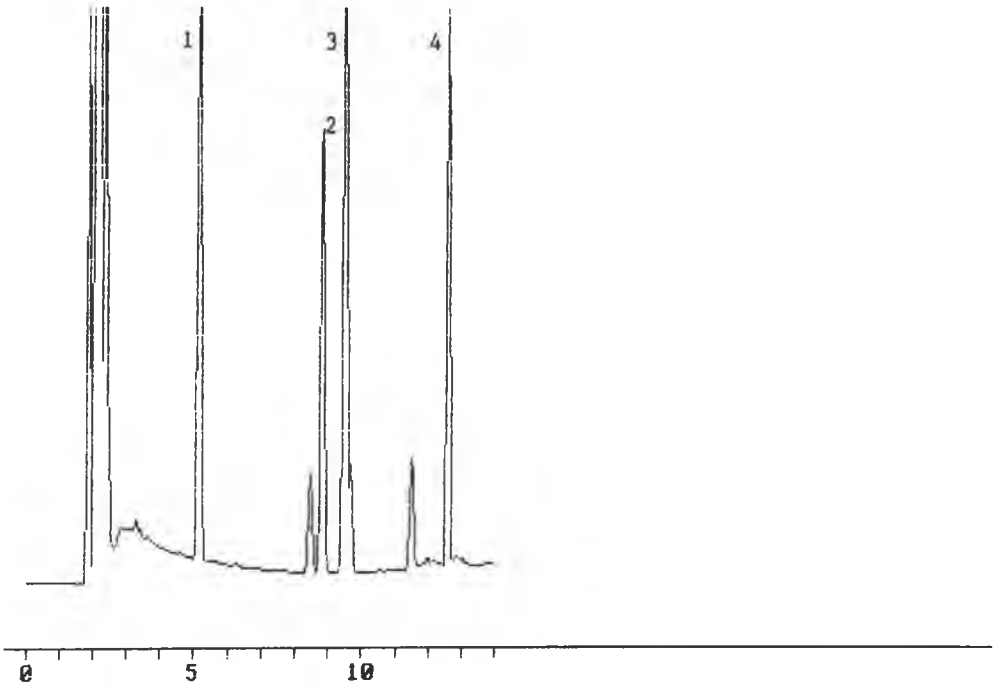

1. **Toluene**
2. **M-xylene**
3. **Styrene**
4. **Decane**

Figure 7.132 GC printout of noncoagulated sample at concentration of 300 ppm, hydrocarbon-water mixture.

Column:	**DB-5**, 30m x 0.45 mm I.D., 1.27 μm
Carrier:	helium at 6.5 mL/min
Oven:	35°C for 6 min., 35-55 at 4° C/min
	55°C for 3 min., 55-105 at 17° C/min
Injector:	Direct injection liner with two restrictions 250° C
Detector:	FID, 250° C

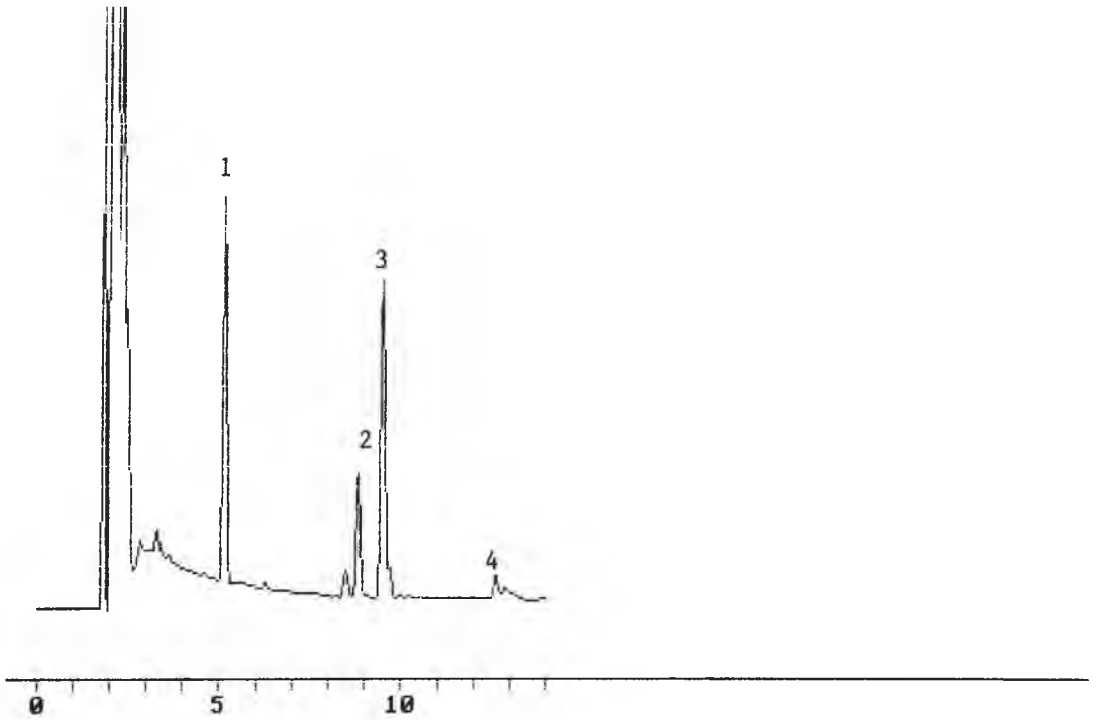

1. **Toluene**
2. **M-xylene**
3. **Styrene**
4. **Decane**

Figure 7.133 GC printout of Cat-Floc 2953 coagulated sample at 300 ppm concentration of hydrocarbon-water mixture.

Column:	**DB-5**, 30m x 0.45 mm I.D., 1.27 μm
Carrier:	helium at 6.5 mL/min
Oven:	35°C for 6 min., 35-55 at 4° C/min
	55°C for 3 min., 55-105 at 17° C/min
Injector:	Direct injection liner with two restrictions 250° C
Detector:	FID, 250° C

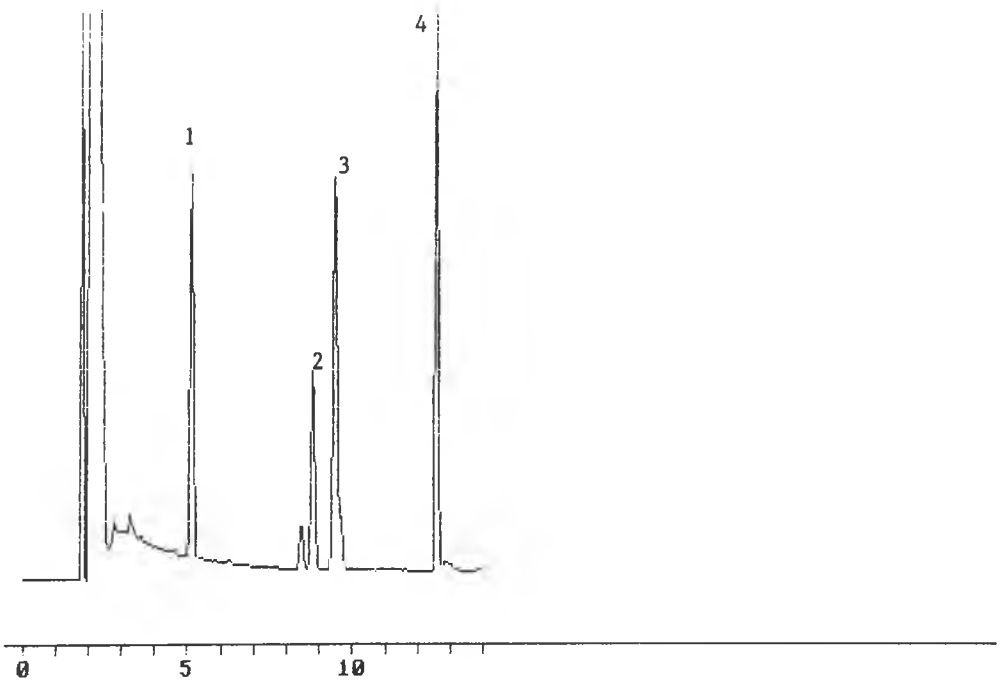

5. **Toluene**
6. **M-xylene**
7. **Styrene**
8. **Decane**

Figure 7.134 GC printout of EB-5000 coagulated sample at 300 ppm concentration of hydrocarbon-water mixture.

Column:	**DB-1**, 30m x 0.53 mm I.D., 1.5 μm
Carrier:	helium at 6.5 mL/min
Oven:	30°C for 6 min., 30-130 at 6° C/min
	130-180°C for 8 min., at 15° C/min
	180-200°C at 25° C/min
Injector:	Direct injection liner with two restrictions 250° C
Detector:	FID, 250° C

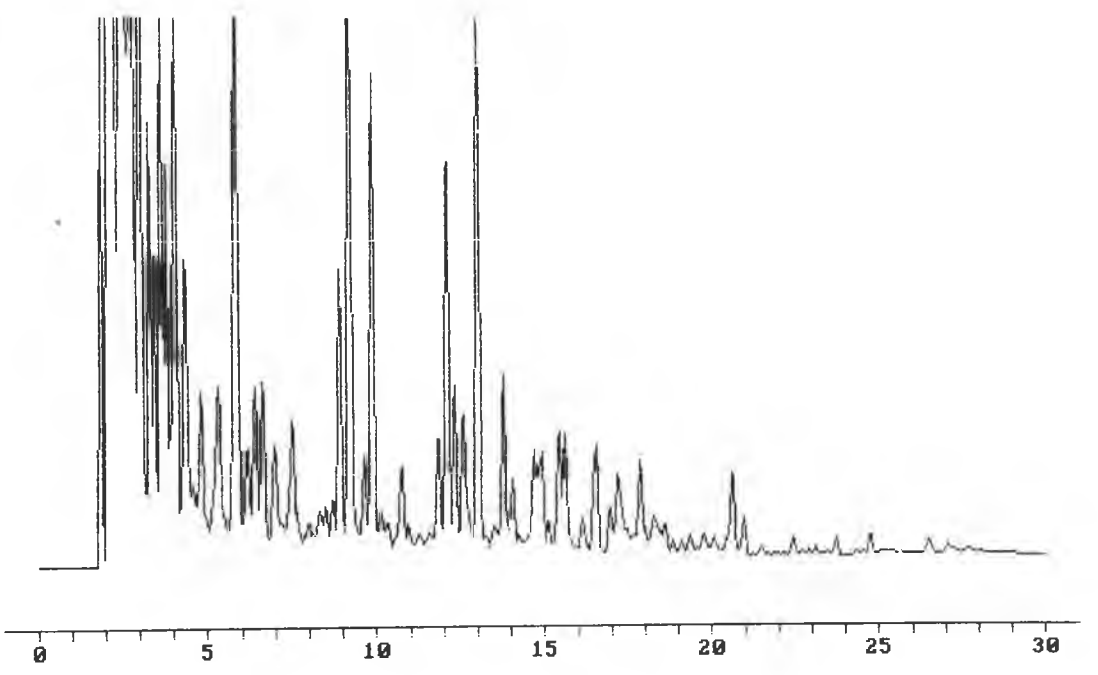

Figure 7.135 GC printout of noncoagulated sample at concentration of 500 ppm, gasoline-water mixture.

Column:	**DB-5**, 30m x 0.45 mm I.D., 1.27 μm
Carrier:	helium at 6.5 mL/min
Oven:	35°C for 6 min., 35-55 at 4° C/min
	55°C for 3 min., 55-105 at 17° C/min
Injector:	Direct injection liner with two restrictions 250° C
Detector:	FID, 250° C

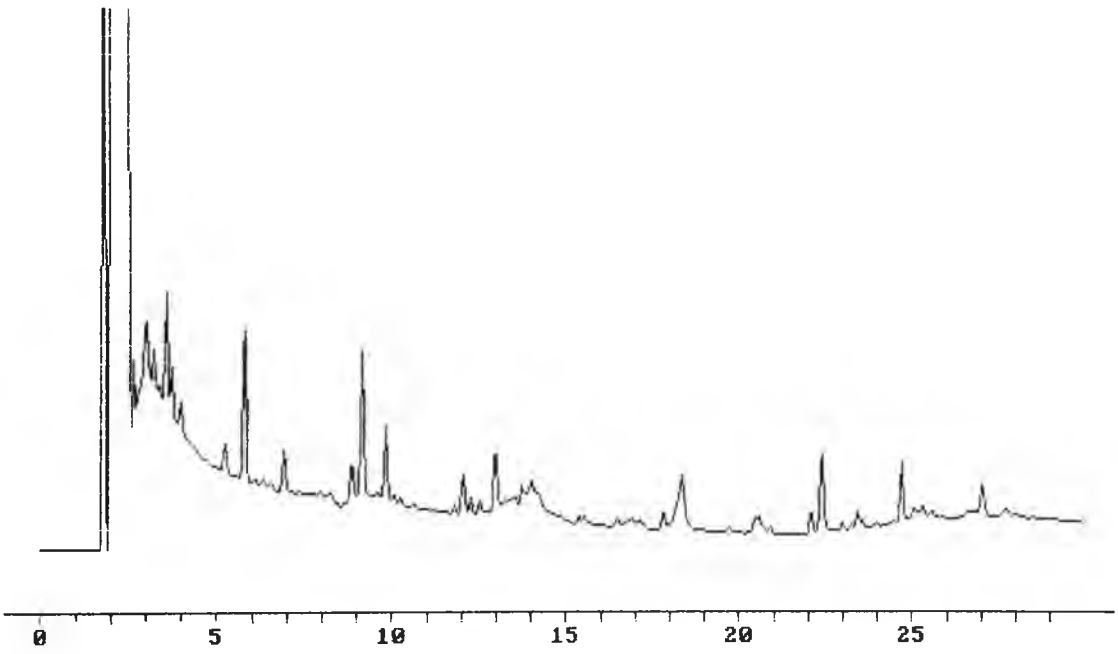

Figure 7.136 GC printout of Cat-Floc coagulated sample at concentration of 500 ppm, gasoline-water mixture.

Column:	**DB-1**, 30m x 0.53 mm I.D., 1.5 μm
Carrier:	helium at 6.5 mL/min
Oven:	30°C for 6 min., 30-130 at 6° C/min
	130-180°C for 8 min., at 15° C/min
	180-200°C at 25° C/min
Injector:	Direct injection liner with two restrictions 250° C
Detector:	FID, 250° C

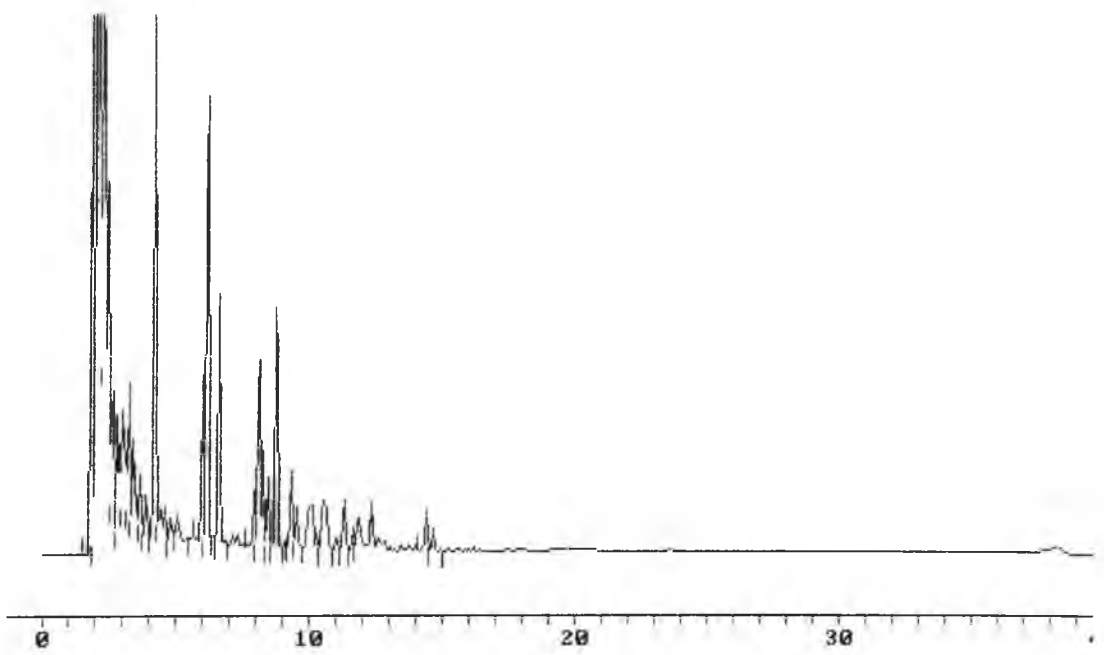

Figure 7.137 GC printout of EB-5000 coagulated sample at concentration of 500 ppm, gasoline-water mixture.

Column:	**DB-1**, 30m x 0.53 mm I.D., 1.5 μm
Carrier:	helium at 6.5 mL/min
Oven:	30°C for 6 min., 30-130 at 6° C/min
	130-180°C for 8 min., at 15° C/min
	180-200°C, at 25° C/min
Injector:	Direct injection liner with two restrictions 250° C
Detector:	FID, 250° C

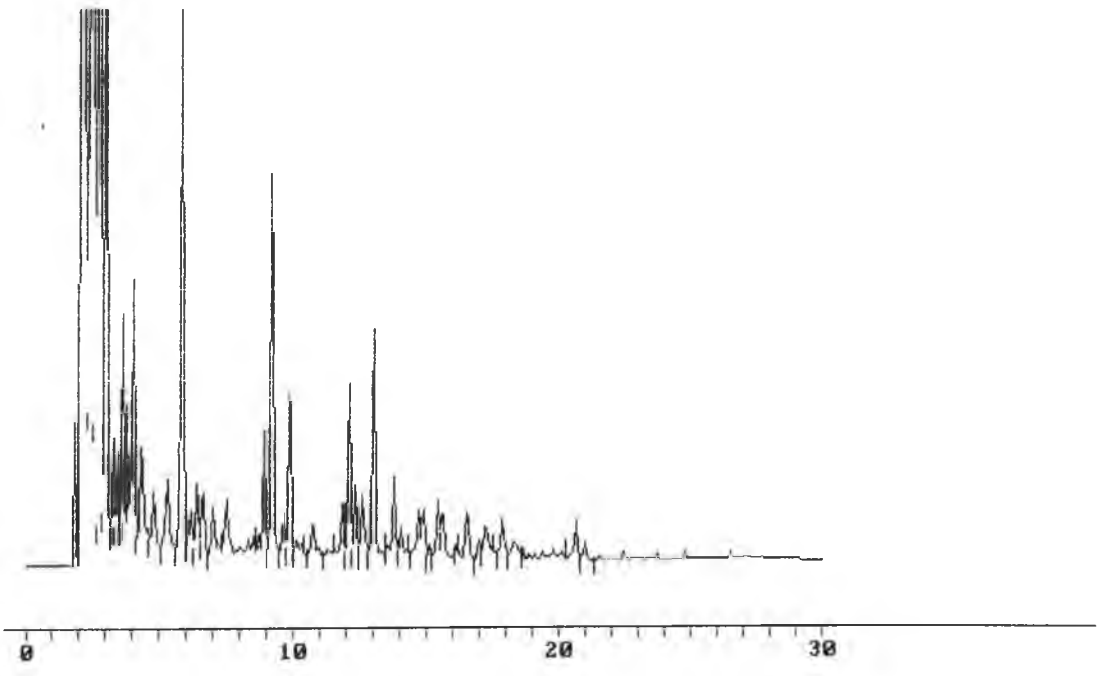

Figure 7.138 GC printout of noncoagulated sample at concentration of 300 ppm, gasoline-water mixture.

Column:	**DB-1**, 30m x 0.53 mm I.D., 1.5 μm
Carrier:	helium at 6.5 mL/min
Oven:	30°C for 6 min., 30-130 at 6° C/min
	130-180°C for 8 min., at 15° C/min
	180-200°C, at 25° C/min
Injector:	Direct injection liner with two restrictions 250° C
Detector:	FID, 250° C

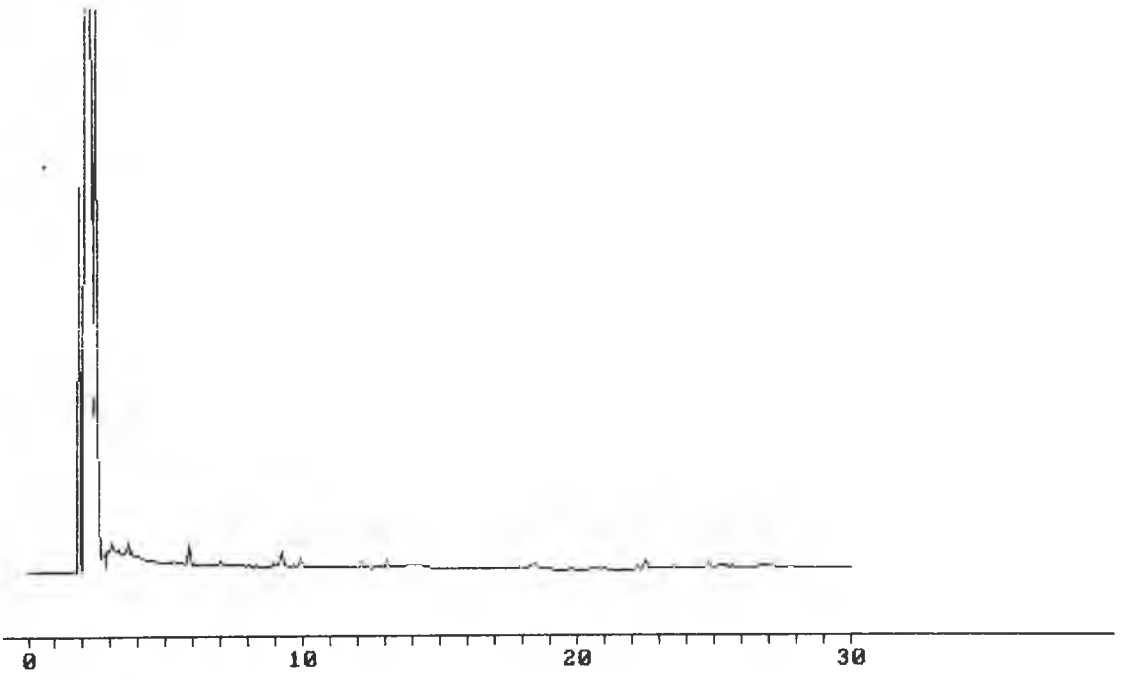

Figure 7.139 GC printout of Cat-Floc 2953 coagulated sample at concentration of 300 ppm, gasoline-water mixture.

Column:	**DB-1**, 30m x 0.53 mm I.D., 1.5 μm
Carrier:	helium at 6.5 mL/min
Oven:	30°C for 6 min., 30-130 at 6° C/min
	130-180°C for 8 min., at 15° C/min
	180-200°C, at 25° C/min
Injector:	Direct injection liner with two restrictions 250° C
Detector:	FID, 250° C

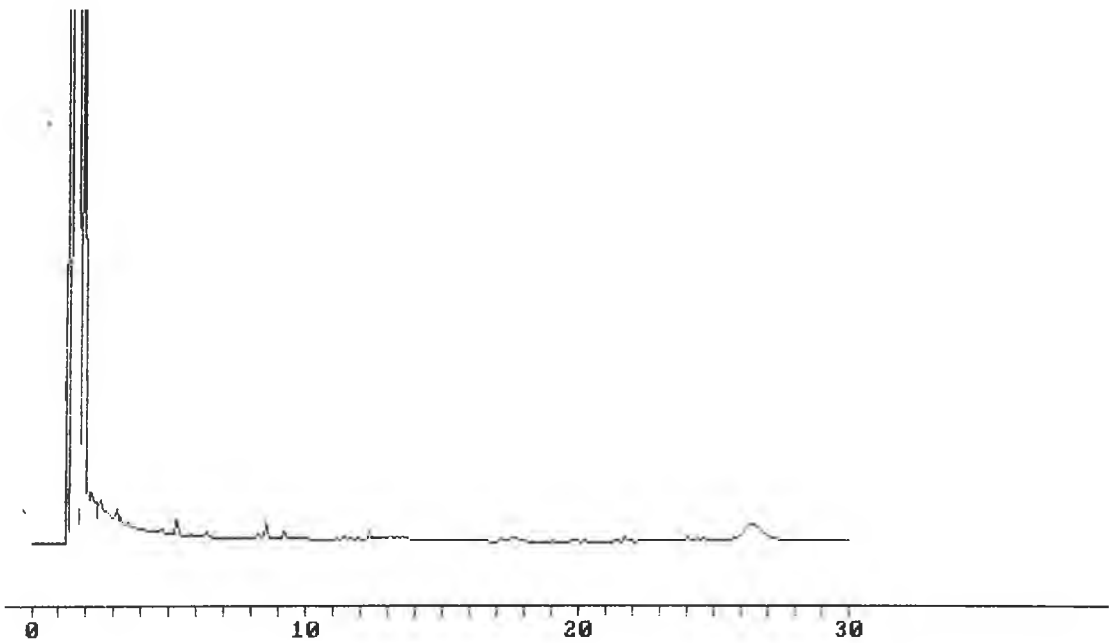

Figure 7.140 GC printout of EB-5000 coagulated sample at concentration of 300 ppm, gasoline-water mixture.

7.3. Settling characteristics

Settling velocity and porosity increases with the floc size while density decreases due to formation of additional pores by linking to other particles and flocs. Average settling velocity vectors are presented in Table 7.2. Figures 7.141 to 7.200 showed velocity profiles, cross-correlation velocity profiles and flow direction of flocs.

Overall findings complied with findings of other researchers, that addition of polymer can have profound effect on development of both, floc size and settling rate. Settling velocity increases with the floc size while density decreases with increase in floc size. Estimated floc density results, for both polymers Cat-Floc 2953 and EB-5000, are presented on Figure 7.201.

Table 7.2. Diameters, settling velocities and densities of the flocs.

Compound	Coagulant	Diameter x10^{-6} (m)	Average settling velocity (m/s)	Estimated floc density (kg/m^3)
Decane*500	CF- 2953	395.05	0.003	1033.03
Decane*500	EB-5000	344.73	0.002	1028.56
Decane*300	CF- 2953	228.68	0.007	1241.38
Decane*300	EB-5000	156.84	0.004	1293.65
Toluene*500	CF- 2953	241.12	0.008	1248.18
Toluene*500	EB-5000	260.90	0.016	1425.38
Toluene*300	CF- 2953	235.95	0.005	1161.29
Toluene*300	EB-5000	300.00	0.023	1462.65
Styrene*500	CF- 2953	343.50	0.005	1075.04
Styrene*500	EB-5000	295.00	0.005	1102.46
Styrene*300	CF- 2953	335.94	0.003	1046.60
Styrene*300	EB-5000	283.68	0.003	1065.78
m-xylene*500	CF- 2953	271.00	0.014	1344.60
m-xylene*500	EB-5000	171.00	0.005	1306.26
m-xylene*300	CF- 2953	234.43	0.004	1130.33
m-xylene*300	EB-5000	220.60	0.004	1147.75
Gasoline*500	CF- 2953	403.16	0.006	1065.12
Gasoline*500	EB-5000	250.49	0.001	1029.98
Gasoline*300	CF- 2953	326.06	0.006	1100.6
Gasoline*300	EB-5000	207.86	0.006	1250.49

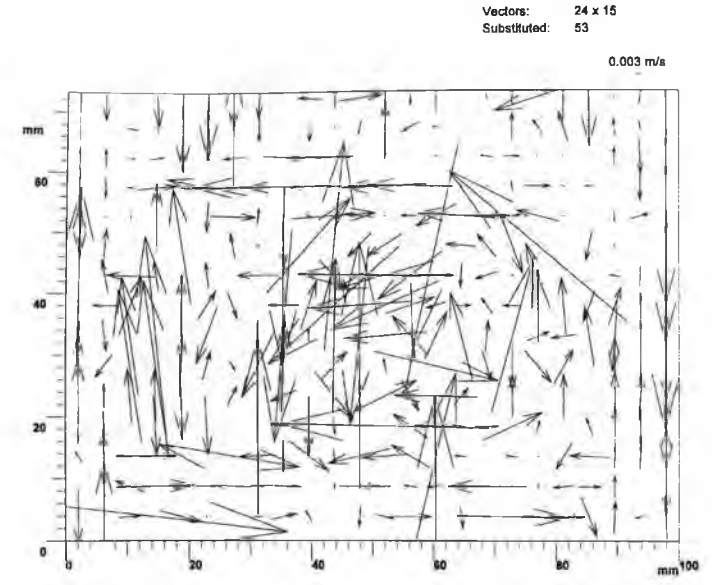

Figure 7.141 Average settling velocity vectors of Decane at concentration of 500 ppm, coagulated with Cat-Floc 2953.

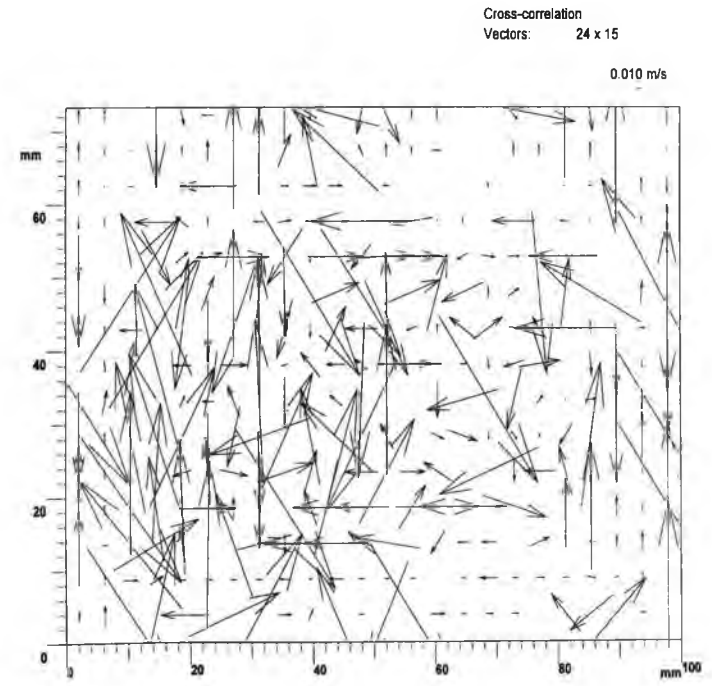

Figure 7.142 Cross-correlation velocity vectors of Decane at concentration of 500 ppm, coagulated with Cat-Floc 2953.

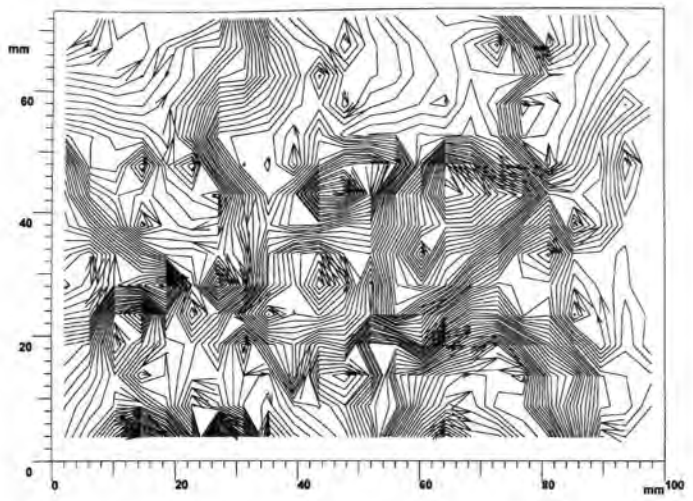

Figure 7.143 Flow direction of Decane flocs at concentration of 500 ppm, coagulated with Cat-Floc 2953.

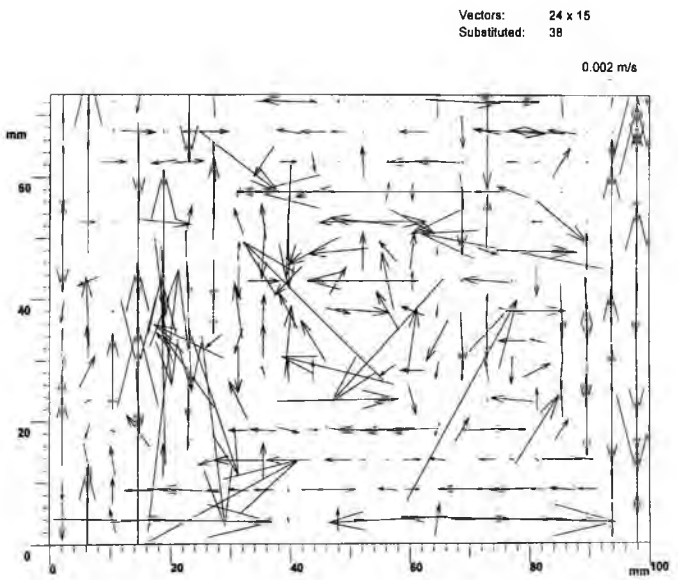

Figure 7.144 Average settling velocity vectors of Decane at concentration of 500 ppm, coagulated with EB-5000.

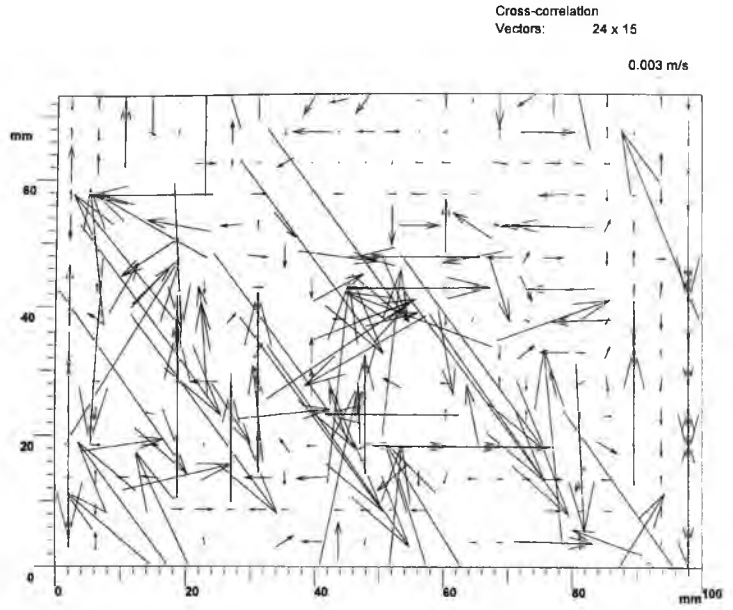

Figure 7.145 Cross-correlation velocity vectors of Decane at concentration of 500 ppm, coagulated with EB-5000.

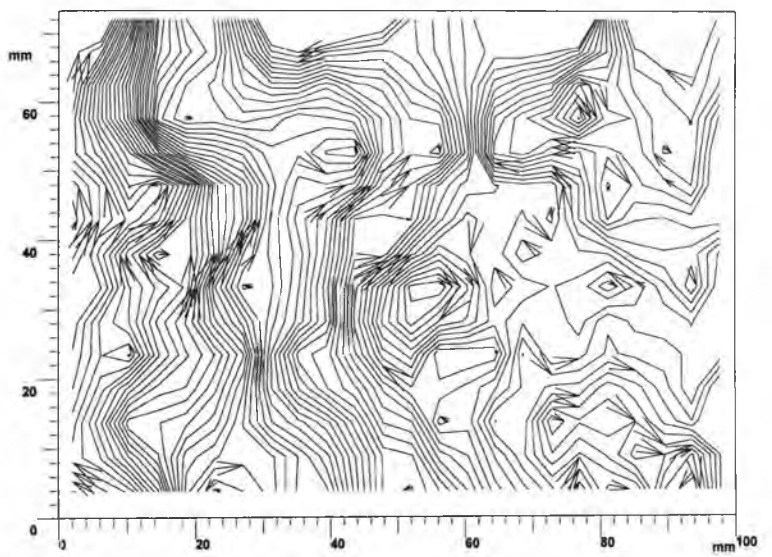

Figure 7.146 Flow direction of Decane flocs at concentration of 500 ppm, coagulated with EB-5000.

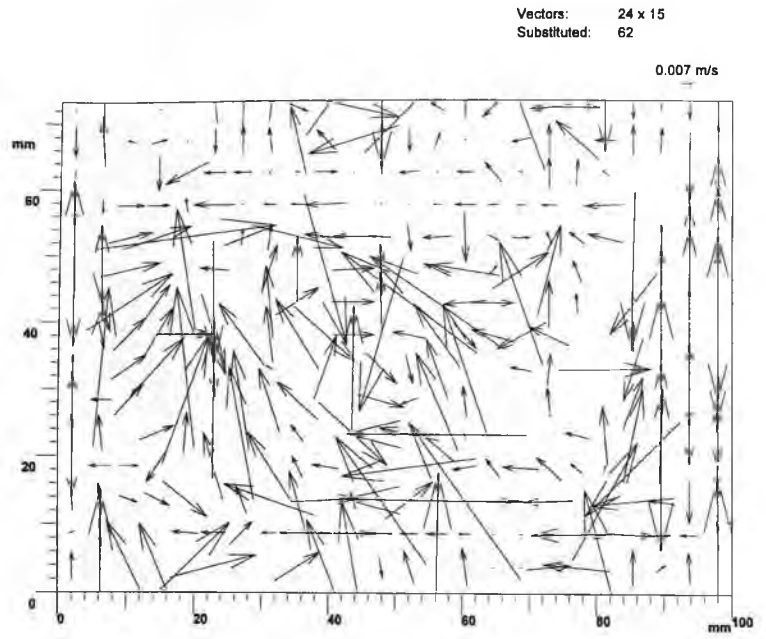

Figure 7.147 Average settling velocity vectors of Decane at concentration of 300 ppm, coagulated with Cat-Floc 2953.

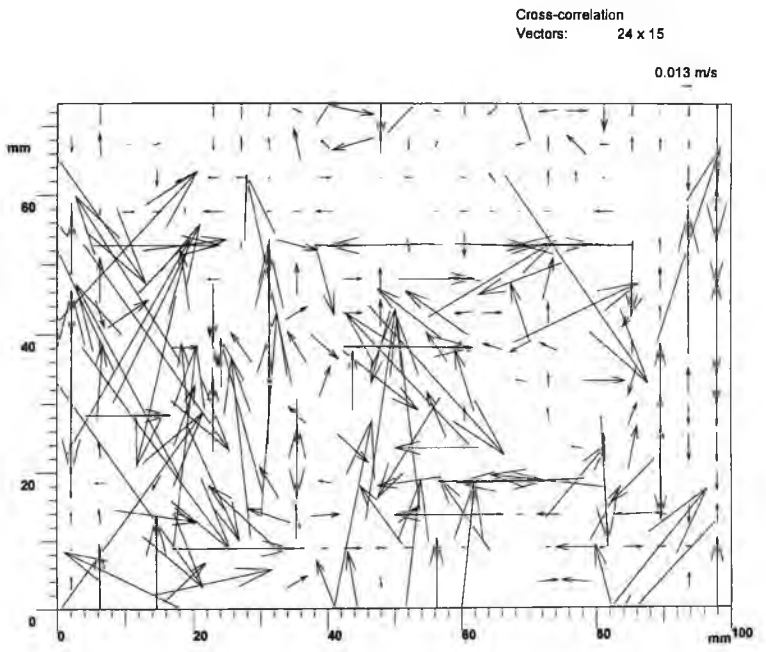

Figure 7.148 Cross-correlation velocity vectors of Decane at concentration of 300 ppm, coagulated with Cat-Floc 2953.

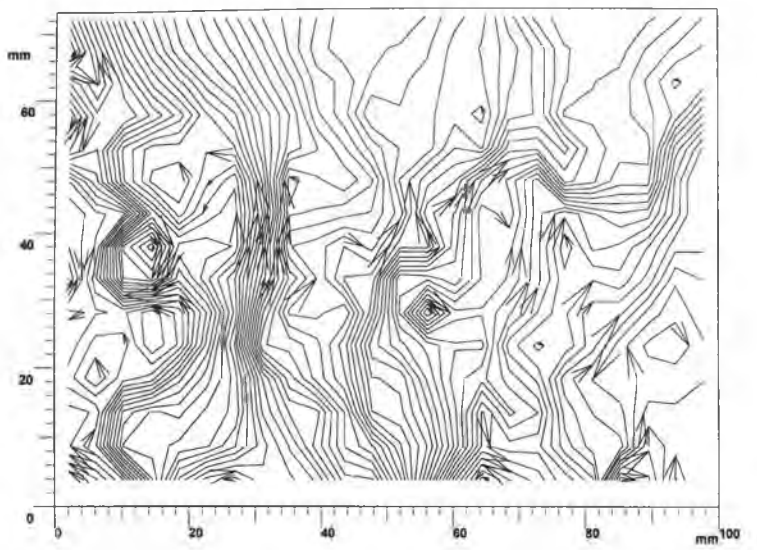

Figure 7.149 Flow direction of Decane flocs at concentration of 300 ppm, coagulated with Cat-Floc 2953.

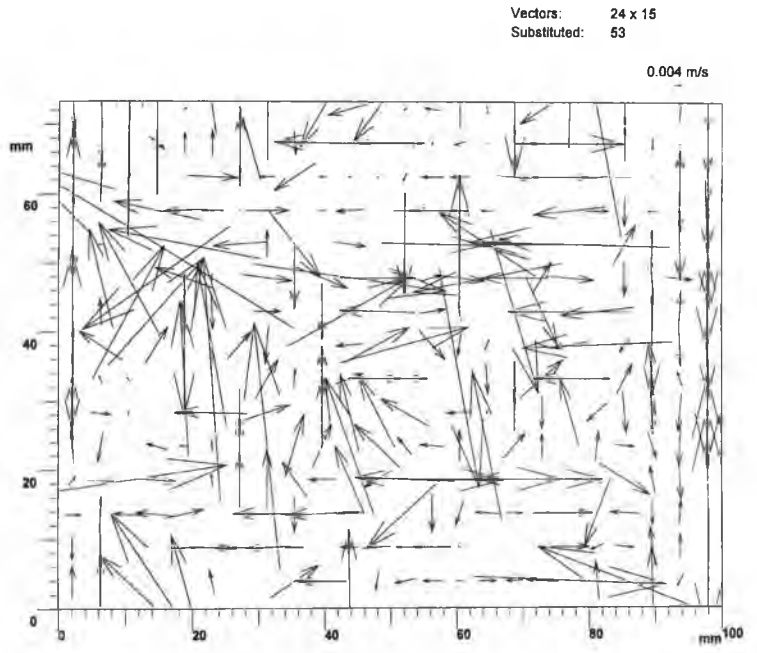

Figure 7.150 Average settling velocity vectors of Decane at concentration of 300 ppm, coagulated with EB-5000.

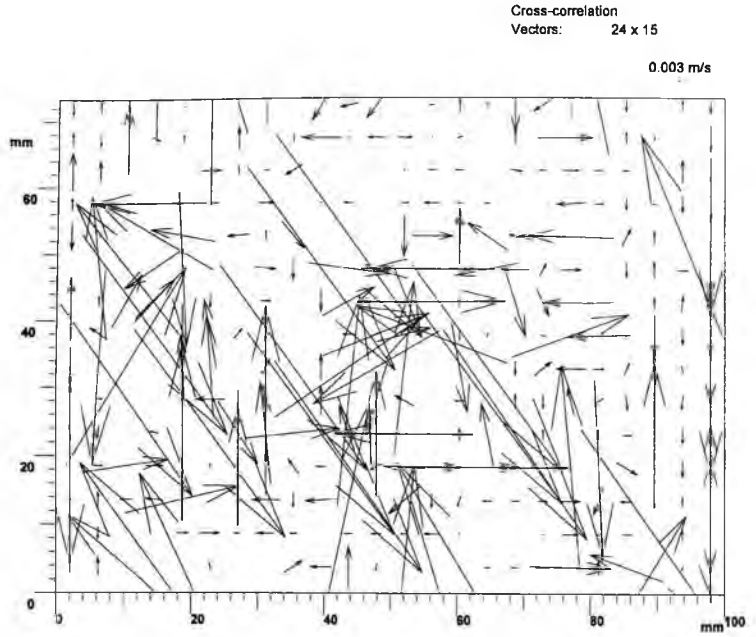

Figure 7.151 Cross-correlation velocity vectors of Decane at concentration of 300 ppm, coagulated with EB-5000.

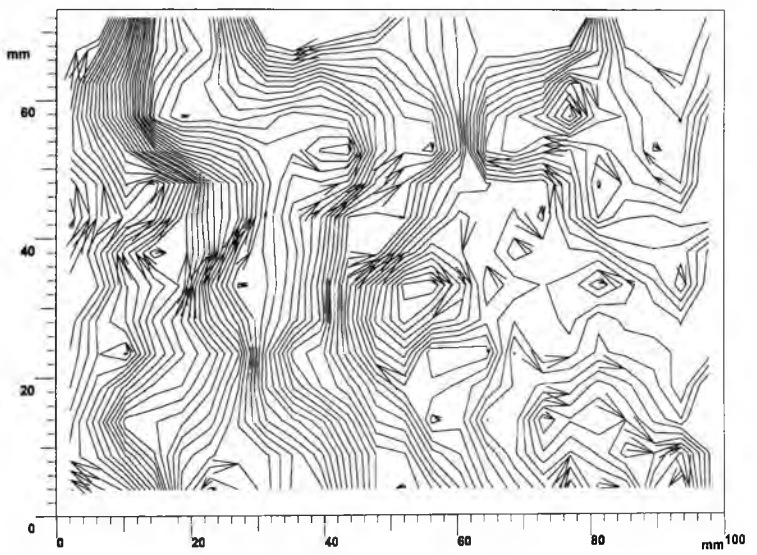

Figure 7.152 Flow direction of Decane flocs at concentration of 300 ppm, coagulated with EB-5000.

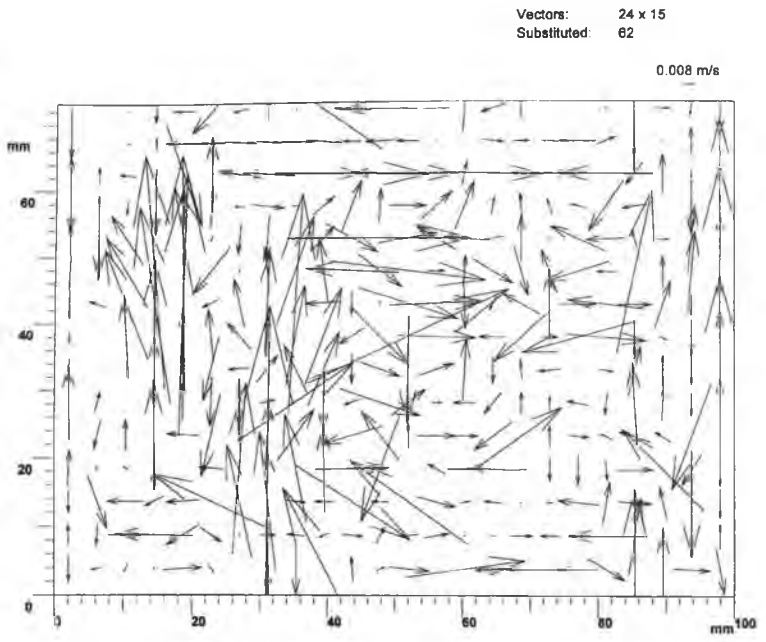

Figure 7.153 Average settling velocity of Toluene at concentration of 500 ppm, coagulated with Cat-Floc 2953.

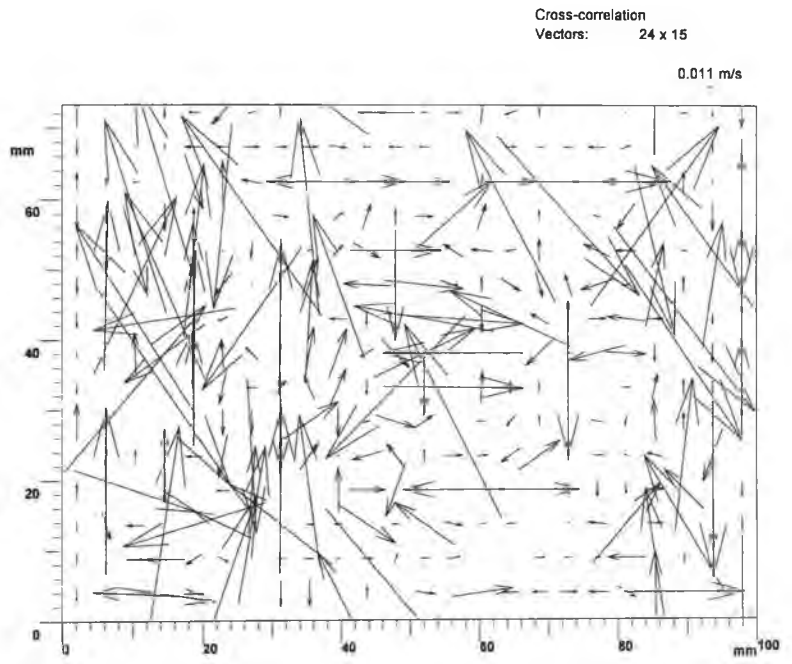

Figure 7.154 Cross-correlation velocity vectors of Toluene at concentration of 500 ppm, coagulated with Cat-Floc 2953.

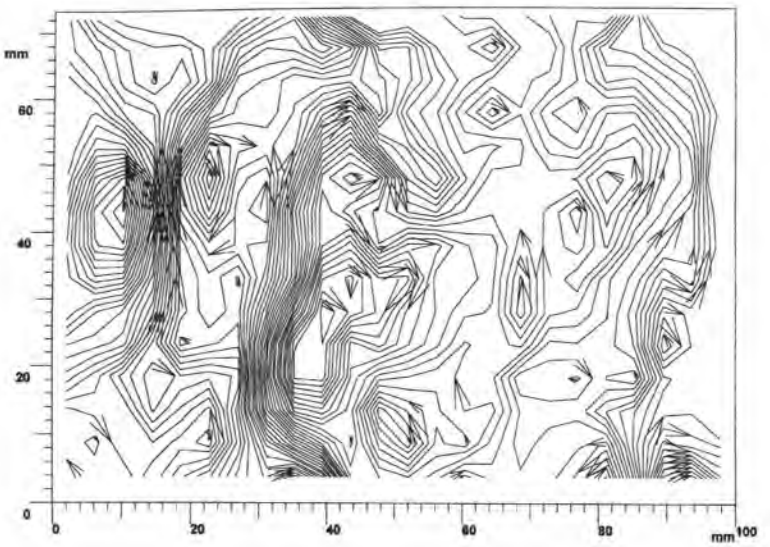

Figure 7.155 Flow direction of Toluene flocs at concentration of 500 ppm, coagulated with Cat-Floc 2953.

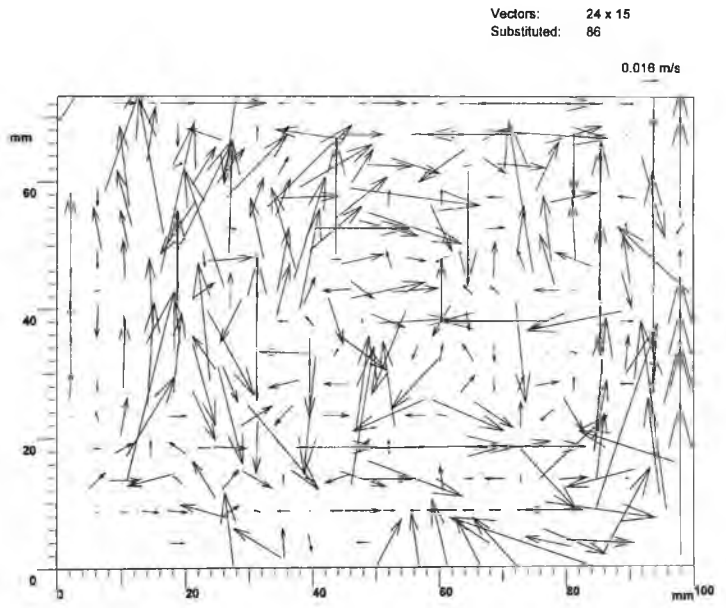

Figure 7.156 Average settling velocity vectors of Toluene at concentration of 500 ppm, coagulated with EB-5000.

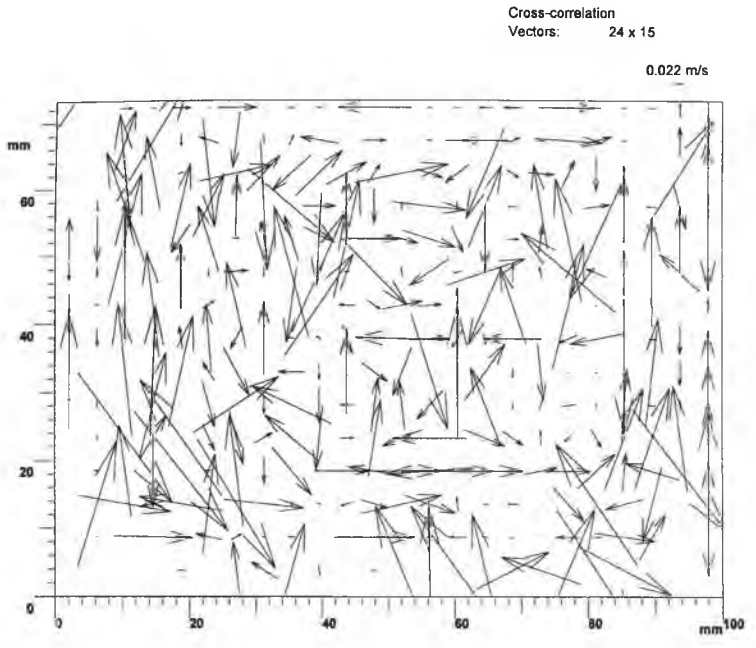

Figure 7.157 Cross-correlation velocity vectors of Toluene at concentration of 500 ppm, coagulated with EB-500.

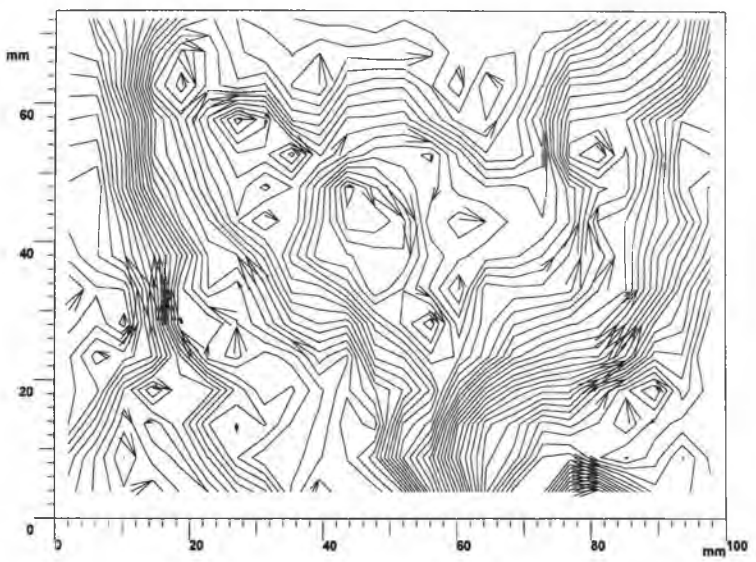

Figure 7.158 Flow direction of Toluene flocs at concentration of 500 ppm, coagulated with EB-5000.

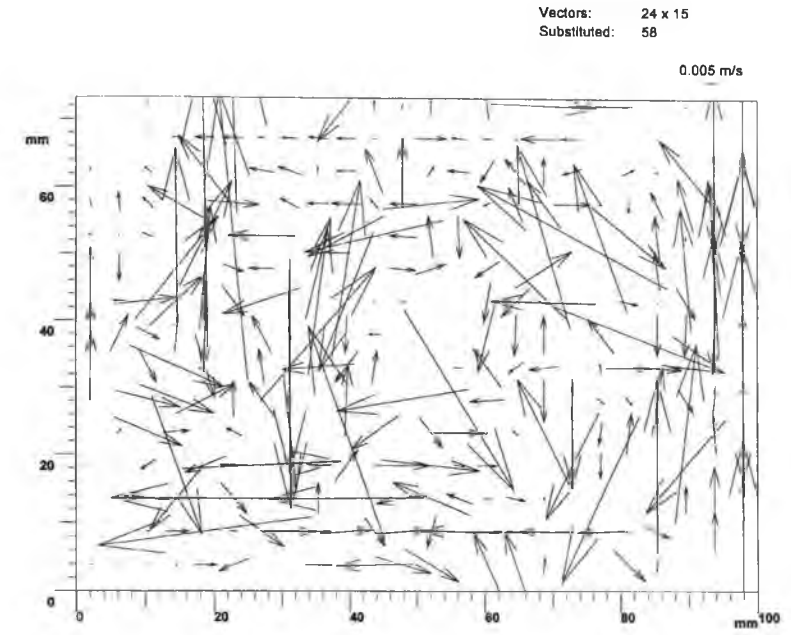

Figure 7.159 Average settling velocity vectors of toluene at concentration of 300 ppm, coagulated with Cat-Floc 2953.

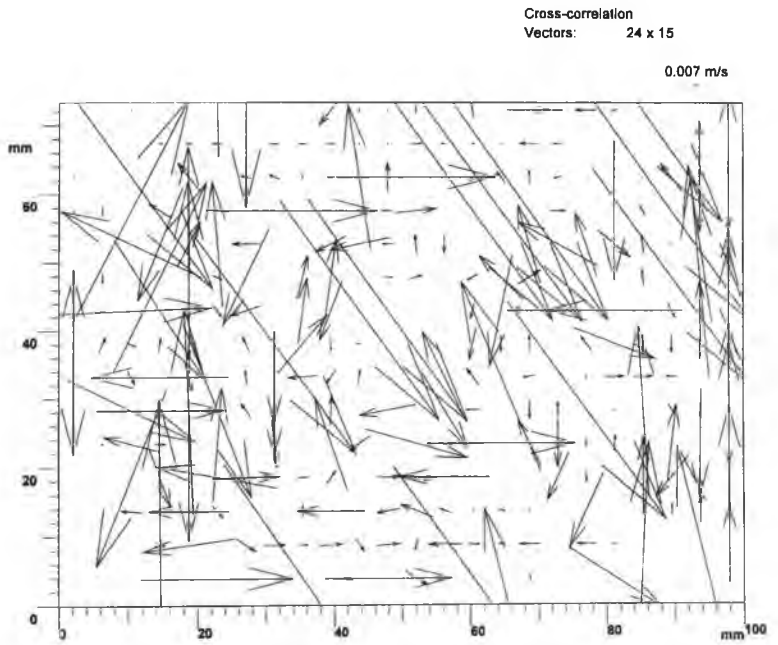

Figure 7.160 Cross-correlation velocity vectors of Toluene at concentration of 300 ppm, coagulated with Cat-Floc 2953.

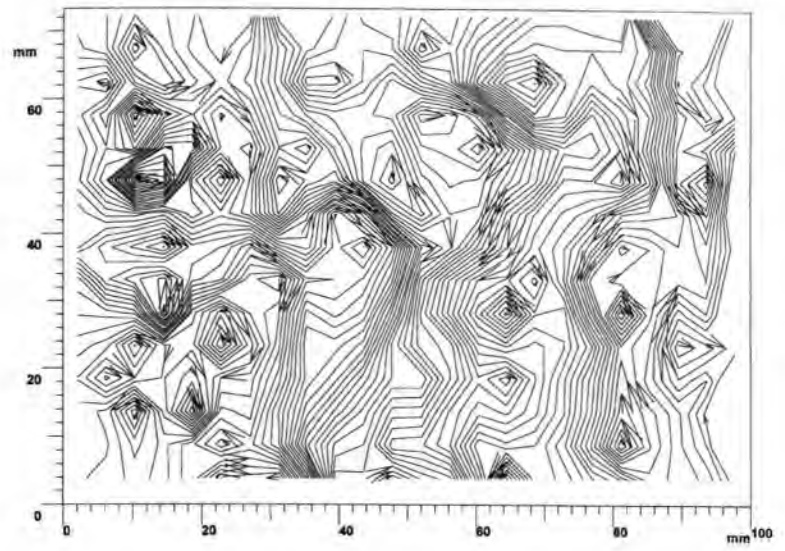

Figure 7.161 Flow direction of Toluene flocs at concentration of 300 ppm, coagulated with Cat-Floc 2953.

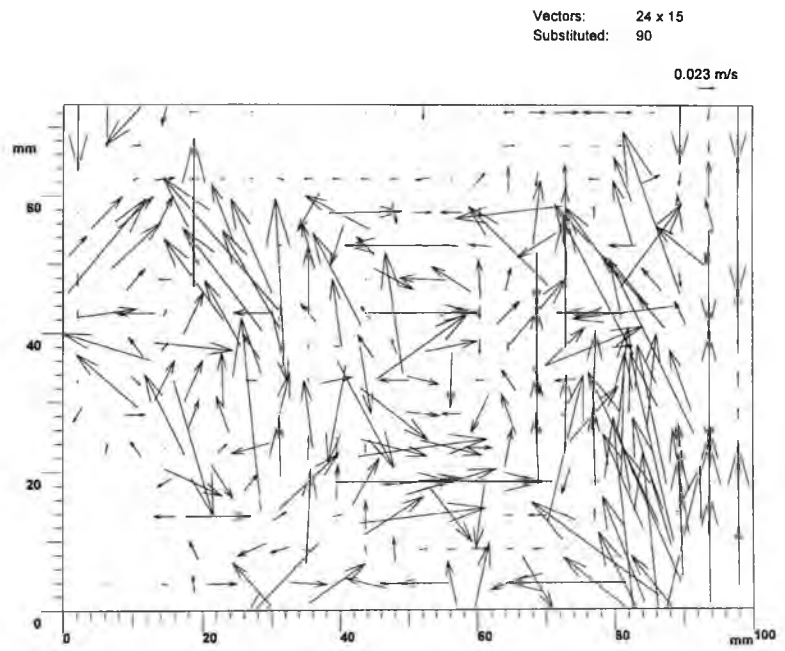

Figure 7. 162 Average settling velocity vectors of Toluene at concentration of 300 ppm, coagulated with EB-5000.

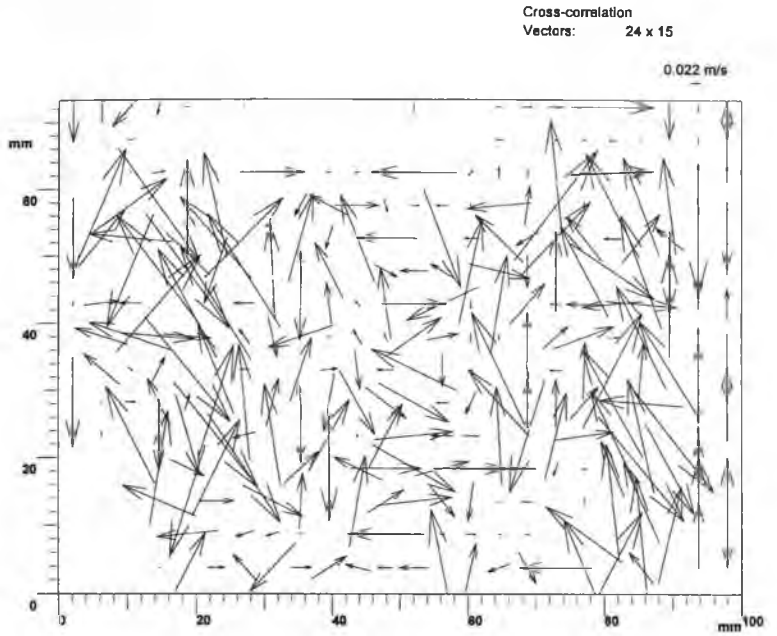

Figure 7.163 Cross-correlation velocity vectors of Toluene at concentration of 300 ppm, coagulated with EB-5000.

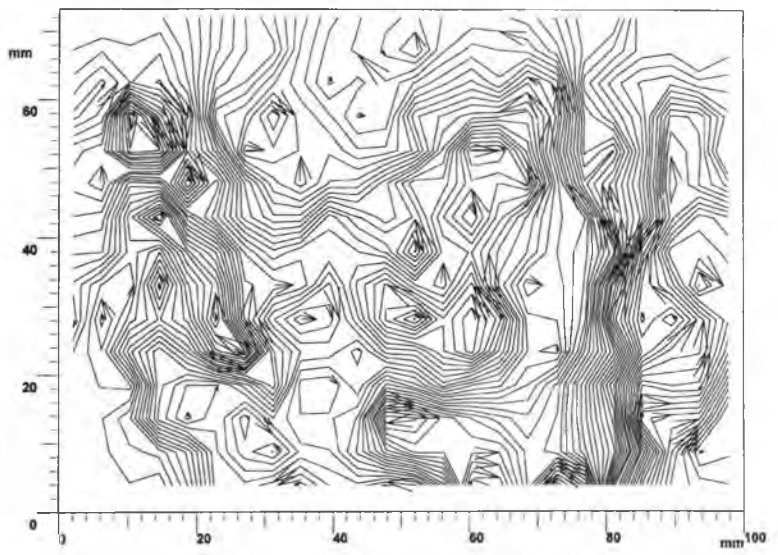

Figure 7.164 Flow direction of Toluene at concentration of 300 ppm, coagulated with EB-5000.

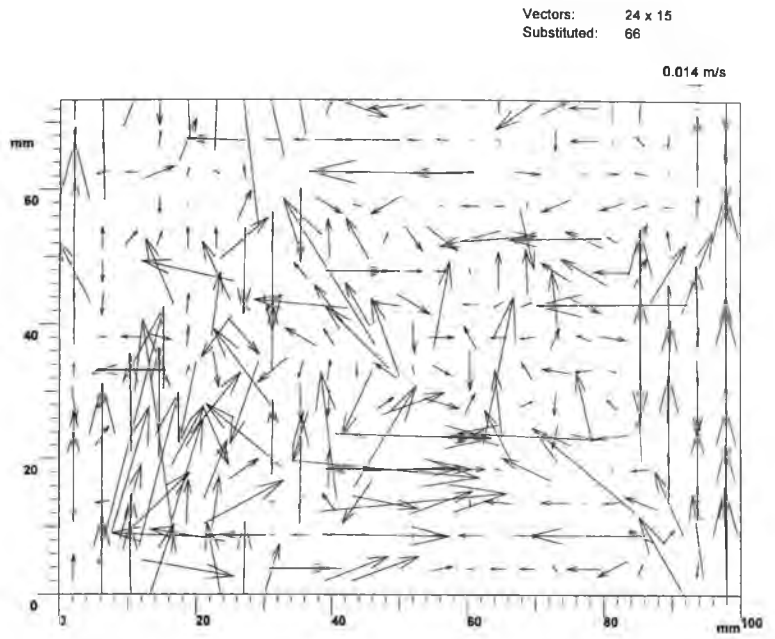

Figure 7.165 Average settling velocity vectors of m-xylene at concentration of 500 ppm, coagulated with Cat-Floc 2953.

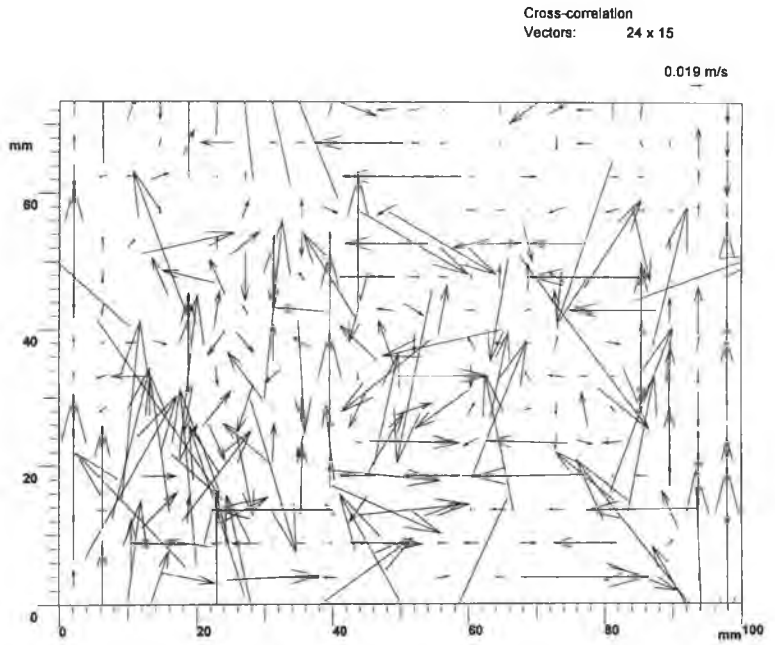

Figure 7. 166 Cross-correlation velocity vectors of m-xylene at concentration of 500 ppm, coagulated with Cat-Floc 2953.

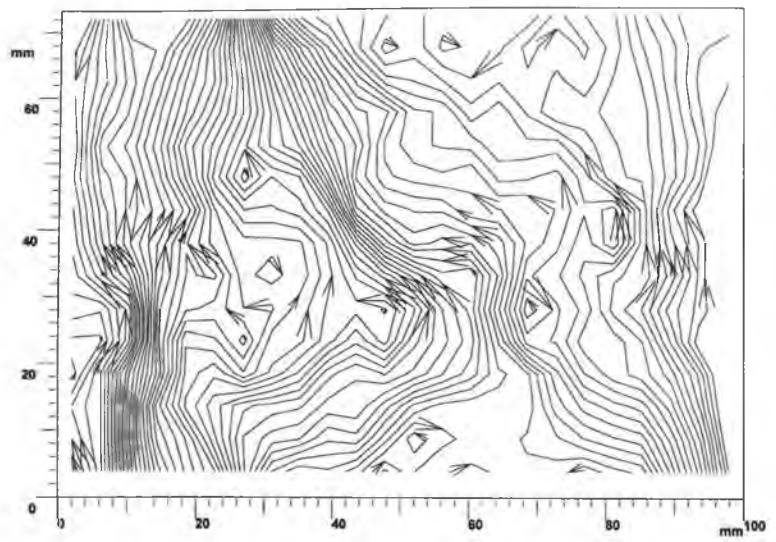

Figure 7.167 Flow direction of m-xylene flocs at concentration of 500 ppm, coagulated with Cat-Floc 2953.

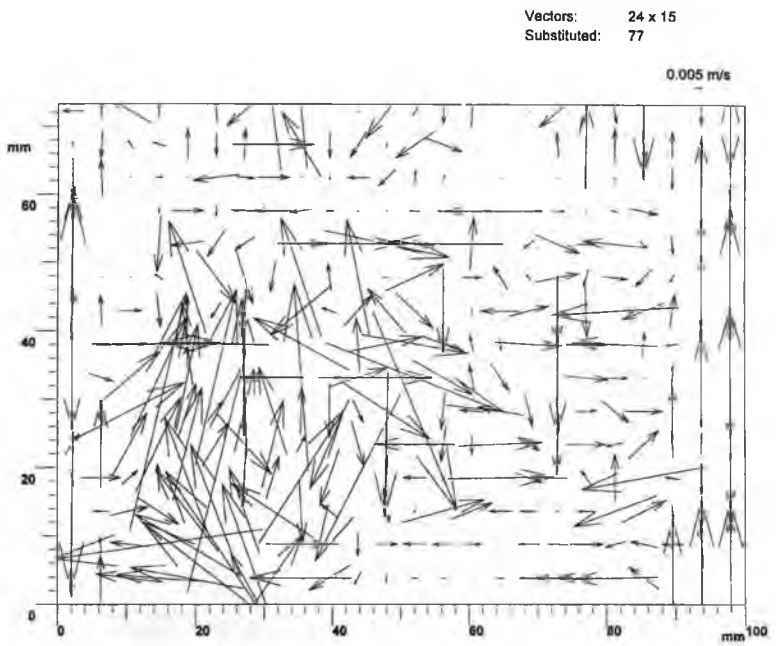

Figure 7.168 Average settling velocity vectors of m-xylene at concentration of 500 ppm, coagulated with EB-5000.

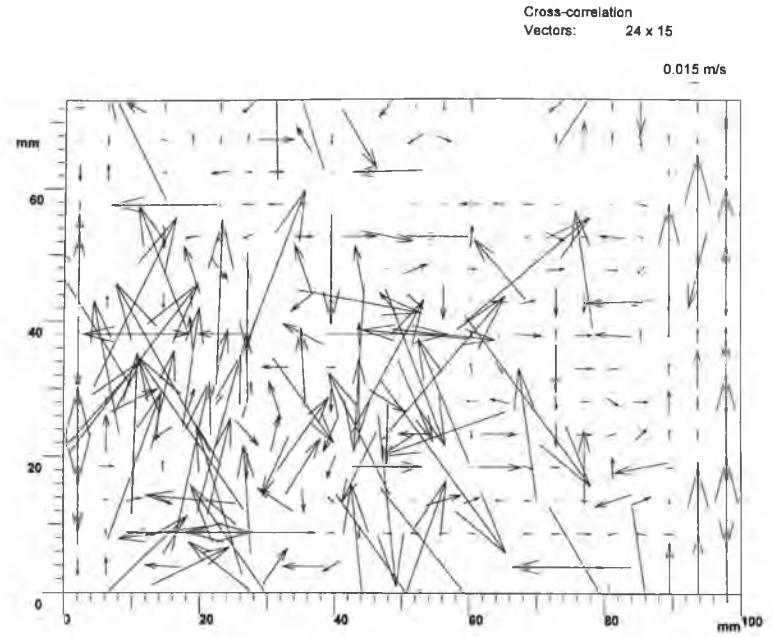

Figure 7.169 Cross-correlation velocity vectors of m-xylene at concentration of 500 ppm, coagulated with EB-5000.

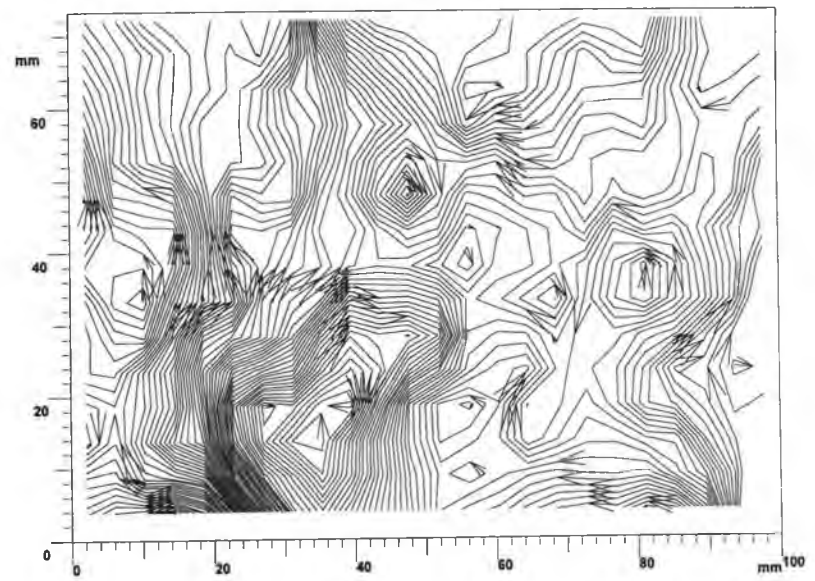

Figure 7.170 Flow direction of m-xylene flocs at concentration of 500 ppm, coagulated with EB-5000.

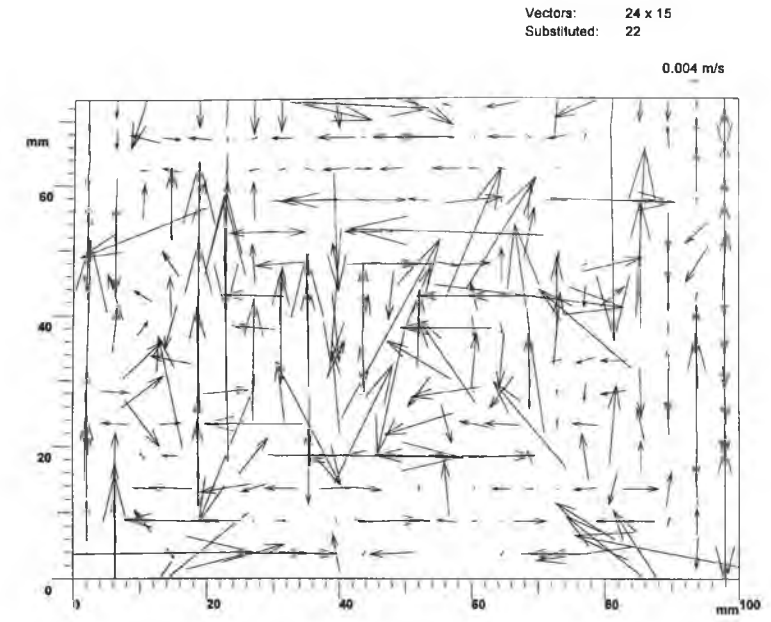

Figure 7.171 Average settling velocity vectors of m-xylene at concentration of 300 ppm, coagulated with Cat-Floc 2953.

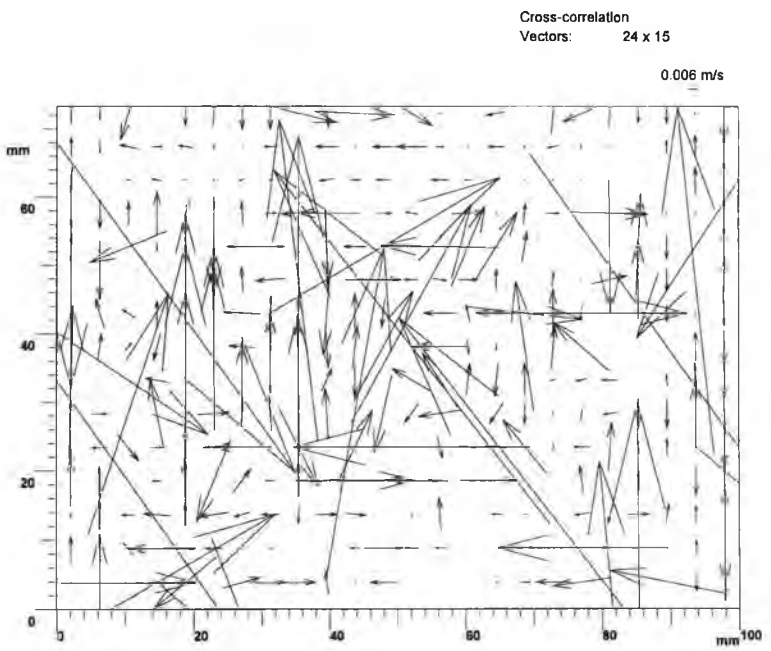

Figure 7.172 Cross-correlation velocity vectors of m-xylene at concentration of 300ppm, coagulated Cat-Floc 2953.

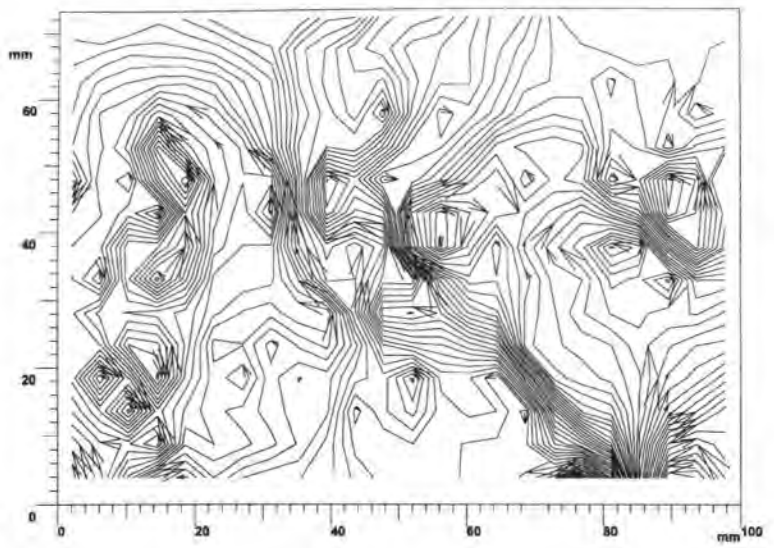

Figure 7.173 Flow direction of m-xylene at concentration of 300 ppm, coagulated with Cat-Floc 2953.

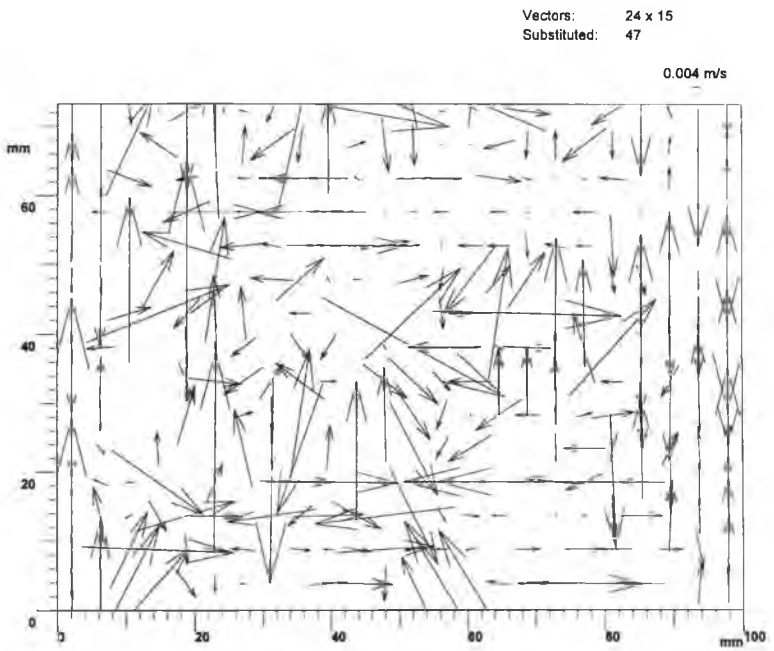

Figure 7.174 Average settling velocity vectors of m-xylene at concentration of 300 ppm, coagulated with EB-5000.

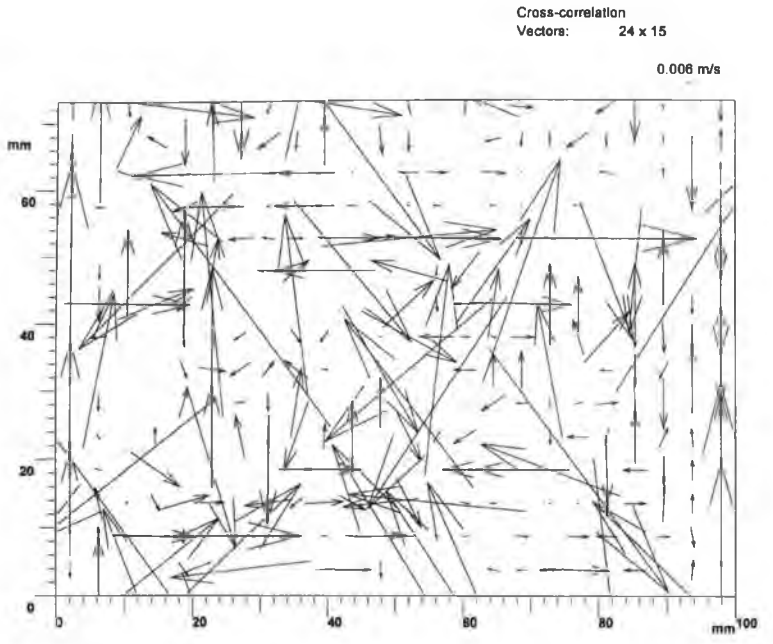

Figure 7.175 Cross-correlation velocity vectors of m-xylene at concentration of 300 ppm, coagulated with EB-5000.

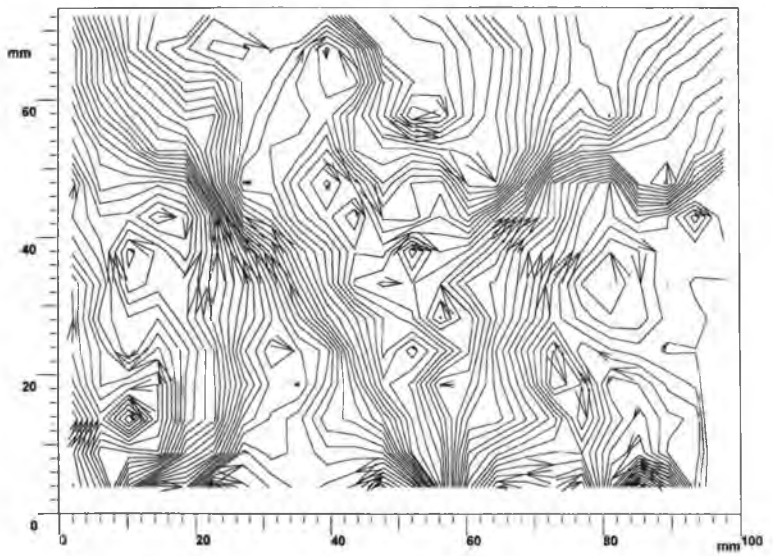

Figure 7. 176 Flow direction of m-xylene flocs at concentration of 300 ppm, coagulated with EB-5000.

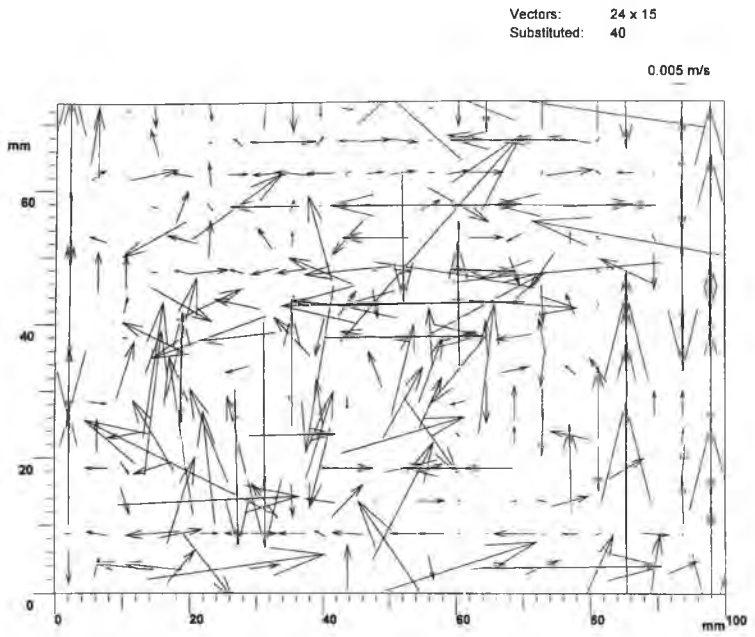

Figure 7.173 Average settling velocity vectors of Styrene at concentration of 500 ppm, coagulated with Cat-Floc 2953.

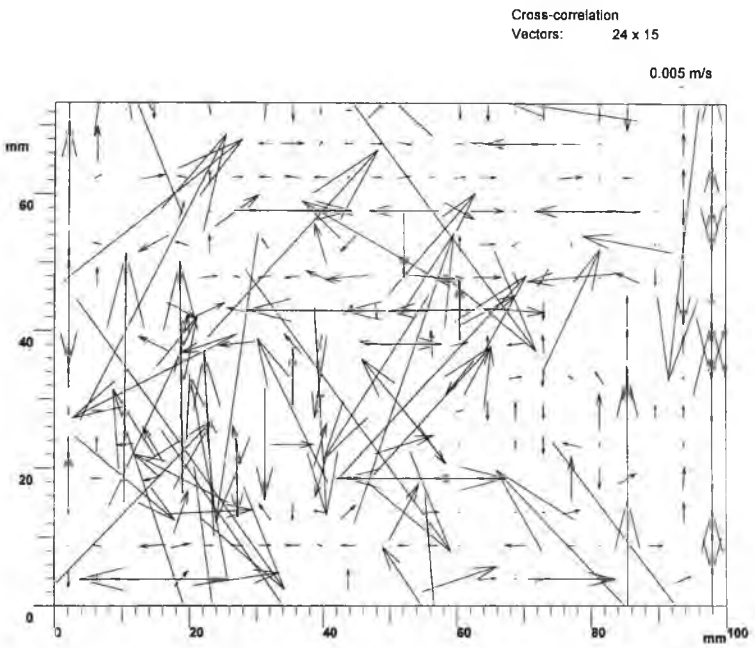

Figure 7.174 Cross-correlation vectors of Styrene at concentration of 500 ppm, coagulated with Cat-Floc 2953.

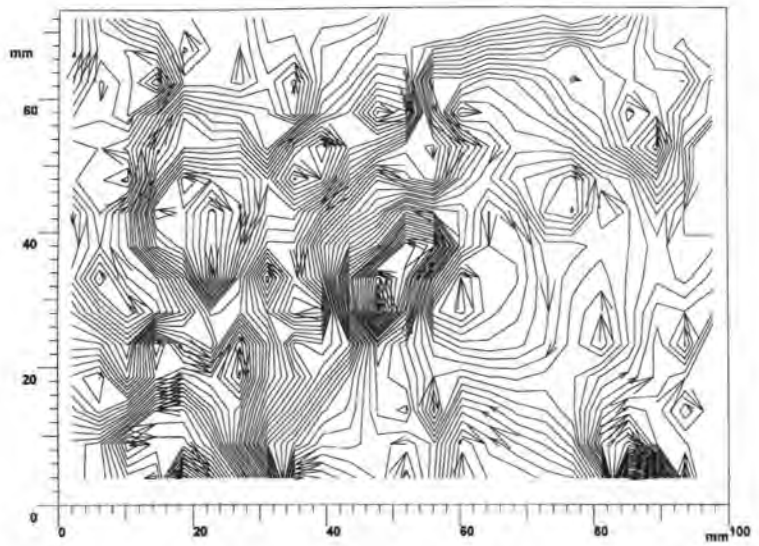

Figure 7.175 Flow direction of Styrene floc at concentration of 500 ppm, coagulated with Cat-Floc 2953.

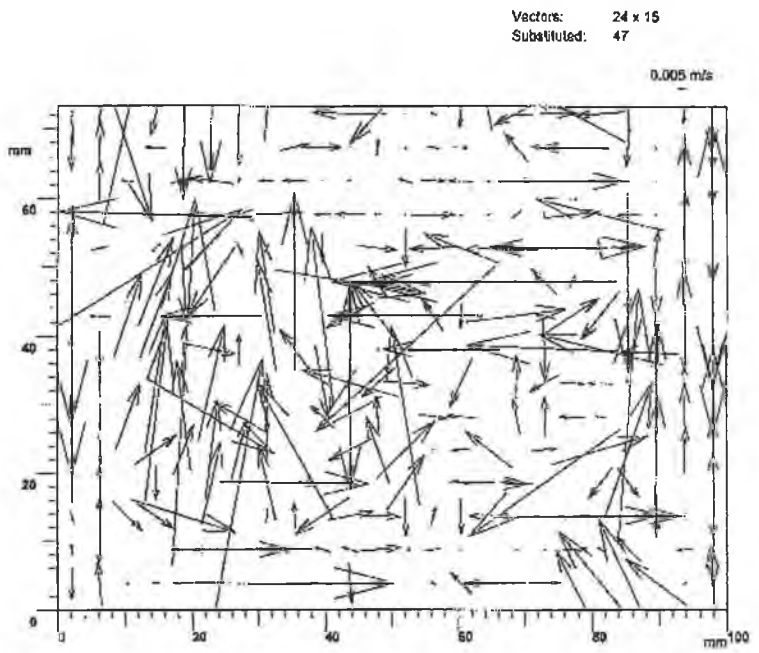

Figure 7.156 Average settling velocity vectors of Styrene at concentration of 500 ppm, coagulated with EB-5000.

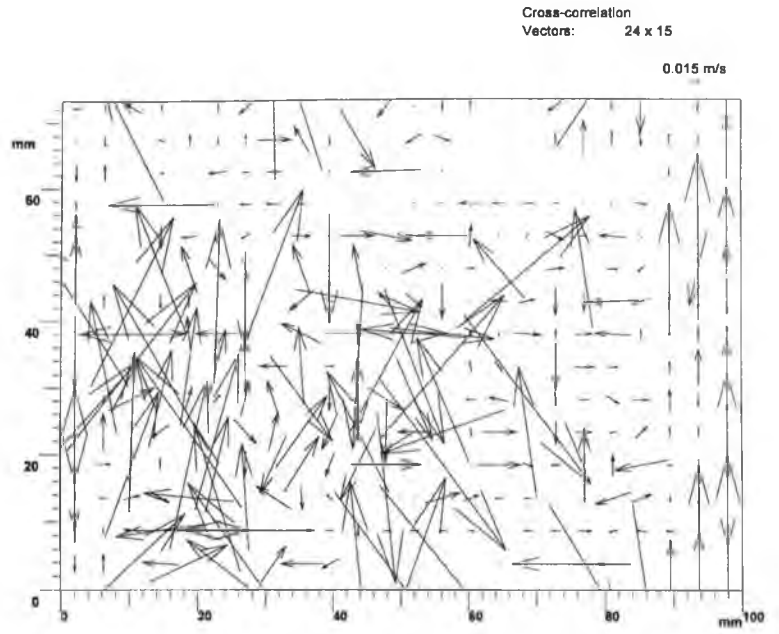

Figure 7.157 Cross-correlation velocity vectors of Styrene at concentration of 500 pm, coagulated with EB-5000.

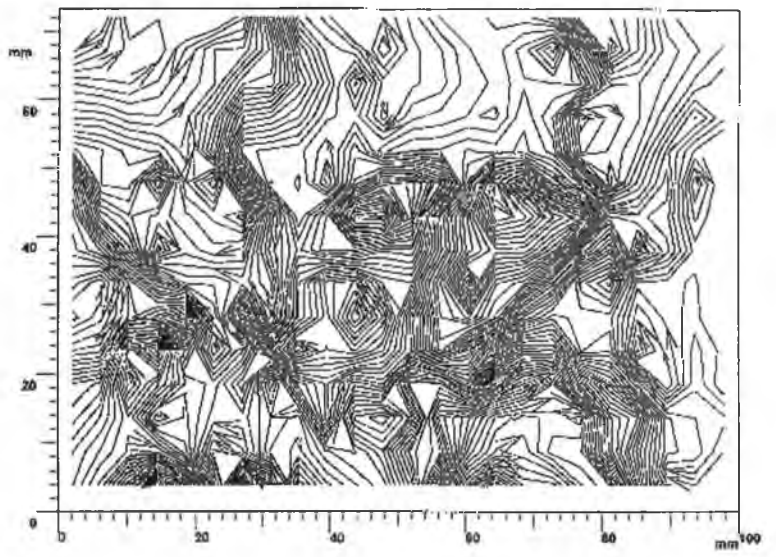

Figure 7.158 Flow direction of Styrene flocs at concentration of 500 ppm, coagulated with EB-5000.

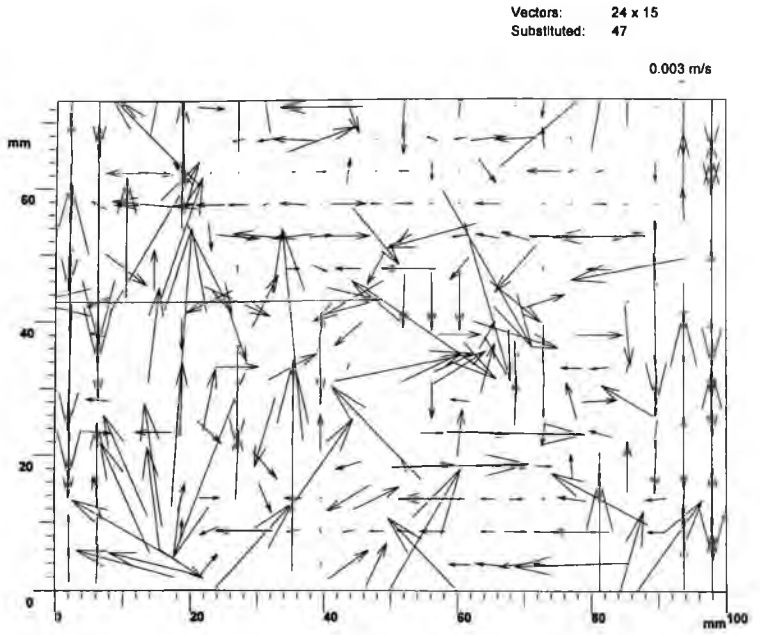

Figure 7.159 Average settling velocity vectors of Styrene at concentration of 300 ppm, coagulated with Cat-Floc 2953.

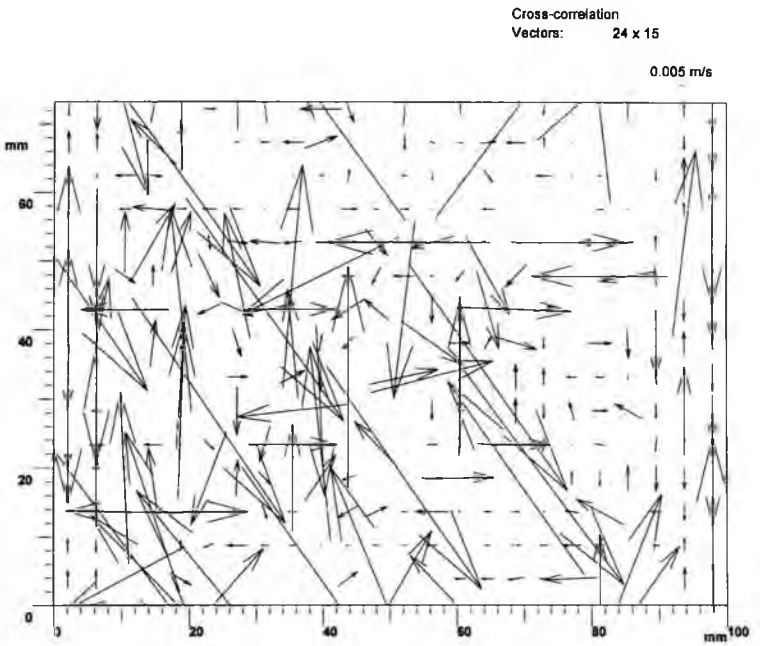

Figure 7.160 cross-correlation velocity vectors of Styrene at concentration of 300 ppm, coagulated with Cat-Floc 2953.

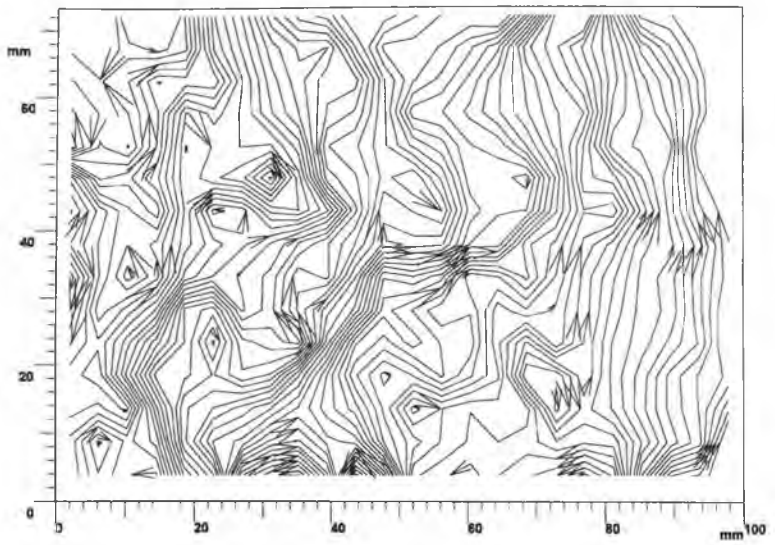

Figure 7.161 Flow direction of Styrene flocs at concentration of 300 ppm, coagulated with EB-5000.

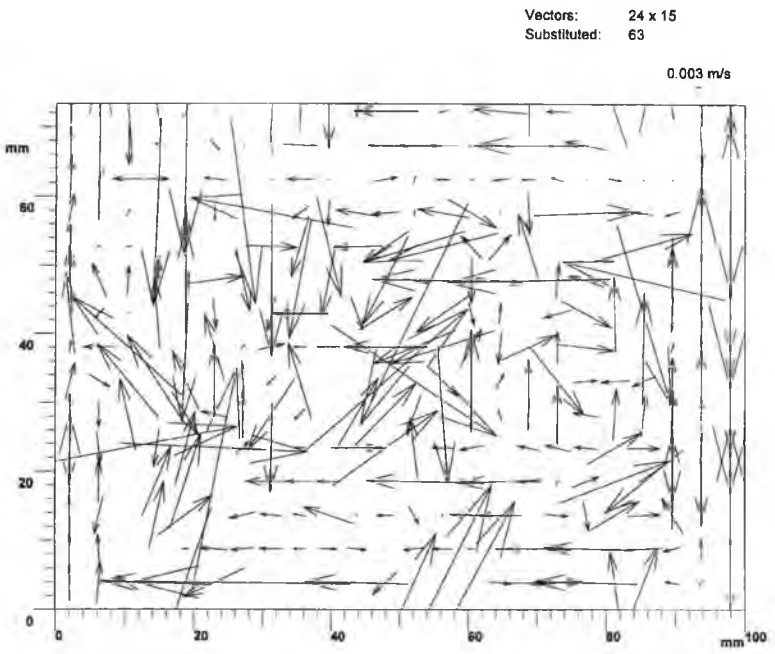

Figure 7.162 Average settling velocity vectors of Styrene at concentration of 300 ppm, coagulated with EB-5000.

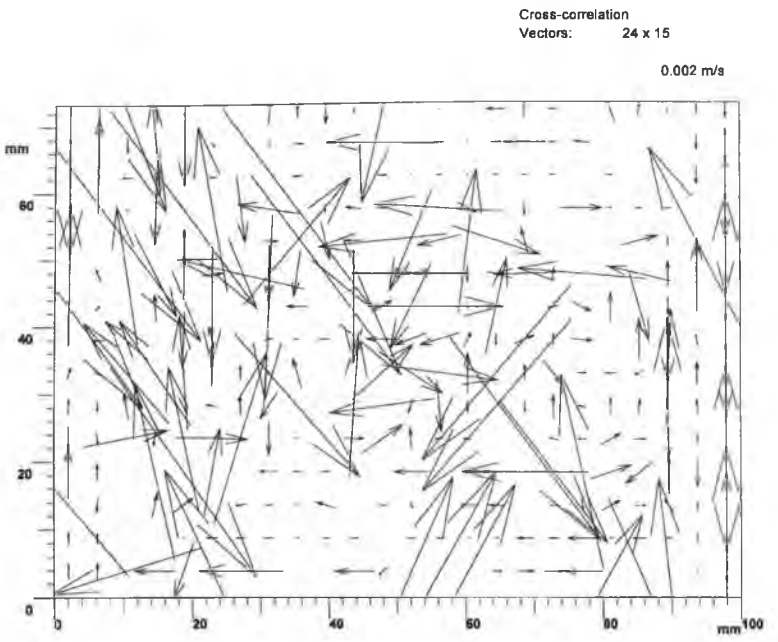

Figure 7.163 Cross-correlation velocity vectors of Styrene at concentration of 300 ppm, coagulated with EB-5000.

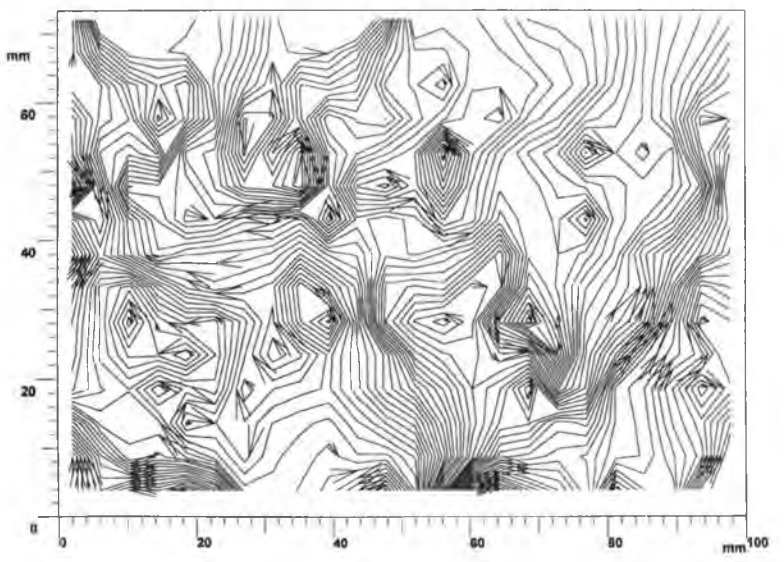

Figure 7. 164 Flow direction of Styrene flocs at concentration of 300 ppm, coagulated with EB-5000.

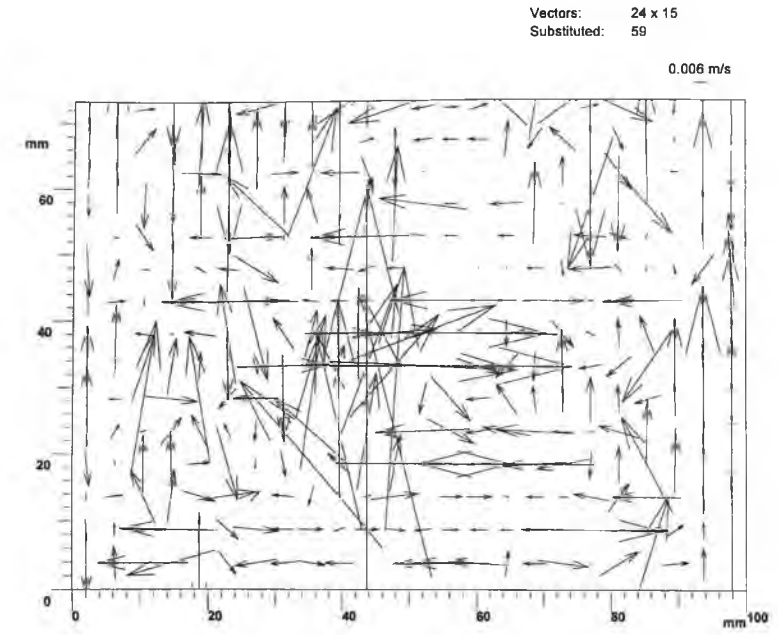

Figure 7.165 Average settling velocity vectors of Gasoline at concentration of 500 ppm, coagulated with Cat-Floc 2953.

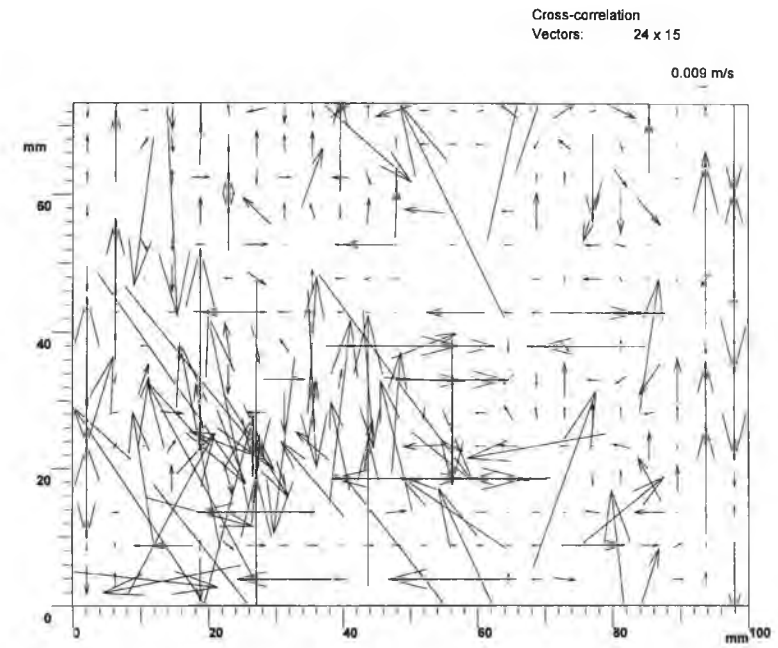

Figure 7.166 Cross-correlation velocity vectors of Gasoline at concentration of 500 ppm, coagulated with Cat-Floc 2953.

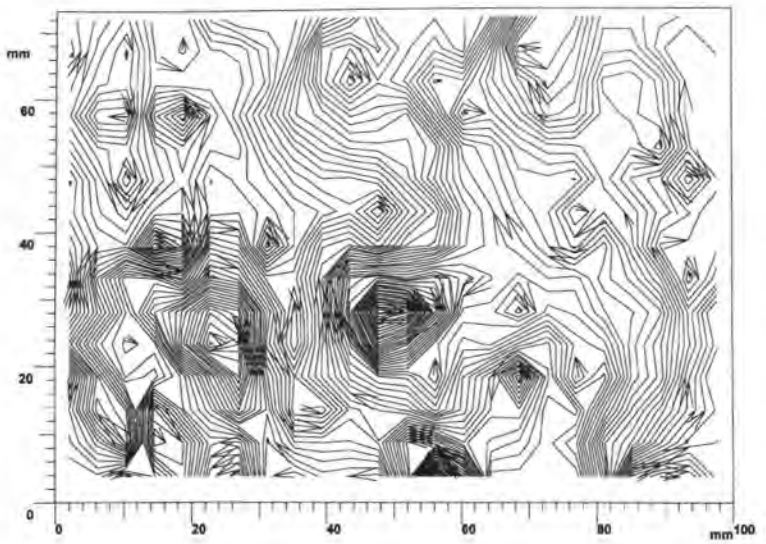

Figure 7.167 Flow direction of Gasoline flocs at concentration of 500 ppm, coagulated with Cat-Floc 2953.

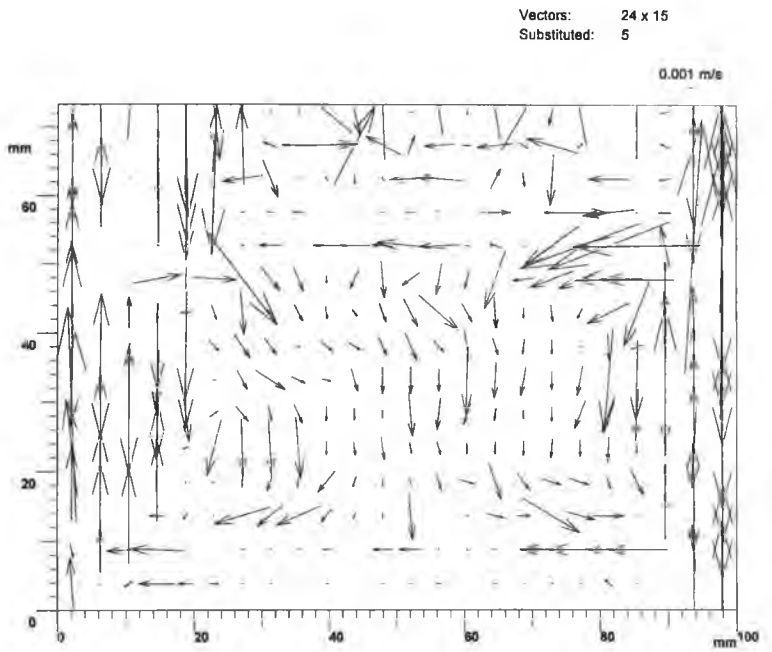

Figure 7.168 Average settling velocity vectors of Gasoline at concentration of 500 ppm, coagulated with EB-5000.

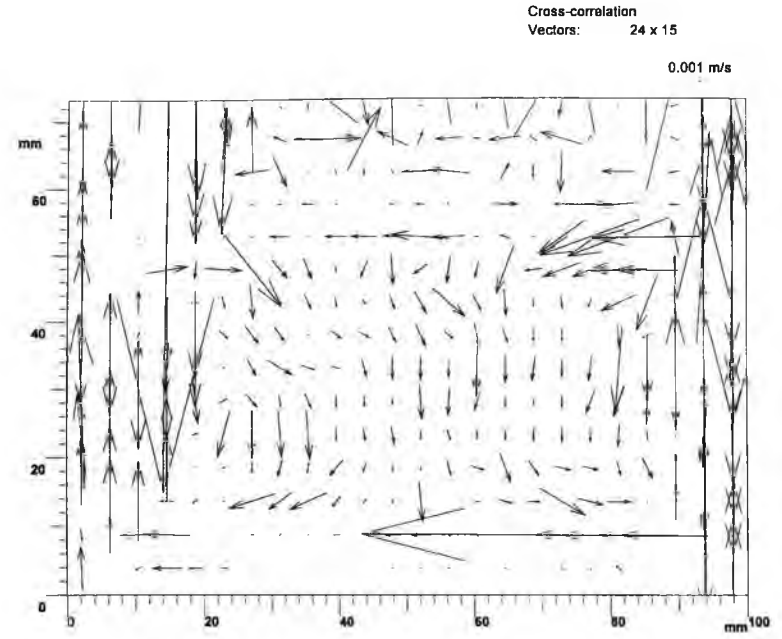

Figure 7.169 Cross-correlation of Gasoline at concentration of 500 ppm, coagulated with EB-5000.

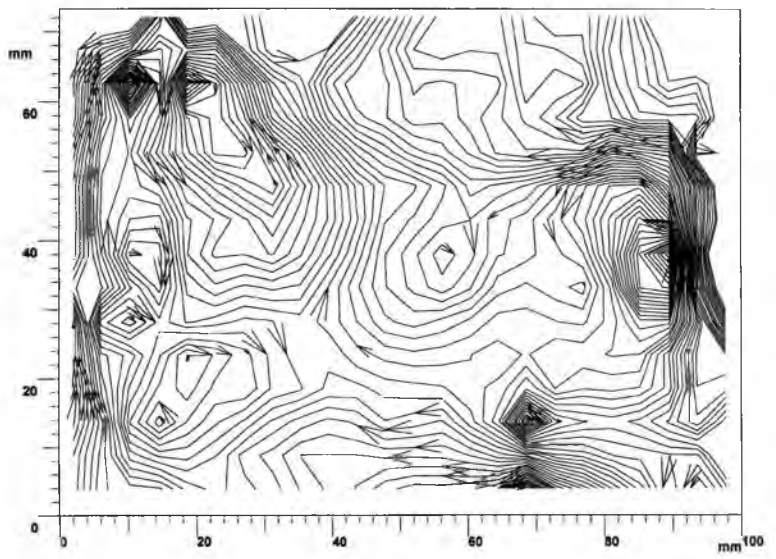

Figure 7.170 Flow direction of Gasoline flocs at concentration of 500 ppm, coagulated with EB-5000.

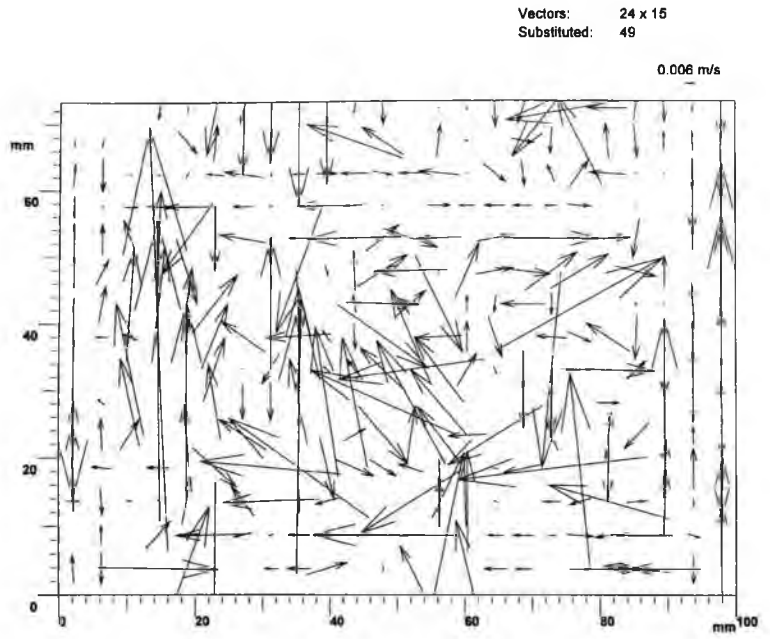

Figure 7.171 Average settling velocity vectors of Gasoline at concentration of 300 ppm, coagulated with Cat-Floc 2953.

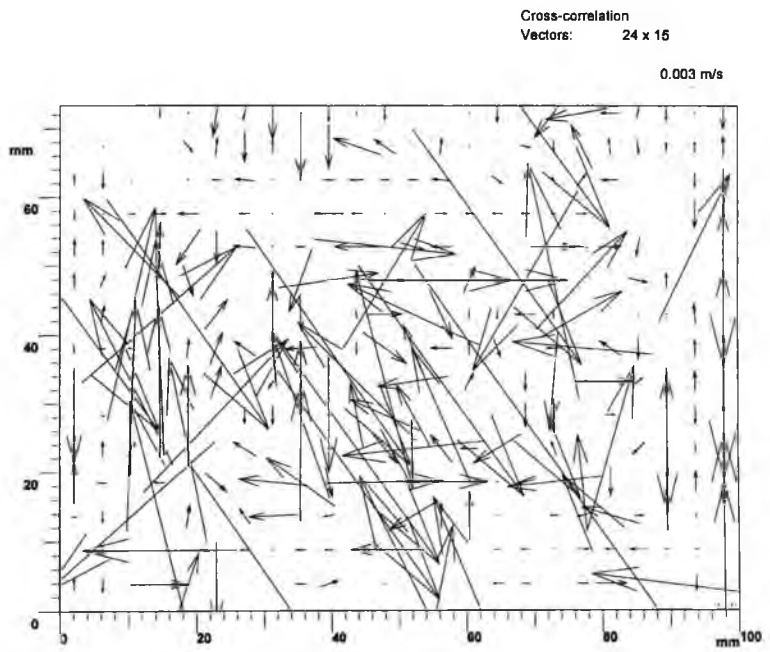

Figure 7.172 Cross-correlation velocity vectors of Gasoline at concentration of 300 ppm, coagulated with Cat-Floc 2953.

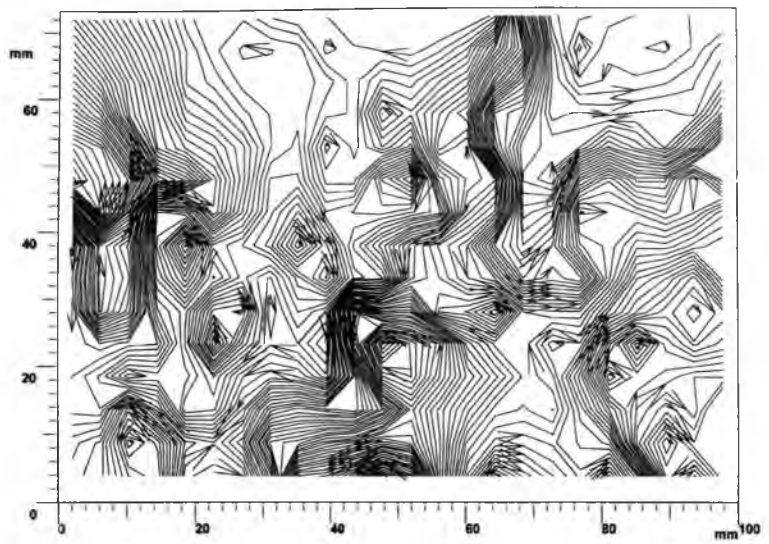

Figure 7.173 Flow direction of Gasoline flocs at concentration of 300 ppm, coagulated with Cat-Floc 2953.

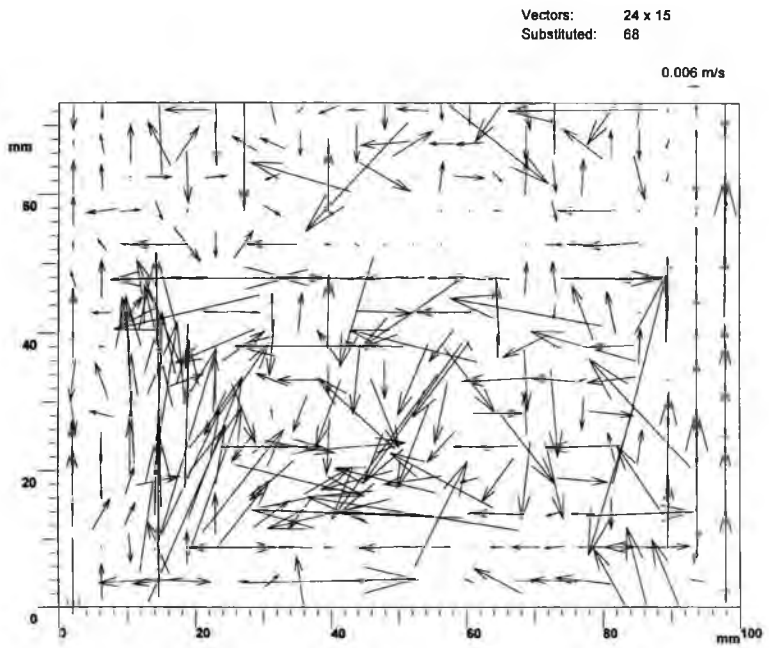

Figure 7.174 Average settling velocity vectors of Gasoline at concentration of 300 ppm, coagulated with EB-5000.

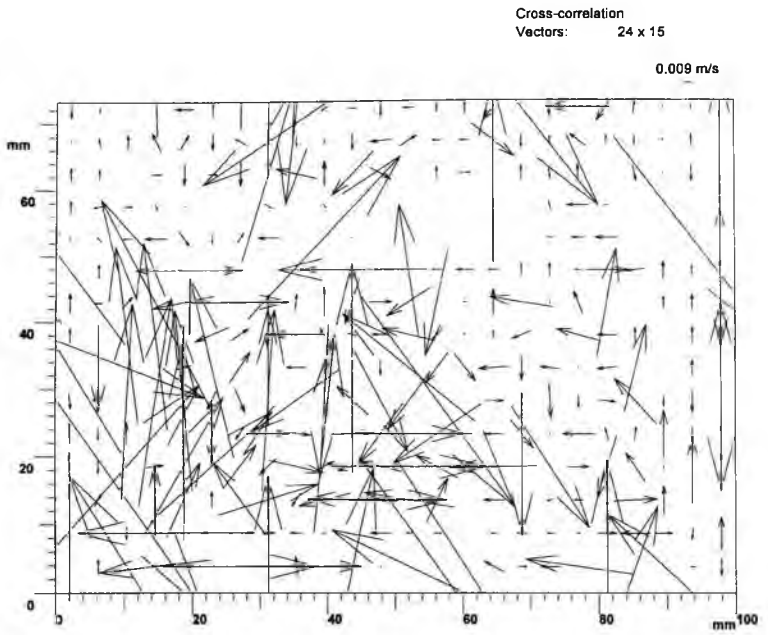

Figure 7.175 Cross-correlation of Gasoline velocity vectors at concentration of 300 ppm, coagulated with EB-5000.

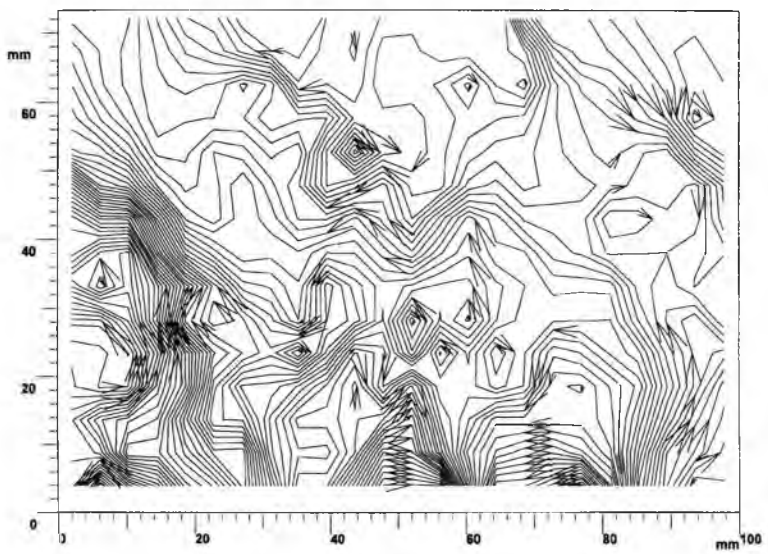

Figure 7.176 Flow direction of Gasoline flocs at concentration of 300 ppm, coagulated with EB-5000.

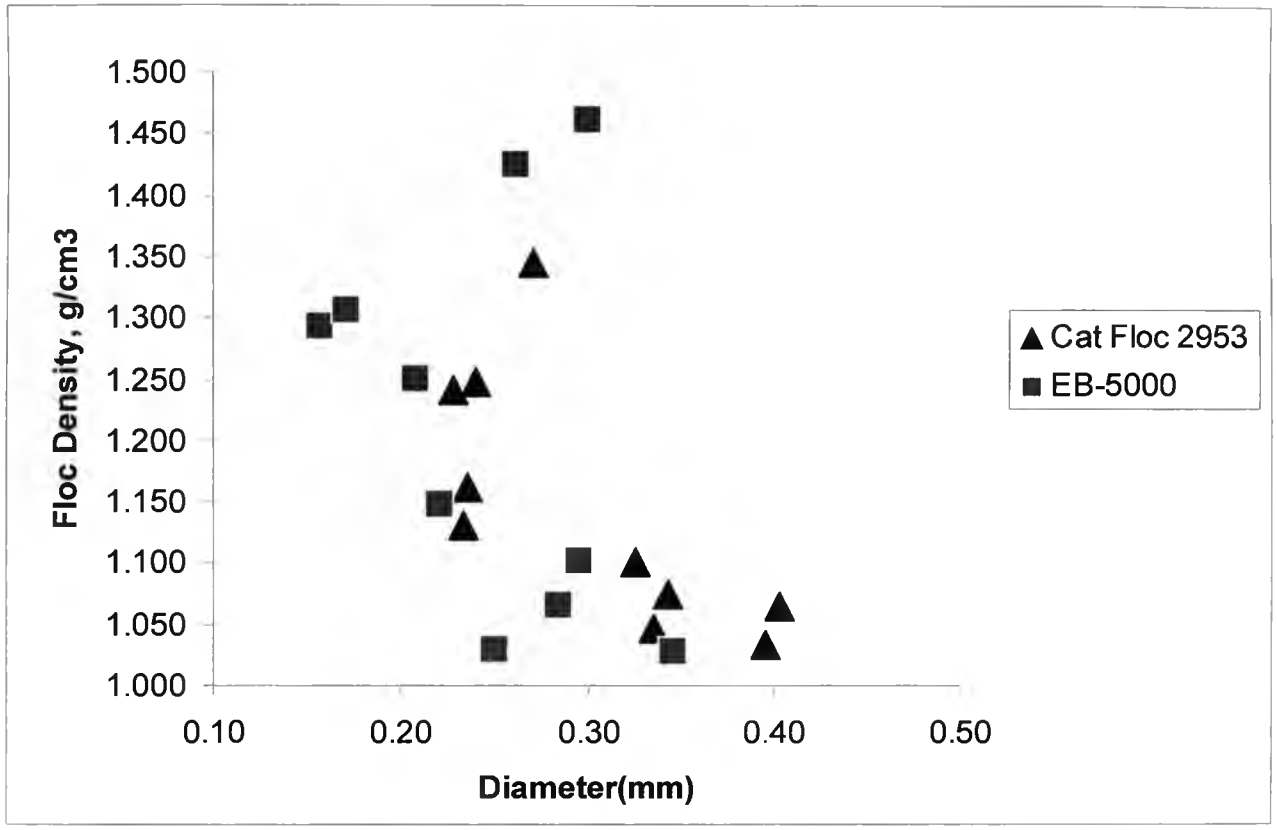

Figure 201. Estimated density of flocs coagulated with polyelectrolytes Cat-Floc 2953 and EB-5000.

7.4. Research Limitations

The research work conducted had the following limitations:

1. The pond water quality parameters (turbidity, humics, and NOM) could not be controlled due to the main feed source being storm water runoff.

2. Volatilization of low molecular weight organics could not be controlled completely, even though they were mixed in closed containers. Volatiles could have escaped during the preparation process, the coagulation process and the preparation for GC analysis (stock solution).

3. Settling velocity calculations based on equation 1, considered the floc as an impermeable spherical particle, while most of the flocs have heterogeneous structure and irregular shapes.

4. Flocs microscopically analyzed may have been damaged during slide preparation due to the size of the pipette used.

5. Ionic concentration and pH effects were considered to be minimal for the duration of research work, nonetheless ionic strength and pH of a solution do effect, to a certain extent the coagulation process.

6. Prior to settling velocity measurements, the hydrocarbon-coagulant flocculated solution was placed in glass cell by pouring the solution into the cell, could have cause breaking some of the flocs.

8. CONCLUSIONS

- Higher removal efficiencies of all hydrocarbons were achieved using coagulant Cat-Floc 2953, which was supported by GC analysis, turbidity measurements and microscopic analysis.

- Floc density calculations confirmed the findings of other researchers, that increase in size of a floc increases settling velocity but decreases density of the floc.

- EB-5000 formed flocs with more dense inner structure except for styrene at concentration 500 ppm and 300 ppm; m-xylene and gasoline at concentration of 300 ppm.

- Cat-Floc 2953 formed larger flocs that settle out faster than flocs produced by EB-5000.

- Overall, high removal of selected hydrocarbons from aqueous solution, with cationic polyelectrolytes were achieved using Cat-Floc 2953 and EB-5000.

9. REFERENCES

Bache, D.H., Rasol, E., Ali, A. and McGiliagan, J.F., (1995). *Floc character: measurement and role in optimum dosing.* Journal of Water SRT-Aqua 44, 2, 83-92.

Bache, D.H., Ali, A., Rasool, E., McGilligan, J.F. and Johnson, C., (1996). *Temperature and coagulation control in the sweep floc domain.* Journal Water SRT-Aqua 45, 4, 195-202.

Bache, D.H. and Al-Ani, S.H., (1989). *Development of a system for evaluating floc strength.* Water Science Technology 21, 529-537.

Bache, D.H., Johnson, C., McGilligan, J.F. and Rasool, E., (1997). *A conceptual view of floc structure in the sweep floc domain.* Water Science Technology 36, 4, 49-56.

Bragg, J.R., (1994). *Clay-Oil Flocculation as a Natural Cleansing Process Following Oil Spills: Part 1 – Studies of Shoreline Sediments and Residues from Past Spills.* Seventeenth Arctic and Marine Oilspill Program Technical seminar.

Becker, C.W. and O'Melia, C., (1996). *Ozone, Oxalic acid and Organic matter molecular weight-Effects on Coagulation.* Ozone Science and Engineering 18, 2, 311-324.

Clark, D.V. and Tansel, B., (1998). *Characterization of microscopic oil-polyelectrolyte interactions during coagulation by image processing.* Proceeding of the International workshop on artificial intelligence and mathematical modeling methods in pavement and geomechanical systems, Florida, USA, 11, 171 – 177.

Crozes, G., White, P. and Marshall, M., (1995). *Enhanced coagulation; its effect on NOM removal and chemical cost.* Journal of American Water Works Association 87, 1, 78-89.

Chang, M.C., Lin, H.L., Huang, C.L., Wang, Y.Y. and Wan, C.C., (1998). *Conditioning characteristics of kaolin sludge with different cationic polyelectrolytes.* Colloids and Surfaces, A: Physicochemical and Engineering Aspects 139, 9,75-80.

Dennett, K.E., Amirtharajah, A., Morgan, T.F. and Gould, J.P., (1996). *Coagulation: its effect on organic matter*. Journal of American Water Works Association 88, 4, 129-142.

Droppo, I.G., Derrick, T.F., Leppard, G.G. Jaskot, C. and Liss, S.N., (1996). *Floc Stabilization for Multiple Microscopic Techniques*. Applied and Environmental Microbiology 62, 9, 3508-3515.

Droppo, I.G., Leppard, G.G., Flannigan, D.T. and Liss, S.N., (1997). *The Freshwater floc: A functional relationship of water and organic and inorganic floc constituents affecting suspended sediments properties*. Water, Air and Soil Pollution 99, 1-4, 43-54.

Eckenfelder, W.W., Jr., (1966). Industrial Water Pollution Control, McGraw-Hill, Inc., New York, NY.

Edwards, M., (May 1997). *Predicting DOC removal during enhanced coagulation.* Journal of American Water Works Association 89, 5, 78-89.

Edzwald, J.K., (1993). *Coagulation in drinking water treatment; particles, organics and coagulants*. Water Science Technology 27, 11, 21-35.

Eifert, L.J., (1995). *Sorption versus coagulation in the treatment of hydrocarbon contaminated waters*. Proceedings – NCUR IX, 1110 – 1113.

Frolov, G.Y. and Mikerova, I.M. (1990). *The turbidity factor as a characteristic of the total content of suspended and colloidal particles in water*. Khimiya I Tekhnologiya Vody (Soviet Journal and Technology) 12, 1, 55-57.

Gagnon, C., Bernard, Grandjean, B.P.A. and Thibault, J., (1997*). Modelling of coagulant dosage in a water treatment plant*. Artificial Intelligence in Engineering 11, 1, 401-404.

Goodger, E.M., (1975). Hydrocarbon fuels: production, properties and performance of liquids and gases, J. Wiley, Inc., New York, NY.

Glasgow, L.A. and Kim, Y.H., (1989). *A review of the role of the physicochemical environment in the production of certain floc properties.* Water, Air and Soil Pollution, 47, 153 – 174.

Gray, S.R., Harbour, P.J. and Dixon, D.R. (1997). *Effect of polyelectrolyte charge density and molecular weight on the flotation of oil in water emulsions.* Colloids and Surfaces, A: Physicochemical and Engineering Aspects 126, 85-95.

Gregory, J. (1997). *The density of particle aggregates.* Water, Science and Technology 36, 4, 1-13.

Huang, C. and Shin, S. (1996). *Interactions between alum and organics in coagulation.* Physicochemical and Engineering Aspects 113, 1,155-163.

Image-Pro Plus (1997). Image-Pro Version 3 for Windows. Media Cybernetics, Silver Spring, Maryland.

Jackson, G.A. (1995). *Comparing observed changes in particle size spectra with those predicted using coagulation theory.* Deep-Sea Research 11, 1, 159-184.

Jordan, E.R. and Payne R.J., (1980). *Fate and weathering of petroleum spills in marine Environment.* Ann Arbor Science Publication. Ann Arbor, Michigan.

Julien, F., Gueroux, B. and Mazet, M., (1994). *Comparison of organic compounds removal by coagulation-flocculation and by adsorption onto preformed hydroxide flocs.* Water Research 28, 12, 2567-2574.

Krasner, S.W. and Amy, G., (1995). *Jar-test evaluations of enhanced coagulation.* Journal of American Water Works Association 10, 10, 93-107.

Laor, Y. and Rebhun, M. (1997). Complex-Flocculation: *A new method to determine binding coefficients of organic contaminants to dissolved humic substances.* Environmental Science Technology, 31, 12, 3558 – 3564.

Leeuwen, van J., Schell, H., Berger, M., Drikas, M., Bursill, D., Chow, C. and Clasen, J. (1997). *Comparison of coagulant doses determined using a charge titration unit with a jar test procedure for eight German surface waters.* Journal of Water SRT-Aqua 46, 5, 261-273.

Lind, C., (1995). *A Coagulant Road Map.* Public Works, 3, 3, 36 – 38.

Lind, C., (1995). *Coagulation control and Optimization I.* Public Works, 10, 1, 56-57.

Lind, C., (1996). *Reducing Total and Dissolved Organic Carbon: Comparing Coagulants.* Environmental Technology, May/June, 54 – 58.

Lurie, M. and Rebhun, M,. (1997). *Effect of properties of polyelectrolytes on their interactions with particulates and soluble organics.* Water, Science and Technology 36, 4, 93-101.

Milligam, T.G., (1996). *In situ particle (floc) size measurements with the benthos 373 plankton silhouette camera.* Journal of Sea Research 36,1/2, 93-100.

Moudgil, M.B. and Prakash, T.S., (1998). *Competitive adsorption of polymer and surfactants on solid substrates.* Colloids and Surfaces, A:Physicochemical and Engineering Aspects 133, 93-97.

Morrison, T.R. and Boyd, N.R., (1975). Organic Chemistry, 3rd edition, Allyn and Bacon, Inc., Boston MA.

Narkis, N., Ghattas, B., Rebhun, M. and Rubin, J.A., (1991). *The mechanism of flocculation with aluminum salts in combination with polymeric flocculants as flocculants aids.* Water Supply, 9, 37 – 44.

Olah, G.A. and Molnar, A., (1995). Hydrocarbon Chemistry, J.Wiley, Inc., New York, NY.

Petrov, A.A., (1987). Petroleum hydrocarbons, Springer-Verlag, Berlin; New York.

Petzold, G., Buchhammer, H.M. and Lunkwitz, K. (1996). *The use of oppositely charged polyelectrolytes as flocculants and retention aids.* Colloids and Surfaces, A: Physicochemical and Engineering Aspects 119, 87-92.

Pizzi, G.N. and Rodgers, L.M., (1989). *Preliminary testing for control of DBPs in Cleveland.* Journal of American Water Works Association 89, 8, 78 - 87.

Plucinski, P. and Reitmeir, J., (1997). *The interactions between polyelectrolytes and AOT in and oil/water system.* Colloids and Surfaces, A: Physicochemical and Engineering Aspects 122, 75-82.

Randtke, J.S., (1988). *Organic Contaminant Removal by Coagulation and Related Process Combinations.* Research and Technology, 5, 40 – 56.

Rebhun, M. and Lurie, M. (1993). *Control of Organic matter by coagulation and floc separation.* Water, Science, Technology, 27, 11, 1- 18.

Regula, J., (1994). Evaluation of ultrafiltration technology for the treatment of PHC contaminated waters. Master thesis.

Schnoor, J.L., (1996). Environmental Modeling, J. Wiley & Sons, Inc., New York, NY.

Solomons, T.W.G., (1992). Organic Chemistry, 5th edition, J. Wiley & Sons, Inc., New York, NY.

Schwarz, S., Buchhammer, H.M., Lunkwitz, K. and Jacobasch, H.J., (1998). *Polyelectrolyte adsorption on charged surfaces: study by electrokinetic measurements.* Colloids and Surfaces, A: Physicochemical and Engineering Aspects 140, 377-384.

Semmens, J.M. and Field, T.K., (1980). *Coagulation: Experiences in Organic removal.* Journal of American Water Works Association 8, 476-483.

Syvitski, J.P.M. and Hutton, E.W.H., (1996). *In situ characteristics of suspended particles as determined by the floc camera assembly FCA.* Journal of Sea Research 36, 1/2, 131-142.

Tambo, N. (1991). *Basic concepts and innovation turn of coagulation/flocculation.* Water Supply: the review journal of the International Water Supply's association, 9, 1, 1-10.

Tambo, N. and Kamei, T., (1980). *Coagulation and flocculation on water quality matrix.* Water, Science and Technology 37, 10, 31-41.

Varanasi, U., (1989). Metabolism of Polyclic Aromatic Hydrocarbons in the Aquatic Environment, CRC Press Inc., Boca Raton, FL.

Verschneren, K., (1983). Handbook of Environmental Data on Organic Chemicals. Second edition, Van Nostrand Reinhold Company Inc., New York, N.Y..

Weber, J.W., Jr., (1972). Physicochemical Processes for Water Quality Control, J. Wiley & Sons, Inc., New York, NY.

Webster, L., Huglin, B. and Robb, D., (1997). *Complex formation between polyelectrolytes in dilute aqueous solution.* Polymer, 38, 6, 1373-1380.

Zunan, Q., Zhang, Y. and Yuqiao, F. (1995). *Removal of Oil from Concentrated Wastewater by Attapulgite and Coagulant.* Water Quality research Journal of Canada, 30, 1, 89 – 99.

APPENDIX

1. Optimum dosages of coagulants obtained from jar tests.

Contaminant	Concentration (ppm)	Cat-Floc 2953 (ml/L)	EB-5000 (ml/L)
Decane	500	7	3
Decane	300	16	3
Toluene	500	4	3
Toluene	300	6	7
m-xylene	500	5	4
m-xylene	300	3	4
Styrene	500	5	3
Styrene	300	5	3
Gasoline	500	4	4
Gasoline	300	7	4

2. Turbidity and pH measurements of Decane at concentration of 500 ppm

Coagulant	pH	Turbidity (NTU)
No coagulant	7.75	12.6
Cat-Floc 2953	7.40	1.55
EB-5000	7.55	1.70

3. Turbidity and pH measurements of Decane at concentration of 300 ppm

Coagulant	pH	Turbidity (NTU)
No coagulant	8.20	6.01
Cat-Floc 2953	7.26	1.18
EB-5000	7.46	2.25

4. Turbidity and pH measurements of styrene at concentration of 500 ppm

Coagulant	pH	Turbidity (NTU)
No coagulant	8.07	7.50
Cat-Floc 2953	7.43	0.40
EB-5000	7.74	0.69

5. Turbidity and pH measurements of styrene at concentration of 300 ppm

Coagulant	pH	Turbidity (NTU)
No coagulant	8.11	4.95
Cat-Floc 2953	7.36	0.35
EB-5000	7.71	0.76

7. Turbidity and pH measurements of m-xylene at concentration of 500 ppm

Coagulant	pH	Turbidity (NTU)
No coagulant	8.08	15.20
Cat-Floc 2953	8.02	0.22
EB-5000	7.96	0.44

8. Turbidity and pH measurements of m-xylene at concentration of 300 ppm

Coagulant	pH	Turbidity (NTU)
No coagulant	7.83	4.01
Cat-Floc 2953	7.69	0.68
EB-5000	7.76	1.39

9. Turbidity and pH measurements of toluene at concentration of 500 ppm

Coagulant	pH	Turbidity (NTU)
No coagulant	8.24	0.79
Cat-Floc 2953	7.56	0.13
EB-5000	7.69	0.15

10. Turbidity and pH measurement of toluene at concentration of 300 ppm

Coagulant	pH	Turbidity (NTU)
No coagulant	8.09	0.64
Cat-Floc 2953	7.41	0.24
EB-5000	7.52	0.31

11. Turbidity and pH measurement of gasoline at concentration of 500 ppm

Coagulant	pH	Turbidity (NTU)
No coagulant	8.00	22.80
Cat-Floc 2953	7.66	0.33
EB-5000	7.58	0.61

12. Turbidity and pH measurements of gasoline at concentration of 300 ppm

Coagulant	pH	Turbidity (NTU)
No coagulant	7.80	9.48
Cat-Floc 2953	7.53	0.21
EB-5000	7.55	0.71